



# **Assessment of the Solar Resource for Non-conventional Solar PV Applications in Highways and Railways**

Pedro Nadais de Vasconcelos

**FACULTY OF ENGINEERING OF THE UNIVERSITY OF PORTO**

Mechanical Engineering  
Thermal Energy Major

Supervisor: Prof. Ana I. Palmero Marrero  
Co-supervisor: Eng. Miguel Marques

February, 2022



*“Concentrate all your thoughts upon the work at hand.  
The sun’s rays do not burn until brought to a focus.”*

*Alexander Graham Bell*



## ABSTRACT

The production of energy using solar photovoltaic (PV) systems requires a considerable area. Given the importance of land as an essential resource for humanity and with a polyvalent potential, there is a strong need to use it as efficiently as possible. In this sense, new photovoltaic applications have emerged in the energy sector.

There is no clear definition for what may be considered as conventional or non-conventional applications solar PV technologies. In this thesis, the term conventional has been reserved for matured and currently widely deployed applications. The more recent and less widespread applications were referred to as non-conventional.

The propound study was performed in conjunction with INEGI (Instituto de Ciência e Inovação em Engenharia Mecânica e Engenharia Industrial) and consists in the evaluation of the solar potential and economic viability of non-conventional highway and railway PV application sites for grid-connected implementation. Its primary objective was to select the 10 most promising locations in a designated area of the Maia County, north from the city of Porto, Portugal.

A first group of 30 sites were initially selected according to surface orientation and near shadings using Google Earth. They were carefully examined according to qualitative solar potential standards and compared amongst each other. The 5 least favourable sites in terms of solar exposure, structural viability for PV module installation, as well as visual and sound impact were excluded. The remaining 25 sites were analysed with ArcGIS software.

ArcGIS analysis allowed to study the local horizontal incident global solar radiation. A second triage was carried out and the 5 locations with the lowest incident radiation were discarded. The remaining 20 sites were analysed using PVsyst software.

Using PVsyst, 3D shading models were created and PV module and inverter were selected for each site. System simulations were conducted and the 15 sites which showed the best performance were identified. Module areas range from 130 m<sup>2</sup> to 5324 m<sup>2</sup> and annual energy production from 37.39 MWh to 1481 MWh. The registered annual performance ratio (PR) was in all cases above 0.811.

Lastly, a brief economic analysis was undertaken, which allowed to determine the 10 sites both with more solar potential and economic viability out of the 30 initially proposed. This analysis took into account exclusively the cost of the modules and inverters used in the simulations. As such, the results are rather optimistic. The initial investment did not exceed 831,834.00 €, the annual return comprised values between 22,806 €/year and 311,010 €/year, and the maximum payback time recorded was less than 5 years.



## RESUMO

A produção de energia com recurso a sistemas solares fotovoltaicos (PV) requer uma área considerável. Atendendo à importância do solo como recurso essencial à humanidade e de potencial plurivalente, há uma forte necessidade de o utilizar da forma mais eficiente possível. Nesse sentido, no ramo energético têm surgido novas aplicações fotovoltaicas.

Não existe uma clara definição para o que pode ser considerado como tecnologias solares fotovoltaicas convencionais ou não convencionais. Nesta dissertação, o termo convencional foi reservado para aplicações maduras e amplamente implantadas nos dias de hoje. As aplicações mais recentes e menos difundidas foram referidas como não convencionais.

O presente estudo foi desenvolvido em conjunto com o INEGI (Instituto de Ciência e Inovação em Engenharia Mecânica e Engenharia Industrial) e consiste na avaliação do potencial solar e da viabilidade económica de locais destinados a aplicações fotovoltaicas não convencionais em rodovias e ferrovias com conexão à rede elétrica. Teve como principal objetivo selecionar os 10 locais mais promissores numa área definida do concelho da Maia, a norte da cidade do Porto, Portugal.

Um primeiro grupo de 30 locais foi selecionado com recurso à ferramenta Google Earth, de acordo com a sua orientação superficial e possível sombreamento causado por edifícios ou árvores na sua proximidade. Os locais foram de seguida comparados entre si e os 5 locais menos favoráveis em matéria de exposição solar, viabilidade estrutural e com maior risco de impacto visual e sonoro foram excluídos. Os 25 locais restantes foram analisados com o software ArcGIS.

A análise realizada com o ArcGIS permitiu estudar a radiação solar global incidente horizontal na área proposta. Uma segunda triagem foi realizada e os 5 locais com menor radiação incidente foram descartados. Os 20 locais restantes foram de seguida analisados usando o software PVsyst.

Com recurso ao PVsyst, foram desenvolvidos modelos de sombreamento 3D para cada local. Tanto módulos PV como inversores foram selecionados para cada local e, após realizadas as simulações para cada sistema, foram identificados os 15 locais com melhor desempenho. As respectivas áreas fotovoltaicas compreenderam valores desde 130 m<sup>2</sup> até 5324 m<sup>2</sup> e produção annual de energia de 37,39 MWh até 1481 MWh. Em todos os casos, o *performance ratio* (PR) registado foi superior a 0,811.

Por último, foi realizada uma breve análise económica que permitiu determinar os 10 locais com maior potencial solar e viabilidade económica. Esta análise teve em conta unicamente o custo dos módulos e inversores utilizados nas simulações e, como tal, os resultados mostram-se bastante otimistas. O investimento inicial não ultrapassou os 831.834,00 €, o retorno anual compreendeu valores entre 22 806 €/ano e 311 010 €/ano, e o máximo *payback time* registado foi inferior a 5 anos.





## **ACKNOWLEDGEMENTS**

I would like to thank first and foremost my parents for their unconditional support in every challenge I face.

I also wish to express my gratitude towards my supervisor, Prof. Ana I. Palmero, and co-supervisor, Eng. Miguel Marques, for their guidance.

I would also like to thank all my professors. Their knowledge and experience have contributed greatly to this work.

Lastly, I would like to thank my friends who have accompanied me for many years.



# TABLE OF CONTENTS

1. INTRODUCTION.....	1
2. STATE OF THE ART.....	3
2.1 Fundamentals of Solar Energy Technologies.....	3
2.1.1 The Solar Resource.....	3
2.1.2 Reckoning of Time.....	6
2.1.3 Solar Angles.....	8
2.1.4 Sun Path Diagrams.....	12
2.1.5 Shadow Determination.....	13
2.2 PV Systems.....	14
2.2.1 PV Cells.....	15
2.2.2 PV Modules.....	17
2.2.3 PV System Components.....	17
2.2.4 PV System Performance.....	19
2.2.5 The Economics of PV Systems.....	22
2.3 Non-Conventional PV System Applications.....	26
3. CASE STUDY.....	41
3.1 Area of Study.....	41
3.2 Site Selection.....	41
4. MODELLING.....	47
4.1 ArcGIS Analysis.....	47
4.2 PVsyst Simulation.....	54
5. RESULTS AND DISCUSSION.....	61
5.1 ArcGIS and PVsyst Comparison.....	61
5.2 Simulation Results.....	63
5.3 Selection.....	71
6. ECONOMIC ANALYSIS.....	73
7. CONCLUSION AND FUTURE STUDIES.....	75
8. REFERENCES.....	77
APPENDIX A: ArcGIS Global Radiation Calculation.....	79
APPENDIX B: 3D Shading Models (PVsyst) .....	80
APPENDIX C: Loss Diagrams.....	88
APPENDIX D: PV Module Datasheets.....	93
APPENDIX E: Inverter Datasheets.....	96

## LIST OF FIGURES

Figure 1 – Work methodology.....	1
Figure 2 - The Sun with its layer structure depicted [4].....	3
Figure 3 - Elliptical orbit of the earth around the sun [5].....	4
Figure 4 - Solar constant in the course of one year [5] .....	5
Figure 5 - Annual total solar irradiation on horizontal surface for Europe [6] .....	6
Figure 6 - Graphical representation of equation of time [3] .....	7
Figure 7 - The sun’s virtual motion coordinate system [4] .....	8
Figure 8 - Definition of the solar angles [3] .....	9
Figure 9 - Celestial representation of the yearly variation of solar declination [3].....	9
Figure 10 - Graphical representation of the yearly variation of solar declination [3].....	10
Figure 11 - Apparent daily path of the sun across the sky from sunrise to sunset [3].....	11
Figure 12 - Solar angles diagram [3] .....	12
Figure 13 - Sun path diagram for 35°N latitude [3] .....	12
Figure 14 - Geometry of the solar profile angle, $p$ , in a window overhang arrangement [3].....	13
Figure 15 – Parameters to calculate the minimum distance between module rows to avoid shading [7] .....	14
Figure 16 – Mono (a) and Poly-Crystalline (b) Silicon PV Cells [9] .....	16
Figure 17 - Photovoltaic cell, module, panel and array [10] .....	16
Figure 18 - Assembly view of a solar PV module [11] .....	17
Figure 19 - Schematic representation of (a) a simple DC PV system to power a water pump with no energy storage and (b) a complex PV system including batteries, power conditioners, and both DC and AC loads [4] .....	18
Figure 20 – Schematic representation of a grid-connected PV system [4] .....	19
Figure 21 – PV LCOE drivers [13] .....	23
Figure 22 - Glass ceiling with transparent BIPV modules [16] .....	27
Figure 23 - PV modules alongside a highway slope [17] .....	28
Figure 24 - Different Possible PVNB Configurations [17] .....	29
Figure 25 - Bifacial PVNBs allow light to enter from both sides [17] .....	30
Figure 26 - Schematic layout of a PV roof structure over a roadway [19] .....	31
Figure 27 - Solar carport [20] .....	32
Figure 28 - Solar PV bus stop shelter in Zagreb, Croatia.....	32
Figure 29 - Time axis of the research on PV pavement structure [24] .....	33
Figure 30 - London’s solar-powered bridge [27] .....	35

Figure 31 - Schematic representation of a typical large-scale floating PV system with its key components [28] .....	36
Figure 32 - Global investment cost for floating solar PV plants [29] .....	37
Figure 33 - The concept of PV integration with swimming pools: (a) PV on the pool edge, and (b) PV on the pool floor [30] .....	38
Figure 34 - (a) APV system installed in Italy [35], and (b) APV facility installed above the potato farm (RESOLA project), Heggelbach, Germany [32] .....	39
Figure 35 – Selected study area (ArcGIS) .....	41
Figure 36 – Selected sites (Google Earth Pro) and their specifications.....	42
Figure 37 – Site 1, sound barrier.....	42
Figure 38 – Site 2, slope.....	42
Figure 39 – Site 3, toll.....	42
Figure 40 - Site 4, sound barrier.....	42
Figure 41 - Site 5, toll.....	43
Figure 42 - Site 6, toll.....	43
Figure 43 - Site 7, toll.....	43
Figure 44 - Site 8, sound barrier.....	43
Figure 45 - Site 9, sound barrier.....	43
Figure 46 – Site 10, toll gate.....	43
Figure 47 - Site 11, slope.....	43
Figure 48 - Site 12, bridge.....	43
Figure 49 - Site 13, sound barrier.....	43
Figure 50 - Site 14, toll.....	43
Figure 51 - Site 15, toll.....	44
Figure 52 - Site 16, slope.....	44
Figure 53 - Site 17, slope.....	44
Figure 54 - Site 18, sound barrier.....	44
Figure 55 - Site 19, slope.....	44
Figure 56 - Site 20, PV canopy.....	44
Figure 57 - Site 21, PV canopy.....	44
Figure 58 - Site 22, PV canopy.....	44
Figure 59 - Site 23, bridge.....	44
Figure 60 - Site 24, PV canopy.....	44
Figure 61 - Site 25, bridge.....	45
Figure 62 - Site 26, bridge.....	45

Figure 63 - Site 27, bridge.....	45
Figure 64 - Site 28, PV canopy.....	45
Figure 65 - Site 29, PV canopy.....	45
Figure 66 - Site 30, train station.....	45
Figure 67 – XY Coordinate System (ArcGIS) .....	47
Figure 68 – Z Coordinate System (ArcGIS) .....	47
Figure 69 - N41W009 layer (ArcGIS) .....	48
Figure 70 - N41W009, roads, and railways of Portugal layers (ArcGIS) .....	48
Figure 71 – N41W009, roads, railway layers, and the polygon representative of the area of interest (ArcGIS) .....	49
Figure 72 – Roads layer, railways layer, and N41W009 layer confined to the area of study (ArcGIS).....	49
Figure 73 – Hillshade layer overlapped by N41W009 layer with 40 % transparency (ArcGIS)	50
Figure 74 – Solar Radiation layer (ArcGIS) .....	51
Figure 75 – Sites of interest (ArcGIS) .....	51
Figure 76 – Sites of interest and solar radiation layer (ArcGIS) .....	52
Figure 77 – Module quality, LID, and mismatch losses (PVsyst) .....	55
Figure 78 – Orientation analysis of site number 3 (PVsyst) .....	56
Figure 79 – 3D shading model of site number 6 (PVsyst) .....	57

## LIST OF TABLES

Table 1 – Renewable Energy Indicators 2020 [8].....	15
Table 2 - Simplified PV system costs, 2008, 2015 and 2025 [13] .....	24
Table 3 - Compiled Highway PVNB Counts [17] .....	30
Table 4 - Commercial achievements of PV pavement [26] .....	34
Table 5 – Numbered sites and respective specification, location, and classification.....	53
Table 6 – Module characteristics.....	57
Table 7 – Inverter characteristics.....	58
Table 8 – Specifications, location, sub-arrays, orientation, modules, and inverters used in each site.....	58
Table 9 – Numbered sites and respective specification, location, and classification.....	60
Table 10 – Results of PV toll sites.....	63
Table 11 – Results of PV slope sites.....	65
Table 12 – Results of PV bridge site.....	66
Table 13 – Results of PVNB sites.....	67
Table 14 – Results of PV canopy sites.....	69
Table 15 – Correlations established between generic components used in the simulations, real component models, and component prices.....	73
Table 16 – Initial investment, annual return, and payback time for each site.....	74

# NOMENCLATURE

## Abbreviations

AC	Alternate Current
APV	Agrophotovoltaic
AST	Apparent Solar Time
BAPV	Building-Attached Photovoltaic
BIPV	Building-Integrated Photovoltaic
BOS	Balance Of System
DC	Direct Current
DS	Daylight Saving
ET	Equation of Time
EVA	Ethyl Vinyl Acetate
FSPV	Floating Solar Photovoltaics
GCS	Geographic Coordinate System
GIS	Geographic Information System
LCOE	Levelized Cost Of Electricity
LL	Local Longitude
LST	Local Solar Time
MPPT	Maximum Power Point Tracker
O&M	Operations and Maintenance
PR	Performance Ratio
PV	Photovoltaic
PVNB	Photovoltaic Noise Barrier
SL	Standard Longitude
SRTM	Shuttle Radar Topography Mission
STC	Standard Test Conditions
UHI	Urban Heat Island



## Symbols

$d$	Row distance	$m$
$G_{sc}$	Solar constant	$W/m^2$
$h$	Module height	$m$
$Ha$	Hour angle	$^\circ$
$I_i$	Irradiance	$W/m^2$
$L$	Local latitude	$^\circ$
$N$	Day of the year	
$p$	Solar profile angle	$rad$
$P_{max}$	Electrical power output	$W/m^2$
$R$	Sun's radius	$km$
$w$	Module width	$m$
$Y_A$	Second Yield	$kWh$
$Y_f$	Final Yield	$kWh$
$Y_r$	Third Yield	$kWh$
$z$	solar azimuth angle	$rad$
$z_s$	Surface azimuth angle	$rad$

## Greek Symbols

$\alpha$	Solar altitude angle	$rad$
$\beta$	Surface tilt angle	$rad$
$\delta$	Declination	$rad$
$\theta$	Incidence angle	$rad$
$\phi$	solar zenith angle	$rad$



# 1. INTRODUCTION

During the past decade, there has been a 50% increase in global solar photovoltaic (PV) demand [1]. While centralized solar power plants require large areas for PV system installation, urban and semi-urban areas might hold the key for a more efficient use of land.

Approximately 55% of the world's population lives in cities, and cities constitute approximately two-thirds of the global primary energy demand [1]. New decentralized PV applications help tackle the geographic problem associated with renewables, particularly solar energy, and at the same time provide energy generation close to its primary consumption location.

Substantial efforts have been made to estimate the solar PV potential of rooftop PV systems in which a large number of small-scale solar PV modules are installed on rooftops, yet the density of high-rise cities means that there is insufficient rooftop space to meet the high electricity demand. Furthermore, rooftop area is also needed for other usages such as Heating, Ventilation, and Air Conditioning (HVAC) systems. In this sense, innovative solutions have been put forth to solve the geographical issue. In this work, these solutions are referred to as non-conventional.

Highways and railways represent a significant area of most developed countries. Moreover, they hold the advantages of general good solar exposure as well as high accessibility. The installation of PV systems applied to these infrastructures seems therefore very promising.

Portugal holds a number of advantages for PV system installation, particularly on highway and railway. It has one of the best solar exposures in Europe and a rather high road and railway density for a country of its size. Portugal has been investing in its renewable energy policies, raising the share of electricity generated by variable renewables (wind power and solar PV). This share reached 27% in 2020 [2] and the goal for 2030 is 47% [3]. In that sense, it is important to reach a solar installed capacity of at least 1 GW by 2030 [3].

In Portugal, there is a special regime of renewable energy production – *Produção em Regime Especial Renovável (PRE)* – which is supported by a set of technologies for the production of electricity through renewable sources, such as wind, water, sun, biomass, etc. This regime is covered by a specific legal framework, its regulation being essentially the responsibility of the Government.

In terms of legislation, the *Decreto-Lei n.º 172/2006, de 23 de agosto*, amended and republished by *Decreto-Lei n.º 76/2019, de 3 de junho*, establishes the legal regime applicable to production, storage, transport, distribution activities and commercialization of electricity, as well as the logistical operation of shifting supplier, the organization of the respective markets and the procedures applicable to access to those activities, in the development of the principles contained in *Decreto-Lei n.º 29/2006, de 15 de fevereiro*, in the wording given by *Decree-Law no. 215-A/2012, of 8 October*. The *Portaria n.º 15/2020, de 23 de janeiro*, sets the amounts of fees due within the scope of administrative procedures relating to the activities of production and sale of electricity [4].

The main aim of this dissertation is to contribute on overcoming the geographical issue associated with PV system installation mentioned before. The primary objective of this work was to select the 10 sites with both higher solar potential and economic viability for the installation of non-conventional highway and railway PV applications in a designated area of the Maia County, north from the city of Porto, Portugal.

This project is organized into the following main chapters. The first chapter comprises an introduction, objective and description of the methodology followed along the work. Chapter 2 includes literature review on the fundamentals of solar energy technologies as well as the components, performance, and economics of PV systems. A list of non-conventional PV applications is also presented as well as an explanation of each technology. The intention is to provide the reader with an introductory technical background.

Chapter 3 explains the case study. A map of the area of study is presented and site selection is described in detail with images of each site. The following chapter 4 portrays the modelling in ArcGIS and PVSyst softwares. In the ArcGIS analysis, the input layers are enunciated and the software functions are explained. In PVSyst, various parameters were defined and these are also carefully elucidated in this chapter.

Chapter 5 includes the PVSyst simulation results and their discussion. Additionally, a comparison between the two softwares (ArcGIS and PVSyst) is made. Chapter 6 comprises a brief economic analysis where the initial investment and payback time are estimated. Lastly, chapter 7 concludes the project and references future works in the area.

The methodology followed in this work was based on a selection process where four main steps were undertaken to identify the 10 sites more suitable. Each of the four selection phases were based on different criteria, as shown in Figure 1.

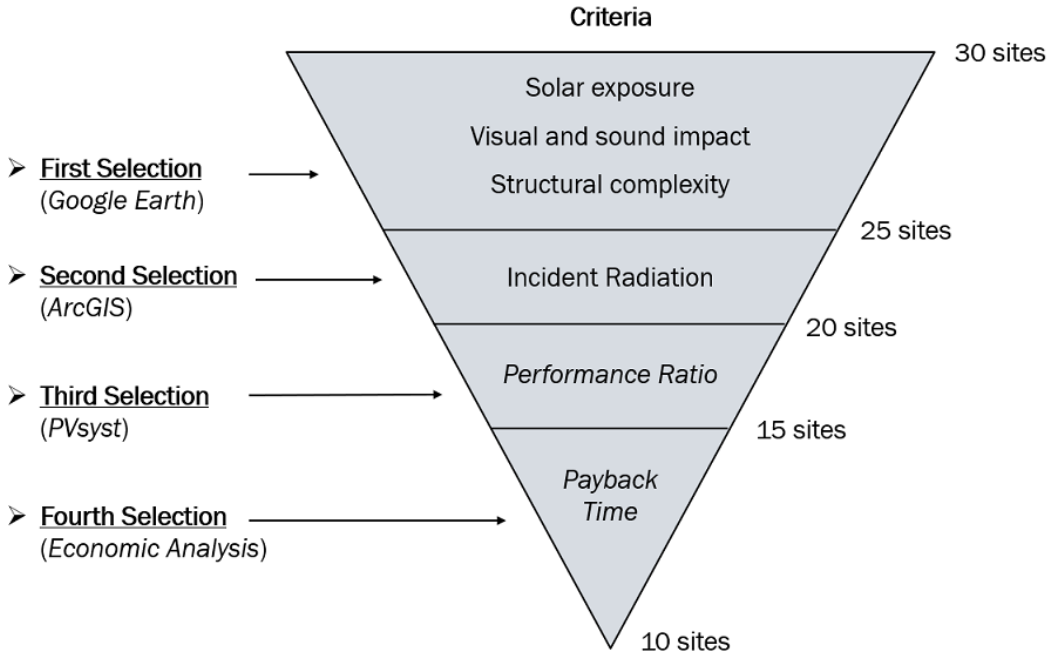


Fig. 1 – Work methodology

## 2. STATE OF THE ART

### 2.1 Fundamentals of Solar Energy Technologies

Solar energy is the most pure, simple, and abundant form of energy that powers our planet. The sun is an incredible resource that not only allows the existence of life on earth but also provides clean, sustainable energy to all of its inhabitants. More energy from the sun reaches our planet in *one hour* than is used by the entire population of the world in *one year* [5]. This makes it clear that the potential power that we can harness from the sun is still far from what our current technologies allow us to, and that there is still a long road for progress, research, and development.

This chapter explains the fundamentals of solar technologies and is mainly based on two books that are considered worldwide references in the subject of solar energy technologies: *Solar Engineering of Thermal Processes, 2013*, by John A. Duffie and William A. Beckman [6], and *Solar Energy Engineering: Processes and Systems, 2009*, by Soteris Kalogirou [7].

#### 2.1.1 THE SOLAR RESOURCE

In order to better understand and take full advantage of PV technologies, it is firstly necessary to comprehend the source of power of these systems – the Sun.

The sun is a sphere of intensely hot gaseous matter with a diameter of  $1.39 \times 10^9$  m and is, on the average,  $1.5 \times 10^{11}$  m from the earth. Because thermal radiation travels with the speed of light in a vacuum (300,000 km/s), solar energy reaches our planet in 8 min and 20 s after leaving the sun.

In essence, the sun is a continuous fusion reactor in which hydrogen is turned into helium (Figure 2). The sun's total energy output is  $3.8 \times 10^{20}$  MW. The earth receives only a tiny fraction of the total radiation emitted, equal to  $1.7 \times 10^{14}$  kW; however, even with this small fraction, it is estimated that 84 min of solar radiation falling on earth is equal to the world energy demand for one year (about 900 EJ) [7].

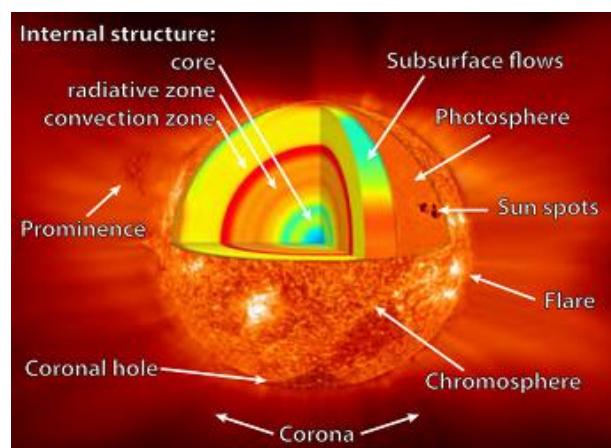


Fig. 2 - The Sun with its layer structure depicted [8].

The sun has an effective blackbody temperature of 5760 K \* but the temperature in the central region is much higher and the density is estimated to be about 100 times that of water. It is estimated that 90% of the energy is generated in the region of 0 to 0.23R (where R is the radius of the sun) [6]. At a distance of 0.7R from the centre, the temperature drops and so does density; here convection processes begin to gain importance. The zone from 0.7 to 1.0 R is known as the *convective zone*.

As observed from earth, the path of the sun across the sky varies throughout the year. The shape described by the sun's position, considered at the same time each day for a complete year, is called the *analemma* and resembles a figure '8' aligned along a north-south axis [7].

The earth rotates not circularly but elliptically around the sun and the eccentricity is such that the distance between the sun and the earth varies by 1.7% throughout the year. Because of this elliptical orbit, there are variations in the sun's path along the sky according to the time of the year. The most noticeable variation in the sun's apparent position along the year is a north-south swing over 47° of angle (because of the 23.5° incline of the earth axis with respect to the sun) called *declination*. This north-south swing in apparent angle is the main cause for the existence of seasons on earth, as shown in Figure 3.

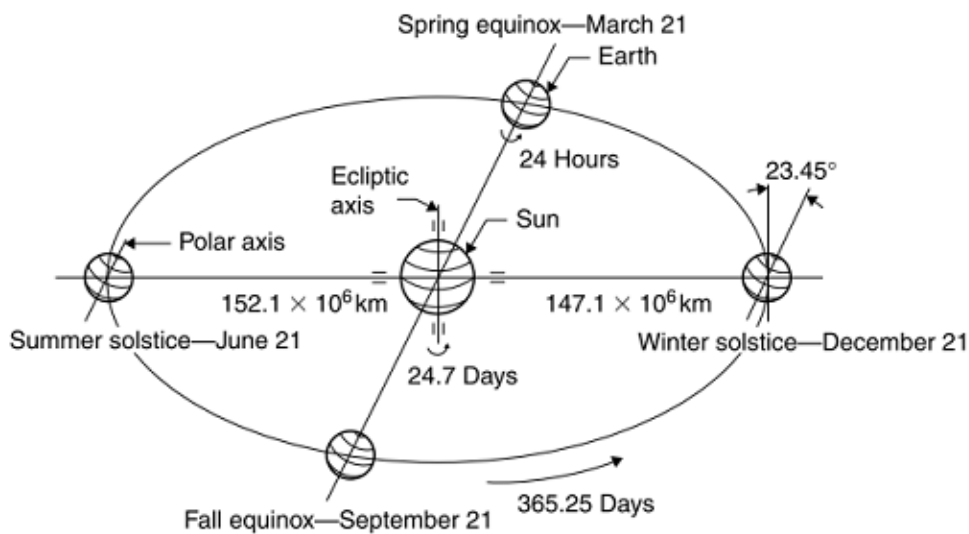


Fig. 3 - Elliptical orbit of the earth around the sun [9]

\*The effective blackbody temperature of 5760 K is the temperature of a blackbody\*\* radiating the same amount of energy as does the sun [2].

\*\* A blackbody, which does not exist in nature, absorbs all the radiation that is incident on it, regardless of wavelength and angle of incidence. Its reflectivity therefore is 0. Of course, since it also will emit light according to its equilibrium temperature, it does not need to appear black to the eye [4].

Knowledge of the sun's path through the sky is necessary to calculate the solar radiation falling on a surface, the solar heat gain, the proper orientation of solar collectors, the placement of collectors to avoid shading, and many more factors [7].

The *solar constant*,  $G_{sc}$ , is defined as the energy from the sun per unit time received on a unit area of surface perpendicular to the direction of propagation of the radiation at mean earth-sun distance outside the atmosphere. It is not in fact constant, as it varies somewhat according to the sun's relative position to the earth throughout the year. The solar constant is largest in January when the earth is nearest the sun, as shown in Figure 4.

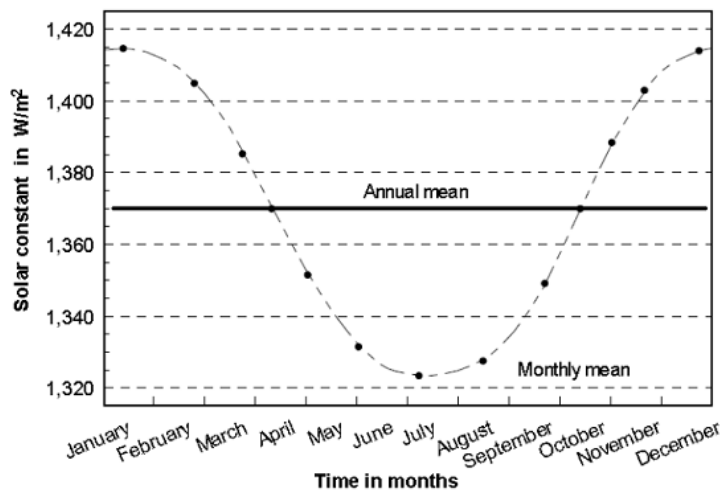


Fig. 4 - Solar constant in the course of one year [9]

## Solar Radiation

In terms of radiation, there are several definitions which prove to be useful in order to better understand the solar resource as well as its relationship with the earth and the various PV technologies.

**Beam Radiation** (often referred to as direct solar radiation): it is the solar radiation received from the sun without having been scattered by the atmosphere.

**Diffuse Radiation**: it is the solar radiation received from the sun after a change in direction as a result of scattering by the atmosphere. In some meteorological literature it is referred to as sky radiation or solar sky radiation.

**Total Solar Radiation** (often referred to as global radiation): it is the sum of the beam and the diffuse solar radiation on a surface.

**Irradiance** ( $W/m^2$ ): defined as the rate at which radiant energy is incident on a surface per unit area of surface. The symbol  $G$  is used for solar irradiance, with appropriate subscripts for beam, diffuse, or spectral radiation.

**Irradiation** or **Radiant Exposure** ( $J/m^2$ ): it is the incident energy per unit area on a surface, found by integration of irradiance over a specified time, usually an hour or a day. **Insolation** is a term applying specifically to solar energy irradiation.

Radiosity or Radiant Exitance ( $W/m^2$ ): it is the rate at which radiant energy leaves a surface per unit area by combined emission, reflection, and transmission.

Emissive Power or Radiant Self-Exitance ( $W/m^2$ ): it is the rate at which radiant energy leaves a surface per unit area by emission only.

Albedo: represents the proportion between the diffuse reflected solar radiation and the total incident solar radiation. It is measured on a scale from 0 to 1, in which 0 corresponds to a blackbody that absorbs all incident radiation and 1 to a body that reflects all incident radiation. Surface albedo is defined as the ratio between *radiosity* and *irradiance*.

The operation of solar technologies and systems depends, among other factors, on the solar radiation input and ambient air temperature. Solar radiation data is available on maps that also take into account local meteorological conditions. Figure 5 displays the annual mean global solar radiation for the years 1981–2000 in Europe. This is based on numerous climatological databases and computational models.

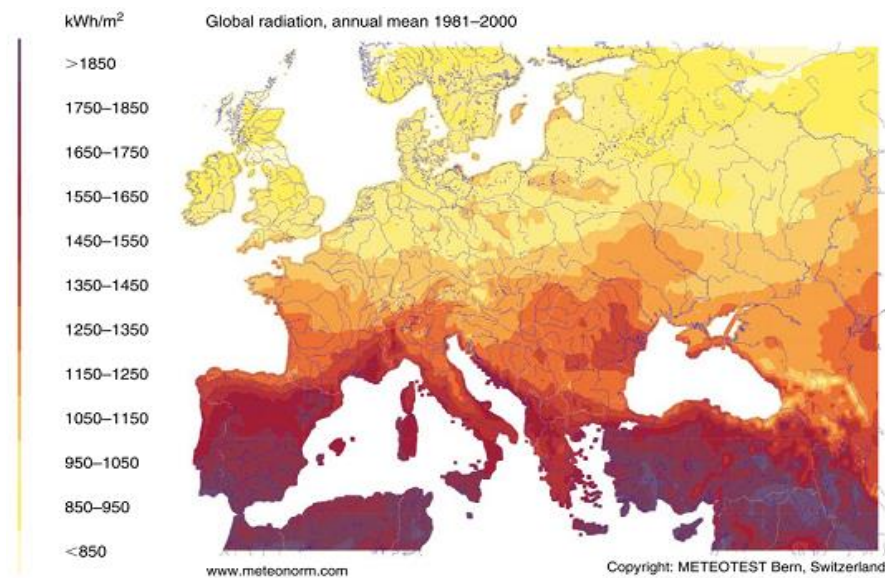


Fig. 5 - Annual total solar irradiation on horizontal surface for Europe [10]

### 2.1.2 RECKONING OF TIME

In solar energy calculations, Apparent Solar Time (AST) must be used to express the time of day. Apparent solar time is based on the apparent angular motion of the sun across the sky. The time when the sun crosses the meridian of the observer is the local solar noon, yet it usually does not coincide with the local 12:00 o'clock time. To convert the Local Standard Time (LST) to apparent solar time, two corrections are applied: the *equation of time* and *longitude correction*.



## Equation of Time (ET)

Due to factors associated with the earth's orbit around the sun, the earth's orbital velocity varies throughout the year, so the apparent solar time varies slightly from the mean time kept by a clock running at a uniform rate [7]. The variation is called the Equation of Time (ET).

This equation arises because the length of a day, that is, the time required by the earth to complete one revolution about its own axis with respect to the sun, is not uniform throughout the year. Over the year, the average length of a day is 24 h; however the length of a day varies due to the eccentricity of the earth's orbit and the tilt of the earth's axis from the normal plane of its orbit [7]. Due to the ellipticity of the orbit, the earth is closer to the sun on January 3<sup>rd</sup> and furthest from the sun on July 4<sup>th</sup>, hence the earth's orbiting speed is faster than its average speed for half the year (from about October until March) and slower than its average speed for the remaining half (from about April until September).

The values of the equation of time as a function of the day of the year ( $N$ ) can be obtained approximately using equations 1 and 2:

$$ET = 9.87 \sin(2B) - 7.53 \cos(B) - \sin(B) \text{ [min]} \quad (1)$$

where

$$B = (N - 81) \frac{360}{364} \quad (2)$$

The equation of time is graphically represented in Figure 6.

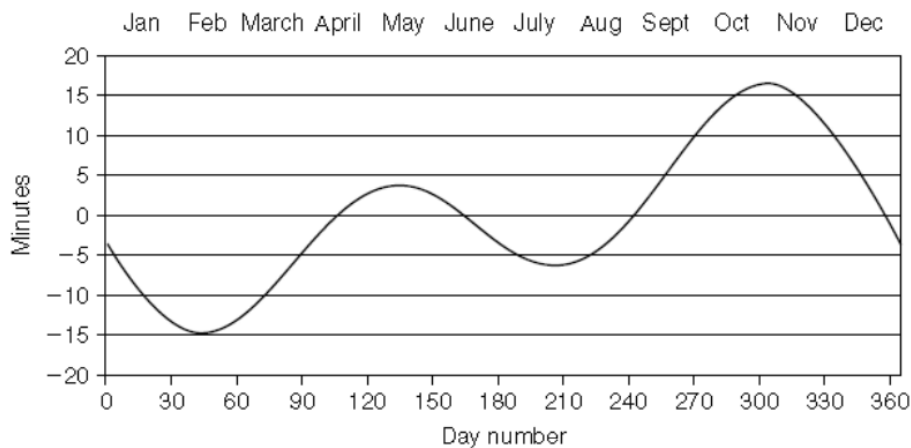


Fig. 6 - Graphical representation of equation of time [7]

## Longitude Correction

The standard clock time is established from a selected meridian near the centre of a time zone or from the standard meridian, the Greenwich, which is at longitude of 0°. The sun takes 4 min to transverse 1° of longitude, therefore a longitude correction term of  $4 \times (\text{Standard longitude} \times \text{Local longitude})$  should be either added or subtracted to the standard clock time of the locality. This correction is constant for a particular longitude, and the following rule must be followed with respect to sign convention: if the location is east of the standard meridian, the correction is added to the clock time; if the location is west, it is subtracted. The general equation for calculating the apparent solar time (AST) is then given by equation 3.

$$AST = LST + ET \pm 4(SL - LL) - DS \quad [\text{min}] \quad (3)$$

where

LST - Local Standard Time

ET - Equation of Time

SL - Standard Longitude

LL - Local Longitude

DS - Daylight Saving (it is either 0 or 60 min)

The term DS depends on whether daylight saving time is in operation (usually from end of March to end of October, where DS = 60 min) or not (where DS = 0). This term is usually ignored from this equation and considered only if the estimation is within the DS period.

### 2.1.3 SOLAR ANGLES

It is known that the sun's position in the sky changes from day to day and from hour to hour. The relative sun-earth motions are not simple, but they are systematic and thus predictable.

To analyse the path of the sun in the sky and explicitly define solar angles, it is convenient to consider the earth as static and to describe the sun's virtual motion in a coordinate system fixed to the earth with its origin at the site of interest, as shown in Figure 7.

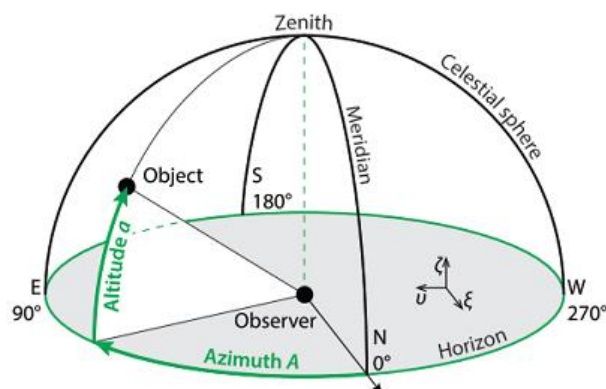


Fig. 7 - The sun's virtual motion coordinate system [8]

In this sense, the sun is constrained to move with 2 degrees of freedom on the celestial sphere; therefore, its position with respect to an observer on earth can be fully described by means of two astronomical angles, the solar altitude ( $\alpha$ ) and the solar azimuth ( $z$ ). An approximate method for calculating these angles is by means of sun-path diagrams. But before giving the equations of solar altitude and azimuth angles, solar declination and hour angle need be defined since these are required in all other solar angle formulations.

### Declination, $\delta$

The solar declination,  $\delta$ , is the angular distance of the sun's rays north (or south) of the equator. As shown in Figure 8, it is the angle between the sun-earth centre line and the projection of this line on the equatorial plane. Declinations north of the equator (summer in the Northern Hemisphere) are positive, and south are negative.

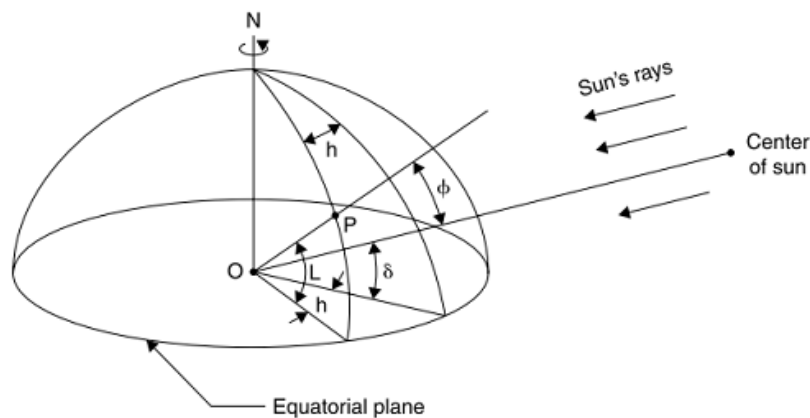


Fig. 8 - Definition of the solar angles [7]

Figures 9 shows the declination during the equinoxes and the solstices. As can be seen, the declination ranges from  $0^\circ$  at the spring equinox to  $+23.45^\circ$  at the summer solstice,  $0^\circ$  at the fall equinox, and  $-23.45^\circ$  at the winter solstice.

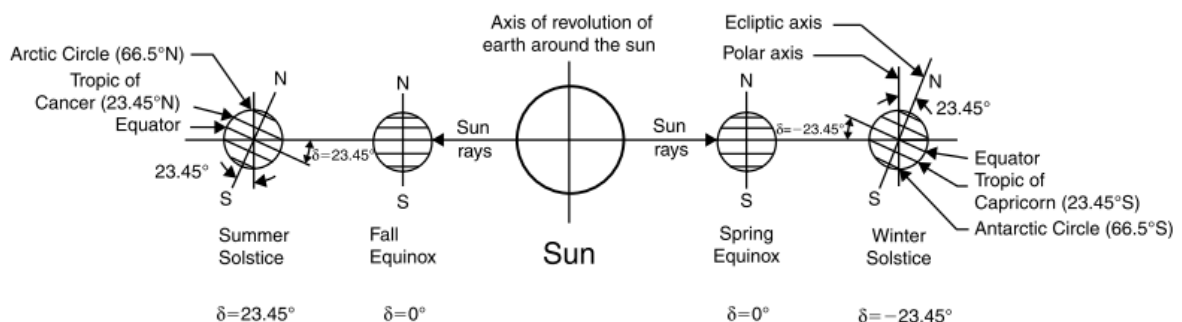


Fig. 9 - Celestial representation of the yearly variation of solar declination [7]

The variation of the solar declination throughout the year is shown in Figure 10. The declination,  $\delta$ , in degrees for any day of the year ( $N$ ) can be calculated approximately by equation 4.

$$\delta = 23.45 \sin \left[ \frac{360}{365} (284 + N) \right] \quad (4)$$

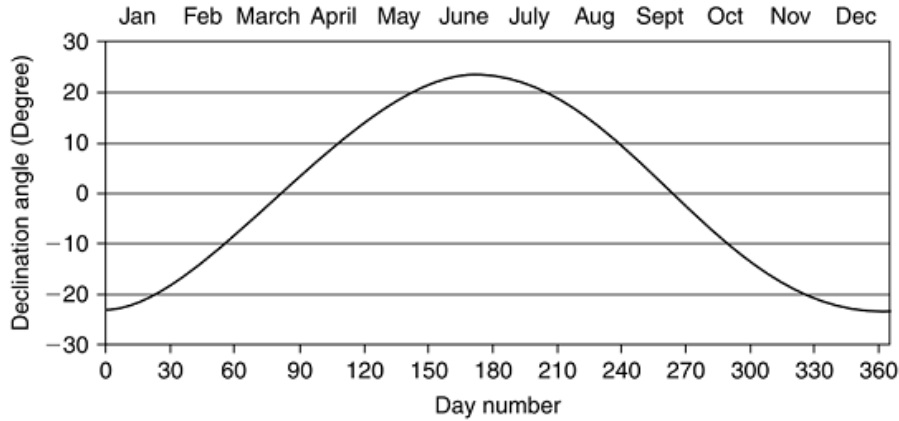


Fig. 10 - Graphical representation of the yearly variation of solar declination [7]

Declination can also be given in radians by the Spencer formula (equation 5):

$$\delta = 0.006918 - 0.399912 \cos(\Gamma) + 0.070257 \sin(\Gamma) - 0.006758 \cos(2\Gamma) + 0.000907 \sin(2\Gamma) - 0.002697 \cos(3\Gamma) + 0.00148 \sin(3\Gamma) \quad (5)$$

where  $\Gamma$  is called the *day angle*, given (in radians) by equation 6.

$$\Gamma = \frac{2\pi(N - 1)}{365} \quad (6)$$

The solar declination during any given day can be considered constant in engineering calculations [6].

### Hour angle, $ha$

The hour angle of a point on the earth's surface is defined as the angle through which the earth would turn to bring the meridian of the point directly under the sun [7]. In other words, it is the angular displacement of the sun east or west of the local meridian due to rotation of the earth on its axis (at  $15^\circ$  per hour). The hour angle,  $ha$ , is negative in the morning, zero at local solar noon, and positive in the afternoon.

Equation 7 expresses  $ha$  in degrees:

$$ha = \pm 0.25 (\text{Number of minutes from local solar noon}) \quad (7)$$

where the plus sign applies to afternoon hours and the minus sign to morning hours. The hour angle can also be obtained from the Apparent Solar Time (AST), as shown in equation 8.

$$ha = 15 \times (AST - 12) \quad (8)$$

### Solar altitude angle, $\alpha$

The solar altitude angle,  $\alpha$ , is the angle between the sun's rays and a horizontal plane (Figure 11). As shown in equation 9, it is related to the solar zenith angle,  $\phi$ , which is the angle between the sun's rays and the vertical [7].

$$\phi + \alpha = \frac{\pi}{2} \text{ rad} = 90^\circ \quad (9)$$

The mathematical expression for the solar altitude angle is given by equation 10.

$$\sin(\alpha) = \cos(\phi) = \sin(L) \sin(\delta) + \cos(L) \cos(\delta) \cos(ha) \quad (10)$$

Where  $L$  is the local latitude, defined as the angle between a line from the centre of the earth to the site of interest and the equatorial plane [7]; values north of the equator are positive and those south are negative.

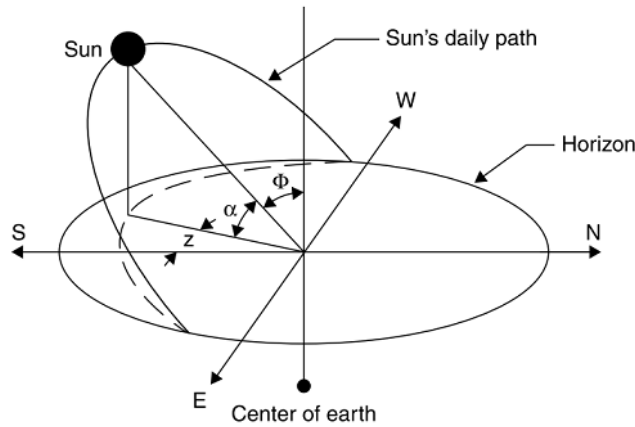


Fig. 11 - Apparent daily path of the sun across the sky from sunrise to sunset [7]

### Solar azimuth angle, $z$

The solar azimuth angle,  $z$ , is the angle of the sun's rays measured in the horizontal plane from due south (true south) for the Northern Hemisphere or due north for the Southern Hemisphere; westward is designated as positive [7]. The mathematical expression for the solar azimuth angle is given by equation 11.

$$\sin(z) = \frac{\cos(\delta) \sin(ha)}{\cos(\alpha)} \quad (11)$$

### Incidence angle, $\theta$

The solar incidence angle, shown in Figure 12, is the angle between the sun's rays and the normal on a surface. For a horizontal plane, the incidence angle,  $\theta$ , and the zenith angle,  $\phi$ , are the same. The expression for the solar incidence angle is given by equation 12.

$$\begin{aligned} \cos(\theta) = & \sin(L) \sin(\delta) \cos(\beta) - \cos(L) \sin(\delta) \sin(\beta) \cos(z_s) + \cos(L) \cos(\delta) \cos(ha) \cos(\beta) \\ & + \sin(L) \cos(\delta) \cos(ha) \sin(\beta) \cos(z_s) + \cos(\delta) \sin(ha) \sin(\beta) \sin(z_s) \end{aligned} \quad (12)$$

where

- $\beta$  is the surface tilt angle from the horizontal
- $z_s$  is the surface azimuth angle, the angle between the normal to the surface from true south (westward is designated as positive)

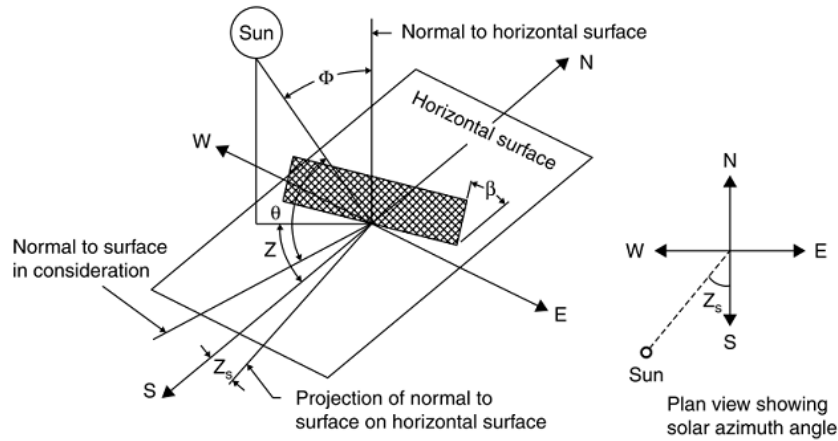


Fig. 12 - Solar angles diagram [7]

### 2.1.4 SUN PATH DIAGRAMS

For practical purposes, instead of using the preceding equations, it is convenient to have the sun's path plotted on a horizontal plane, called a sun path diagram, and to use the diagram to find the position of the sun in the sky at any time of the year [7]. The solar altitude angle,  $\alpha$ , and the solar azimuth angle,  $z$ , are functions of latitude,  $L$ , hour angle,  $ha$ , and declination,  $\delta$ . In a two-dimensional plot, only two independent parameters can be used to correlate the other parameters; therefore, it is usual to plot different sun path diagrams for different latitudes. Such diagrams show the complete variations of hour angle and declination for a full year. An example of a sun path diagram for 35°N is shown in Figure 13.

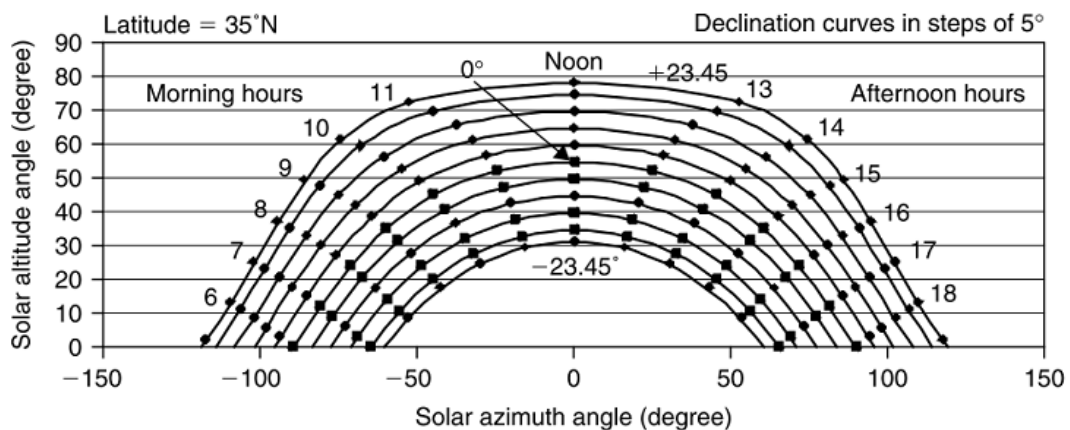


Fig. 13 - Sun path diagram for 35°N latitude [7]

### 2.1.5 SHADOW DETERMINATION

In the design of many solar energy systems, it is often required to estimate the possibility of the shading of solar modules by surrounding structures or shading caused by the modules themselves. Solar panels are usually installed in multi-rows facing south, hence there is a need to estimate the possibility of shading by the front rows of the second and subsequent rows.

Shadow determination is facilitated by establishing a surface oriented solar angle, called the *solar profile angle*. As shown in Figure 14, the solar profile angle,  $p$ , is the angle between the normal to a surface and the projection of the sun's rays.

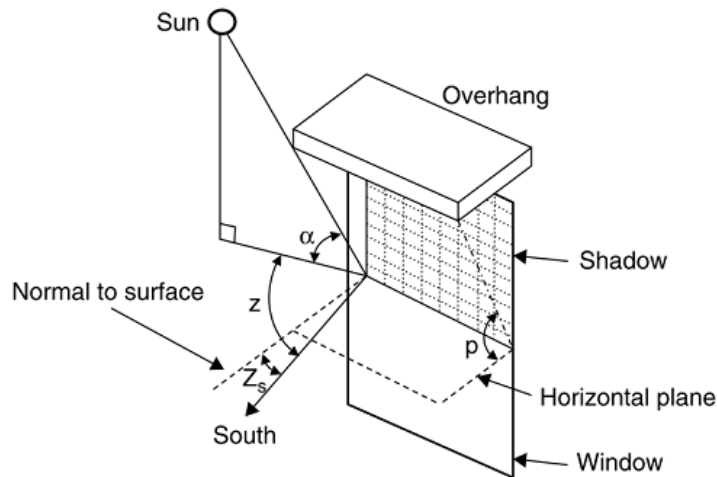


Fig. 24 - Geometry of the solar profile angle,  $p$ , in a window overhang arrangement [7]

In terms of the solar altitude angle,  $\alpha$ , solar azimuth angle,  $z$ , and the surface azimuth angle,  $z_s$ , the solar profile angle,  $p$ , is given by equation 13.

$$\tan(p) = \frac{\tan(\alpha)}{\cos(z - z_s)} \quad (13)$$

For a better understanding, in a horizontal plane, Figure 15 shows the parameters that need be calculated to estimate shading and determine optimum distance,  $d$ , between rows of PV modules.

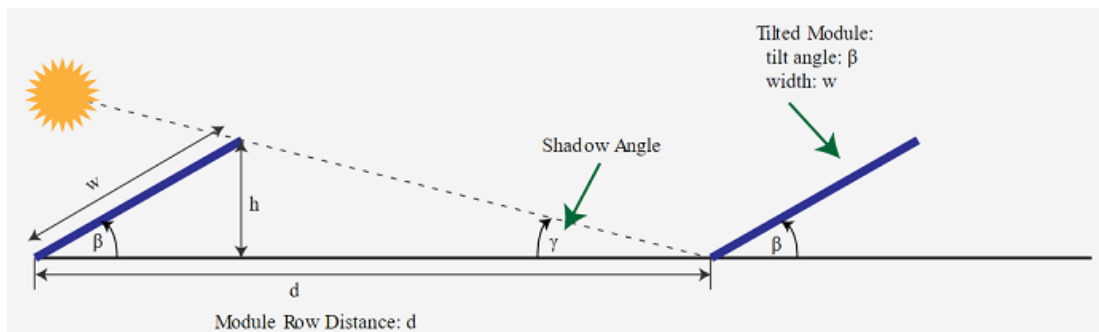


Fig. 15 - Parameters to calculate the minimum distance between module rows to avoid shading [11]

Equations 14 and 15 are derived by geometry.

$$d = \frac{h}{\tan(\alpha)} + w \cdot \cos(\beta) \quad (14)$$

where

$$h = w \cdot \sin(\beta) \quad (15)$$

The solar altitude angle,  $\alpha$ , is obtained by solar angle equations which were previously discussed. Knowing the module's width,  $w$ , height,  $h$ , and orientation,  $\beta$ , row distance is determined to avoid shading.

## 2.2 PV Systems

Photovoltaic (PV) modules are solid-state devices that convert sunlight (the most abundant energy source on the planet) directly into electricity without the need of a heat engine or rotating equipment. PV technology is designed to generate electricity without producing emissions of greenhouse or any other gases; in addition, its operation is virtually silent. Photovoltaic systems can be built effectively in any size, ranging from milliwatt to megawatt, and they are modular, which means that panels can be easily added to increase output.

The modular nature of PV technology and its lack of mechanical machinery allows its installation to be located where the electric loads are effectively being consumed, such as: residences, commercial buildings, farms, and so on. This characteristic distinguishes PV from many other types of electrical generation, including wind. Furthermore, PV systems are highly reliable and require little maintenance.








PV systems can be classified as either flat plate or concentrator systems. In the latter, optical components, namely lenses or mirrors, are used to increase the intensity of the solar radiation falling on the PV modules. Only flat plate systems will be considered in this thesis.

60 years ago, in the early days of photovoltaics, the energy required to produce a PV panel was more than the energy the panel could produce during its lifetime. Since the beginning of the XXI century, due to improvements in the efficiency of the panels and manufacturing methods, the payback times have been greatly reduced.

Solar PV deployment has grown at an astonishing pace. Of all renewable sources, it has registered the greatest increase in power capacity between 2019 and 2020, adding as much as 136 GW, as can be observed in Table 1.



Table 1 – Renewable energy investment and installed capacity [2]

		2019	2020
<b>INVESTMENT</b>			
New investment (annual) in renewable power and fuels <sup>1</sup>	billion USD	298.4	<b>303.5</b>
<b>POWER</b>			
Renewable power capacity (including hydropower)	GW	2,581	<b>2,838</b>
Renewable power capacity (not including hydropower)	GW	1,430	<b>1,668</b>
 Hydropower capacity <sup>2</sup>	GW	1,150	<b>1,170</b>
 Solar PV capacity <sup>3</sup>	GW	621	<b>760</b>
 Wind power capacity	GW	650	<b>743</b>
 Bio-power capacity	GW	137	<b>145</b>
 Geothermal power capacity	GW	14.0	<b>14.1</b>
 Concentrating solar thermal power (CSP) capacity	GW	6.1	<b>6.2</b>
 Ocean power capacity	GW	0.5	<b>0.5</b>

1 USD (\$) = 0.88 EUR (€) (verified in 18/02/2022)

The top five national markets – China, the United States, Vietnam, Japan and Germany – were responsible for almost 66% of newly installed capacity in 2020 [2].

### 2.2.1 PV CELLS

The working principle of solar cells is based on the photovoltaic effect, i.e., the generation of a potential difference at the junction of two different materials in response to electromagnetic radiation [8].

A basic solar cell contains two layers of a semiconductor material. One layer is of n-type (negative) and the other is p-type (positive). An electrical field is created near the top surface of the cell where the two layers are in contact, called a p-n junction. When solar radiation is absorbed by the solar cell, photons hit the semiconductor material and cause a movement of electrons to the n-type side and holes to the p-type side of the junction, which generates a voltage difference between the front and the back of the cell and a dissipation of power in the load.

PV cells consist of:

- ***Active photovoltaic material:*** two or more thin layers of a semiconducting material. PV cells range in colour from black to blue, depending on the type of material, as shown in Figure 16.
- ***Metal grids:*** they conduct the electrical charges as direct current and enhance the current collection from the front and back of the solar cell.
- ***Antireflection coating:*** applied to the top of the cell to maximize the light going into the cell. In some types of photovoltaic cells, the top of the cell is covered by a semi-transparent conductor that functions as both the current collector and the antireflection coating.
- ***Supporting material.***

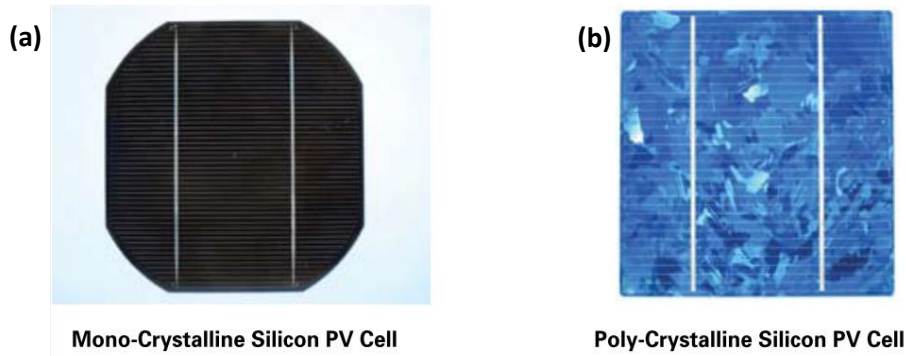


Fig. 36 - Mono (a) and Poly-Crystalline (b) Silicon PV Cells [12]

Nowadays, there are many types of PV cells with different photovoltaic materials. Silicon is the most traditionally used semiconductor due to its stability in high-temperature processing, nontoxicity, and high abundance. It covers about 25% of the earth's crust and for this reason, it is also cheap. In fact, labour now accounts for almost all the cost of a silicon solar cell. Fabrication techniques and automation of the manufacturing process have been improving to continuously lower the price of these cells.

Many types of PV cells are available today, such as: mono-crystalline silicon cells (made from pure monocrystalline silicon, high efficiency – around 15%); multi-crystalline silicon cells (simple to manufacture and therefore cheaper than mono-crystalline ones, slightly less efficient - around 12%); amorphous silicon (composed of silicon atoms in a thin homogenous layer, low efficiency – around 6%), etc.

A typical silicon PV cell produces 0.5 V and up to 3 A under Standard Test Conditions (STC) of solar irradiance  $1000 \text{ W/m}^2$  and temperature  $25^\circ\text{C}$ . The electrical output from a single cell is small, so multiple cells are connected and encapsulated (usually glass covered) to form a module [7]. One or more PV modules assembled together form a PV panel and various panels together complete a PV array, as it can be observed in Figure 17.

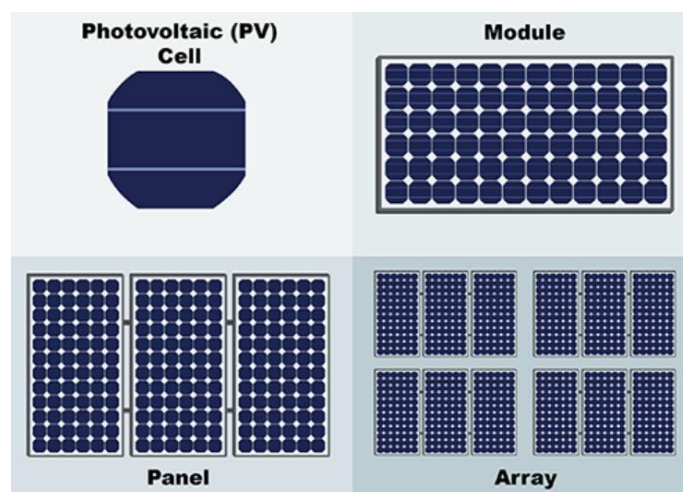
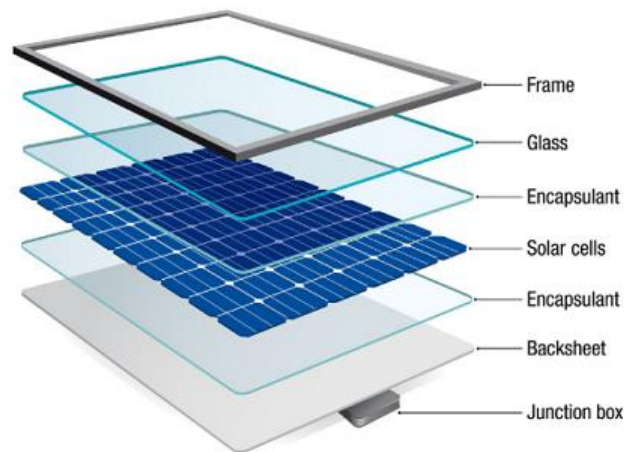


Fig. 17 - Photovoltaic cell, module, panel and array [13]

### 2.2.2 PV MODULES

Standard PV modules are composed by 60 solar cells. The cells are encapsulated by a thin sheet of Ethyl Vinyl Acetate (EVA) and sandwiched between a glass and the back sheet. An aluminium frame is fixed on all four sides and a junction box with cables and connectors is fixed on the rear side of the module. Figure 18 shows a typical assembly view of a PV module.



*Fig. 18 - Assembly view of a solar PV module [14]*

Solar modules are built to work for 25 to 30 years and to withstand harsh weather conditions such as high and low temperatures, storms, rain, dusty environments, etc.

### 2.2.3 PV SYSTEM COMPONENTS

The heart of a photovoltaic system is the PV array itself. However, the installation of PV modules comes associated with a number of different Balance Of System (BOS) components, which may include:

- **Batteries:** required in many PV systems to supply power at night or when the PV system cannot meet the demand. The selection of battery type and size depends mainly on the load and availability requirements. When batteries are used, they must be located in an area without extreme temperatures, and the space where the batteries are located must be adequately ventilated [7];
- **Inverters:** used to convert the Direct Current (DC) into Alternate Current (AC). The output of the inverter can be single or three phase. The designer should specify both the type and size of the load the inverter is intended to service [7];

- **Controllers:** regulate the power from PV modules to prevent the batteries from over-charging. The controller can be a shunt type or series type and also function as a low-battery voltage disconnect to prevent the battery from over-discharge [7];
- **Peak-power trackers:** these components use the Maximum Power Point Tracker (MPPT) method, which lets the controller operate at the optimum operating point. It's a high-efficiency DC-to-DC converter that compensates for the changing voltage against current characteristic of a solar cell by converting the power to a voltage or current level that is more suitable to whatever load the system is designed to drive. MPPT charge controllers are desirable for off-grid power systems.

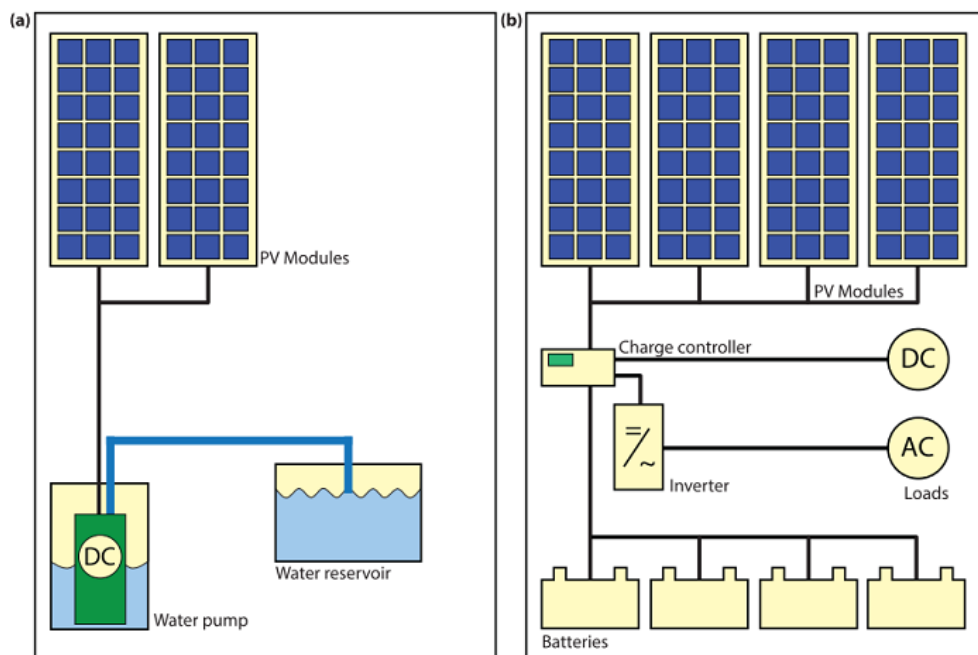


Fig. 19 - Schematic representation of (a) a simple DC PV system to power a water pump with no energy storage and (b) a complex PV system including batteries, power conditioners, and both DC and AC loads [8]

According to network connection, PV systems can be classified as:

- **Stand-alone PV systems (Off-grid):** used in areas that are not easily accessible or have no access to main electricity grids. A stand-alone system is independent of the electricity grid, with the energy produced normally being stored in batteries. A typical stand-alone system would consist of the PV module or modules, batteries, and a charge controller. An inverter may also be included in the system to convert DC current generated by the PV modules to the AC current form [7]. Figure 19 shows schematically examples of stand-alone systems.

- **Grid-connected systems (On-grid):** these systems are connected to the grid via inverters and do not require batteries, since they are connected to the electricity network (Figure 20). The electricity generated can either be used immediately (which is normal for systems installed in offices and other commercial buildings) or sold to an electricity supply company (which is more common for domestic systems, where the occupier may be out during the day) [7]. In the evening, when the solar system is unable to provide the electricity required, power can be bought back from the network [7]. Large PV fields act as power stations from that all the generated PV electricity is directly transported to the electricity grid [8].

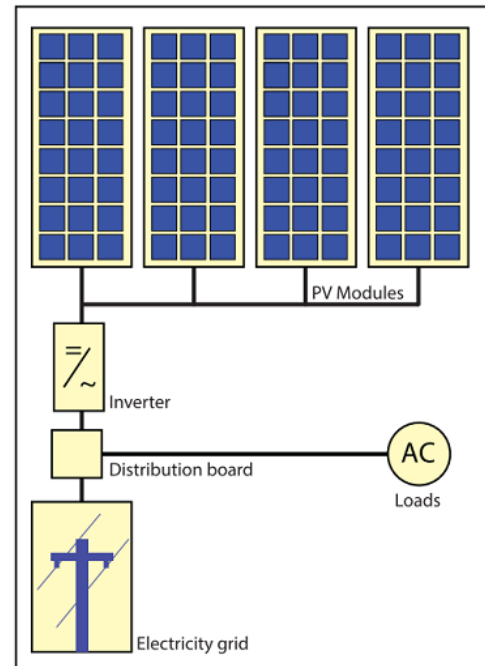


Fig. 20 - Schematic representation of a grid-connected PV system [8]

There is also a third type of PV system called a *hybrid system*, which consists of a combination of PV modules and a complementary electricity generation system, such as a diesel, gas or wind generator. This thesis focuses on grid-connected systems.

## 2.2.4 PV SYSTEM PERFORMANCE

This section explains the fundamentals of PV system performance and is based on the book *The Performance of Photovoltaic (PV) Systems, 2017*, by Pearsall, N. M. [15].

The performance of a system sets its technical and practical feasibility. It is directly related to its energy output and depends on both the operating conditions and the configuration of the system. The operation conditions depend on variables like location, which dictates the solar irradiation received, ambient temperature, humidity, and other climate-related aspects.

In terms of the configuration of the system, its network connection plays a big role on performance. Grid-connected PV systems are generally designed to produce their maximum energy output at all times in order to meet network and/or local electrical loads. In turn, stand-alone systems run independently from the grid and are designed to supply the required amount of electricity for the specified load, which does not necessarily mean they provide always the maximum energy output. Obviously, equipment characteristics also affects system performance depending on the cell type, the module type, and the BOS components.

PV system performance can be expressed by five main parameters:

- *Conversion efficiency;*
- *Energy yield;*
- *Solar installed capacity;*
- *Specific production;*
- *Performance ratio (PR).*

These parameters are related but express different aspects of the overall performance. *Loss factors* must also be considered.

### **Conversion Efficiency**

The *conversion efficiency* is the ratio between the electrical power output,  $P_{max}$ , and the solar irradiance received,  $I_i$ , under specified operating conditions (equation 16).

$$\eta = \frac{P_{max}}{I_i} \quad (16)$$

### **Energy Yield**

The *energy yield* is the output of a system, in other words, the *produced energy*. Three types of energy yields can be defined: the *final yield*, the *second yield*, and the *third yield*.

The *final yield* or simply *energy yield*,  $Y_f$ , expresses the energy delivered to the load per unit capacity of the system. In the case of a grid-connected system providing power directly to the grid rather than to local loads, the final yield would be calculated using the energy to the grid.

The *second yield*,  $Y_A$ , also known as array yield, is defined in a similar way as the final yield but using the energy output from the PV array (before conversion to AC in the inverter). This gives a measure of the performance of the array itself. Naturally, it is only possible to determine the array yield if there is a measurement of the array output at the relevant point in the system.

The *third yield* or *reference yield*,  $Y_r$ , represents the output of the system if there were no losses, i.e., in the ideal case.

### **Solar Installed Capacity**

*Solar installed capacity* is the amount of energy a module can produce at its peak performance, such as in the afternoon of a clear, sunny day. This parameter is rated by the manufacturer and calculated by a standardized test (1000 W/m<sup>2</sup> of solar radiation at an ambient temperature of 25°C and a clear sky). It is given in kWp which is the commonly used unit to indicate the peak power capability of a solar module.

## Specific Production

The *specific production* expresses the relation between the produced energy (*energy yield*) and the solar installed capacity, i.e., it represents the amount of energy (kWh) produced for each kWp.

## Performance ratio (PR)

As discussed, the performance of a system and its efficiency depends on module choice. In turn, the final yield relies mainly on the solar irradiation received. The lack of some benchmark of efficiency or yield for each system makes it difficult to determine performance quality. In this sense, the *Performance Ratio (PR)* takes into account both system design and solar irradiation by comparing the final yield of the system with its reference yield. It is the ratio between the effectively produced energy and the energy which would be produced if the system was continuously working at its nominal Standard Test Conditions (STC) efficiency. It is a useful tool to compare performance quality between different systems. PR is expressed by equation 17.

$$PR = \frac{Y_f}{Y_r} \quad (17)$$

The PR is a widely used parameter that compares the actual yield attained by a system to the yield in the ideal case. This translates into a measure of the overall losses, and hence the quality, of the system.

In practice, the determination of PR requires only the measurement of energy output from the system and the solar irradiation received by the PV array over the defined period, together with knowledge of the nominal rating of the system.

## Loss factors

The typical loss factors for grid-connected PV systems include:

- Module operating temperature;
- Angle of solar radiation incidence (depending on module orientation and solar position);
- Low light levels (below 100 W/m<sup>2</sup>);
- Module mismatch (typical when modules with different operating characteristics are electrically connected);
- Shading (results both in a loss of output and increased mismatch between shaded and unshaded modules);
- Dirt or ice/snow accumulation;
- MPP tracking losses;
- Inverter efficiency;
- Cabling losses.

## 2.2.5 THE ECONOMICS OF PV SYSTEMS

The economics of PV systems is fundamentally different from that of traditional energy generation, namely, fossil fuel. In the latter, it is easy to measure the actual cost to generate electricity based on the price of fuel, the efficiency of the generating unit, the operating costs, and the depreciation of the facility.

On the contrary, for PV systems, the cost of electricity depends on a forecast of the future, since in essence the electricity is being paid for upfront in the higher capital cost of the system. Because there is no fuel involved, and the operating costs are relatively low, the purchase price must be amortized across the asset's useful life in order to derive an average cost of electricity.

The widespread global deployment of PV systems is contingent on reducing the cost of generated electricity to levels that make systems economically competitive without incentives, this is a milestone also referred to as solar "grid-parity" [16].

### Payback Time

Payback time can be defined as the amount of time required to recover the cost of an investment [16]. It can be calculated by equations 18 and 19.

$$\text{payback time [years]} = \frac{\text{initial investment [€]}}{\text{annual return [€/year]}} \quad (18)$$

where

$$\text{annual return [€/year]} = \text{produced energy [kWh/year]} \times \text{energy price [€/kWh]} \quad (19)$$

The initial investment comprises the initial costs of the PV system, while the annual return expresses the relation between energy production (*produced energy*) and its price per kWh (*energy price*).

Payback time is therefore strongly influenced by:

- Annual solar radiation: in general, we can say that the sunnier the location, the greater the PV yield and the shorter the payback time;
- Grid electricity costs: the higher these costs, the shorter the payback time;
- Initial costs of the PV system.



## Levelized Cost of Electricity (LCOE)

The Levelized Cost Of Electricity (LCOE) is the most commonly referenced parameter of PV system economics. Essentially, it gives a levelized (average) cost per kWh of electricity produced over the life of the asset. The LCOE can be used to compare alternative technologies with different scales of operation, investment, or operating time periods. It is calculated using the equation 20.

$$LCOE \text{ [€/kWh]} = \frac{\text{Total Life Cycle Cost [€]}}{\text{Total Lifetime Energy Production [kWh]}} \quad (20)$$

The LCOE is influenced by five key high-level drivers listed in Figure 18:

- Cost of Capital;
- System Life / Residual Value;
- Plant Energy Production;
- Annual Operating Costs;
- PV System Cost.

Under these five categories dozens of variables influence LCOE (Figure 21), and each can have a material influence on system economics.

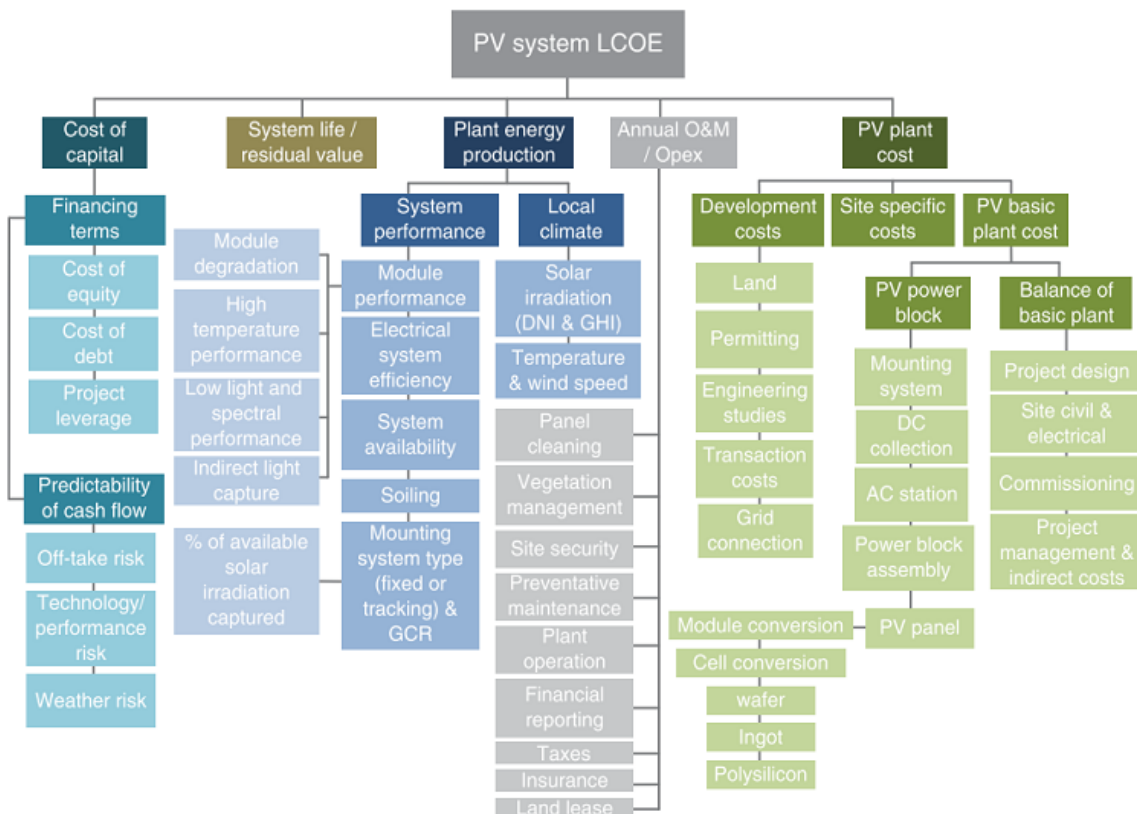


Fig. 21 - PV LCOE drivers [16]

## PV System Cost

The first major LCOE driver is PV system initial cost. The primary focus of PV technology development and innovation during the past three decades has been to reduce this factor. The steady decline of module and balance of system (BOS) costs is a result of this effort.

PV system costs also depend on further considerations such as site-specific costs. These may include foundations, roof repair work, road building, fencing, etc. Development costs which include site acquisition, engineering studies, permits, project financing, and interconnection costs are also site-specific.

Table 2 gives a simplified view of what a large (10 MW+) system cost in 2008, its cost in 2015, and a simplified projection for 2025.

*Table 2 - Simplified PV system costs, 2008, 2015 and 2025 [16]*

Generic PV System Costs (\$/Wp) @ 10MW + Project Size				
	2008*	2015**	2025 Estimate***	
PV module price	\$ 4.02	\$ 0.55	\$	0.41
Balance of system (power block & construction)	\$ 1.77	\$ 0.68	\$	0.50
Interconnection costs	\$ 0.07	\$ 0.06	\$	0.05
Development costs	\$ 0.06	\$ 0.04	\$	0.03
<b>Total system price</b>	<b>\$ 5.92</b>	<b>\$ 1.33</b>	<b>\$</b>	<b>0.99</b>
<i>% of 2008 baseline</i>	<i>100%</i>	<i>22%</i>		<i>17%</i>

\*Deutsche Bank, January 2011 Report; also consistent with SunPower projects at that time

\*\*Cost for a generic fixed tilt system built in 2015 with commodity modules in a moderate or low labor cost country – estimate by the author based on project experience

\*\*\*Estimate based on an extrapolation of 2015 system costs and applying a simple 3% annual improvement rate through experience curve effects

1 USD (\$) = 0.88 EUR (€) (verified in 18/02/2022)

As can be observed, PV system costs have fallen considerably, largely due to PV module price reduction but also seen across almost all the other system components.

## System Energy Production

The second key driver of the LCOE in PV system economics is the system's annual energy production. Energy production (kWh) is frequently correlated with specific production (kWh/kWp). The kWh/kWp is a function of:

- the amount of sunshine the project site receives in a year and the local weather (wind, temperature, humidity);
- how the system is mounted and oriented (e.g., flat, fixed tilt, tracking, etc.);
- the spacing between PV panels as expressed in terms of system Ground Coverage Ratio (GCR), more spacing reduces shading losses and improves yield but requires more space;

- the energy harvest of the PV panel (e.g., performance sensitivity to high temperatures, efficiency as affected by low or diffuse light, etc.);
- system losses from soiling, transformers, inverters, and wiring inefficiencies;
- system availability, largely driven by inverter reliability improvements.

Improved system performance plays a significant role on curtailing the LCOE: more energy directly reduces the LCOE. PV system performance has improved over the past ten years due to a number of factors, including: high levels of system availability, improvements in inverter efficiency, improvements in cleaning, development of modules with improved temperature coefficient, and widespread adoption of trackers for large power plants in high-sunshine markets.

In spite of the improvements on system performance, PV systems still experience an unavoidable phenomenon: degradation. This translates into a reduction of the energy yield. The durability of the components exposed to environmental variables such as high temperature, moisture, wind, and UV will influence the rate of average annual performance. Project investors consider annual degradation rates from 0.25% to 2.00% per year [17] depending on the system, location, and technology type. Annual degradation can have a major impact on system LCOE, since it represents an annual decrease in energy production.

### **Cost of Capital**

The cost of capital is the third major driver of the LCOE and is defined as the level of interest rate required to finance a system. It is as important as system cost and its performance.

The average cost of financing a system is directly linked to the real and/or perceived risk of the asset. The potential risks to investors in a PV power plant can be classified as:

- Off-take risk: represents the risk of the electricity from a plant being sold for a lower price and/or volume than expected by project investors;
- Performance risk: stands for the risk that the system will not generate the expected energy and/or achieve the operating costs in line with original project estimates, therefore reducing expected cash flows;
- Property risks: these are the risks associated with property damage or theft, exchange rate, and inflation.

As investor understanding of PV power plants has grown, the industry has seen a decrease in the financing costs of PV systems.

### **System Life**

The fourth key driver of PV system economics is a system's operational life. Although PV power plants are commonly designed to operate for around 20 years, studies have shown that there is no fundamental barrier for a PV system to operate during more than 30 years.

Comparing the longevity advantage of other technologies, such as fossil fuel, hydro, or nuclear over PV, the reality is that conventional power plants must contend with a much harsher operational environment than PV. Steam generation units, industrial pollution, corrosion, and complicated

mechanical systems that require constant maintenance are some examples of why conventional power plants face larger operational hurdles than PV, yet continue to operate for more than 50 years [16]. In contrast, PV systems have few moving parts and a much benevolent operating environment.

This leads to the conclusion that PV technology has the potential for a long economic life which influences on a positive way a system's LCOE.

### **Annual Operating Costs**

The annual operating cost of a system is the fifth major contributor of PV system economics. It includes:

- Operations and Maintenance (O&M) of the plant;
- Administrative costs, such as: tax reporting, property insurance, land lease (when applicable), site security and property or revenue taxes that may apply.

Generally, annual operating costs of PV systems contribute less than 5% to a project's LCOE. However, given the substantial declines in PV system prices and cost of capital, they are becoming gradually more important to manage and reduce.

## **2.3 Non-Conventional PV System Applications**

There is no clear definition for what may be considered as conventional or non-conventional applications solar PV technologies. In this thesis, the term conventional has been reserved for matured and currently widely deployed applications, such as: *PV fields*, where solar modules are simply disposed on-land in an equator-oriented direction; and *Building-Attached Photovoltaic Systems (BAPVs)*, which consist in the installation of PV modules on existing buildings.

This chapter focuses on the considered non-conventional PV applications, that is, the more recent and less widespread technologies. These include:

- Building-Integrated PV Systems (BIPVs);
- **PV systems alongside highways and railways;**
- PV carports;
- PV bus-stop shelters;
- PV pavement;
- Solar bridges;
- Floating PV systems;
- Submerged PV systems;
- Agriphotovoltaic systems (APVs).

Of all these technologies, the installation of PV systems along highways and railways is the central area of study in this dissertation.

## BUILDING-INTEGRATED PHOTOVOLTAIC SYSTEMS (BIPVS)

Building-Integrated Photovoltaic Systems (BIPVs) today are viewed as state-of-the-art systems that offer innovative solutions for PV integration into buildings. They differ from Building-Attached Photovoltaic Systems (BAPVs), which require additional components and materials to be mounted onto existing surfaces. In addition, BIPV systems are aesthetically pleasing and generally prone to follow the architectural flows of the building.

BIPVs are the result of integrating or combining building construction materials with photovoltaic solar cells in order to make urban edification structures (buildings) power generators, therefore sustainable [18, 19]. The building construction materials typically used in BIPV systems can be integrated in either the façade, walls, windows, curtains, or in roofs as tiles, shingles, and skylights. The main objective of BIPVs is to achieve multifunctionality by integrating solar materials into existing building materials while serving as a protective, sustainable, and aesthetically pleasing construction, as shown in Figure 22.



*Fig. 22 - Glass ceiling with transparent BIPV modules [19]*

By deploying solar energy harvesting technologies on all suitable rooftops, the EU could meet about 25% of its electricity consumption with clean energy. However, today only 10% of the EU's rooftop potential is used and BIPV represents about 3% of all the solar installed capacity in the EU. The first BIPV system installed in Portugal was in Proença-a-nova, Castelo Branco, in 2009. Despite currently being a young innovation, BIPV systems have the potential to grow considerably in a near future.

## PV SYSTEMS ALONGSIDE HIGHWAYS AND RAILWAYS

Highways and railways represent a large area of most developed countries. These infrastructures hold the advantages of general good solar exposure as well as high accessibility on the side slopes. This implies that no additional construction is required to build access roads to PV systems.

There are various ways to implement PV systems alongside highways and railways, which can work as on-grid technologies and/or off-grid to feed public lighting along highways/railways.

One way is to incorporate PV panels on the side slopes (Figure 23), according to solar orientation and slope inclination. This is a relatively simple technology that only requires a strip of land parallel to the highway or railway. Naturally, it works best on east-west oriented highways or railways as the solar panels should face south to maximize their efficiency, on the north hemisphere.



*Fig. 23 - PV modules alongside a highway slope [20]*

Other technologies that can be used are Photovoltaic Noise Barriers (PVNBs), introduced for the first time in Switzerland in 1989. These systems consist in the incorporation of PV panels on existing or newly designed noise barriers. In either case, the noise barrier serves as a substructure for PV modules.

The literature on PVNBs, most of which is several years old, generally agrees that there is great potential to use both existing and planned new noise barriers to produce solar power [20]. It is also agreed upon that noise barriers can be designed in such a way that power production doesn't compromise their abilities to safely reduce noise, and in some cases may even improve their performance. In many cases, sound absorption is not required for the noise barrier to achieve its intended acoustical purpose. In fact, materials such as solid concrete, wood, or metal do not provide sound absorption, and PV modules are acoustically no less satisfactory.

There are various types PVNB configurations, as shown on Figure 24, being top-mounted retrofit designs the most common. They provide additional area to an existing noise barrier structure.

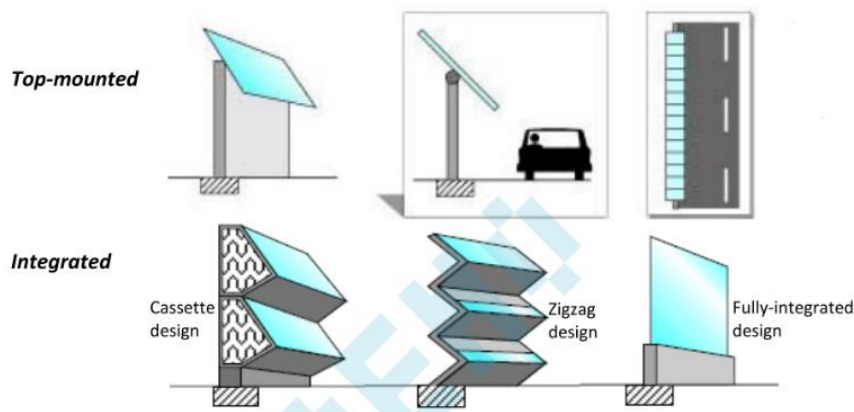


Fig. 24 - Different Possible PVNB Configurations [20]

A PVNB is most appropriately located along a highway or railway nearby a densely populated area for a number of reasons.

Firstly, noise barriers are generally more needed in these locations because of the number of local residents which can be affected by the noise.

Secondly, in a crowded area there is not much room available to install conventional PV systems and this makes sound barriers an interesting alternative to mount PV panels on. Although there might be a considerable area of rooftops, there are many specific issues regarding the integration of PV systems in roof structures. The roof tilt angle can influence the efficiency of the panels, structural roof characteristics are not always ideally suited for the installation of solar panels, and the use of roof space for other applications such as HVAC installations or roof terraces should be taken into account. It is also possible that residents do not agree with the installation of solar panels on their roofs, due to concerns about economic and financial risks or aesthetic matters.

Finally, when energy supply systems, in this case PVNBs, are located in densely populated areas (near to the consumer), this translates in decentralized electricity generation. This brings certain advantages, such as: reduced energy transportation costs, savings in primary energy consumption, and emission reduction of CO<sub>2</sub> and other pollutants [21].

Road orientation dictates noise barrier orientation, hence it will also affect PVNBs orientation and therefore its efficiency. East-west oriented roads were initially viewed as the only roads suitable for PVNBs, but the emergence of bifacial panel technology (Figure 25) has presented a potentially attractive option given their ability to produce electricity in any orientation - particularly on north-south oriented highways [20]. Bifacial PVNBs were first installed in a highway setting in Aubrugg, near Zürich Airport in Switzerland in 1997. The system was later expanded in 2005, and several others have been constructed since then.



Fig. 25 - Bifacial PVNBs allow light to enter from both sides [20]

In terms of driver safety, there is little to no evidence to date that PVNBs significantly affect it. Driver distraction and glare can be minimized by locating the PV modules high on noise barriers and/or set back from the roadway, and by ensuring that the panels are at proper angles to minimize glare [20]. Studies have reported that PVNBs with a vertical design, such as the Australian PVNB, do not enhance glare. Moreover, solar panels are designed to absorb light, rather than to reflect it.

The advantages of PVNBs have turned these systems into a growing phenomenon. Since 1989, when the Swiss first retrofitted a highway noise barrier with PV modules, PVNBs have been deployed in at least 14 countries (Table 3) and are planned in others.

Table 3 - Compiled Highway PVNB Counts [20]

Country	Earliest Implementation	Count (at least)
Australia	2007	2
Austria	1992	3
Croatia	2010	1
Denmark	1991	2
France	1999	2
Italy	2006	2
Germany	1992	18
The Netherlands <sup>a</sup>	1995	4
Slovenia	2012	1
Sweden	2014	1
Switzerland	1989	9
United Kingdom (U.K.)	2006	3

\* Confirmed by available documentation;  
planned not included

<sup>a</sup> Includes luminescent solar concentrator pilot

Sources<sup>10</sup>

Apart from PVNB systems, there is another way to implement PV modules alongside highways and railways which is using a land above type of approach: a PV roof structure (canopy) on top of the highway/railway, schematically represented in Figure 26. The Austrian Institute of Technology, the



Fraunhofer ISE in Germany, and the Forster Industrietechnik in Switzerland are currently working together to develop this kind of technology.

A PV highway canopy may have many advantages in terms of energy efficiency, such as improved vehicle movement and minimum energy destined for air conditioning of vehicles (as it creates shade). It also helps prevent road detrition, allowing road repairs to be less frequent, and provides longer vehicle tire life due to the effect of sun shade.

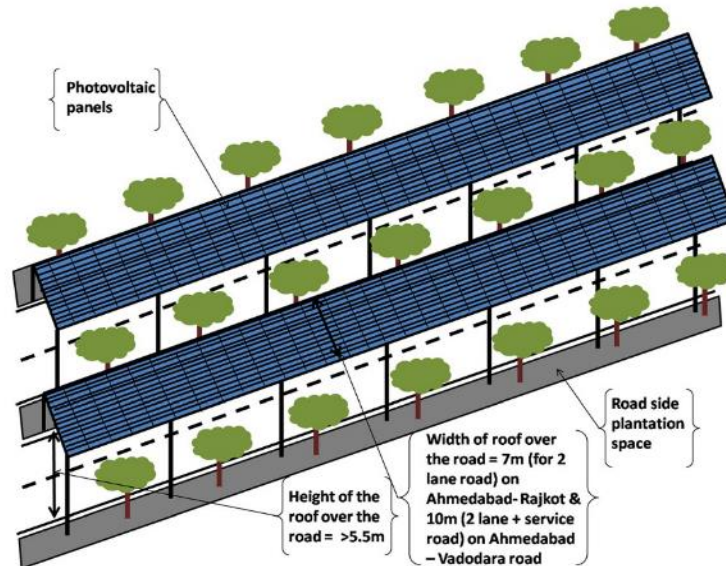


Fig. 26 - Schematic layout of a PV roof structure over a roadway [22]

Although this type of structure may have some advantages, it may pose some concerns in terms of proper implementation. Setting the solar panels at an elevated location (about 9 to 10m above the ground) may be quite challenging and it is very important to firmly fix the structure at a ground base level as it may be vulnerable to heavy winds. Dust and smoke particles may also pose a problem due to the movement of the vehicles (which can also happen to PVNBs). Nevertheless, highways/railways are generally wide and much cleaner than roads and it is proven that rain can be very effective on cleaning the PV modules.

Thus, although there are a few matters to be considered, disadvantages can be undertaken with proper planning.

## PV CARPORTS

Similarly to the roof-over-highway technology, PV carports like the one in Figure 27 are an efficient way to generate clean energy. This type of system is much simpler and can also work as an on-grid and/or off-grid technology to feed public lighting but also to charge parked electric cars.



*Fig. 27 - Solar carport [23]*

Nowadays, PV carports can be found in various different countries around the world, including Portugal.

### **PV BUS STOP SHELTERS**

Bus stop shelters can also serve as a means of clean energy generation. There are countless of these structures on any country and they can work in the same way as the parking canopies.

Bus shelters can even be used as an off-grid technology to charge peoples' phones while they wait for the bus, or even spare some electricity for power heaters inside the shelter in cold countries. Figure 28 shows a PV bus stop shelter in Zagreb, Croatia.

This type of technology is one of the most simple and useful non-conventional ways to generate power using PV modules.



*Fig. 284 - Solar PV bus stop shelter in Zagreb, Croatia*










Several conclusions are drawn based on these studies:

- there are still unsolved conflicts between the electrical and mechanical performance;
- the effects of PV cell operating temperature on the power generation efficiency should be more emphasised;
- standardised structural design of PV pavements and methods on connecting the unit structures should be proposed;
- material specification of PV pavements should be able for further discussion.

It is, therefore, clear that research on PV pavements is still at its early age and requires overall improvement.

Besides the technical issues enumerated above, there can be listed some commercial accomplishments, as shown in Table 4.

*Table 4 - Commercial achievements of PV pavement [29]*

Time/Country	Picture	Details
2014 U.S.		The world's <b>first</b> PV car park; It was designed by Brusaw couple; Hexagonal solar panel.
2014 Holland (Krommenie)		The world's <b>first</b> PV bicycle lane; Scale: 70 m-long; Rectangular PV plate; Structure: tempered glass plate + PV cell + concrete plate.
2016 Franch (Normandy)		The world's <b>first</b> PV road 'Wattway'; Scale: 1 km-long, 2,800 km <sup>2</sup> ; Rectangular PV plate; Structure: silicon resin coating + PV cell + polymer and gum plate
2016 China (Beijing)		Experimental road; Scale: 70 m-long.
2016 Belgium, Holland		Thin-membrane flexible PV pavement; It was developed by Hanergy Group; Demonstration bicycle lane sections;
2017 China (Zhejiang)		"Sun No.1" PV road section; It was laid by Zhejiang Lanting Solar Energy Corporation;
2017 China (Shandong)		The world's <b>first</b> PV highway; It was constructed by Qilu Group and Shandong Guangshi Energy Corporation; It can carry heavy load.

Based on the available research and development on PV roads/pavements, several limitations are found and concluded as below:

- 1) Effective power generation of PV cells is low while it is still costly;
- 2) PV pavements cannot obtain full solar radiation due to shadow and blocking effects from the existing adjacent buildings, car movement, and walking pedestrians;
- 3) The mechanical properties of PV pavement structure may not meet full requirement;
- 4) High operating temperature of the PV cell is the main problem occurred in the block structures of PV pavement, which further reduces the power generation efficiency [27].

PV pavement is thus a very recent technology and there are still lots of improvements to be made. Nonetheless, it has proven its potential.

## **SOLAR BRIDGES**

Solar bridges can be implemented in a very similar way as the PV systems alongside highways and railways by installing a PV roof and/or a vertical PV structure on the bridge.

London is home to the world's largest solar bridge, shown in Figure 30. Thanks to it, Blackfriars rail station secures half its power from the 4,400 roof-mounted solar panels. The bridge was originally built in 1886 but has now been upgraded by the London rail network.



*Fig. 30 - London's solar-powered bridge [30]*

## FLOATING PV SYSTEMS

In Floating Solar Photovoltaics (FSPVs), the PV modules are designed and installed to float on water bodies such as: reservoirs, hydroelectric dams, industrial ponds, water treatment ponds, mining ponds, lakes, and lagoons.

In FSPV systems, solar panels, inverters, and cables are mounted upon a pontoon-based floating platform, and the floating structure is anchored and moored (Figure 31) [14].

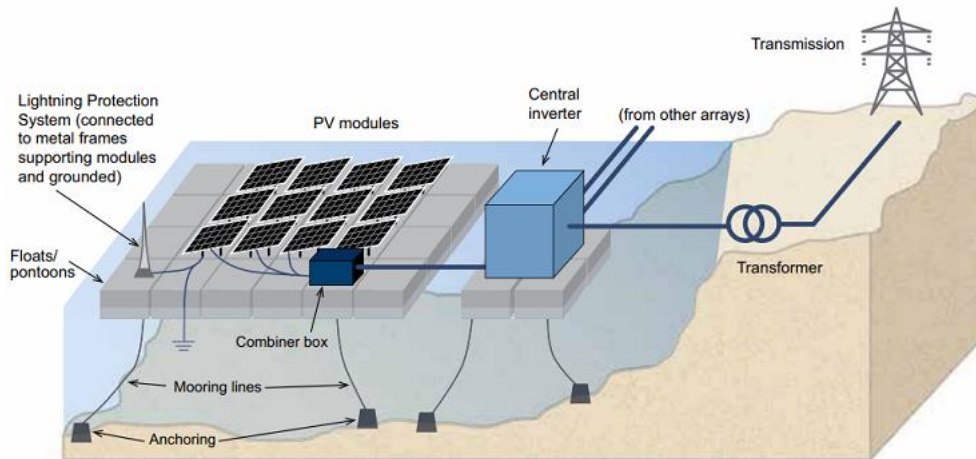


Fig. 31 - Schematic representation of a typical large-scale floating PV system with its key components [31]

Floating PV systems are conceptually very similar to conventional solar parks, with the particularity of being deployed on water bodies as opposed to on land. There are countless water bodies throughout the world and this technology solves in a sense the big geographic problem associated with PV systems.

FSPV systems are also known for the following benefits:

- Improved energy yield performance: The evaporative cooling effect of water results in lower operating temperatures of the PV modules [14];
- Water evaporation control: FSPV causes shading of water surfaces. With floating solar, around 70% of the evaporation could be prevented which would in turn help in retaining sufficient amount of water in the canals and small river bodies [32];
- Restriction of algae growth: Since FSPV plants provide shade to the water surface, they reduce the amount of sunlight reaching the water surface, which may cause a reduction in algae growth [14]. This makes water less contaminated and helps in production of oxygen necessary for the aquatic life in sustaining and minimizing the associated water treatment and labour costs [14].

Disadvantages of FSPV plants may include:

- Cost of installation: an on-water-type PV system is more expensive than, for instance, a ground/roof top-based one. PV modules are exposed to high humidity levels so more care has to be taken in selecting them. Also, in terms of maintenance, the algae that grow on the floats and panels need to be removed;
- Impact on the ecosystem: particularly in aquaculture, due to reduced sun light;
- Obstruction for marine activities, such as boats;

The first floating PV system was deployed in the year 2008 in California with a 175 kW peak capacity. Since then, FSPV technology has been growing and is considered nowadays to be nearly mature.

China has the world’s biggest FSPV plant of 150 MW capacity installed at Huainan, south Anhui province. Most of the FSPV plants in China are installed at unused mining ponds [32]. However, in terms of total numbers of installation, Japan is a leading country: it is home to 73 of the world’s 100 largest FSPV plants.

The First-ever hydropower-connected floating solar operation was deployed in Montalegre, Portugal. In terms of global investment cost for floating solar PV plants, Portugal is well positioned, as shown in Figure 32.

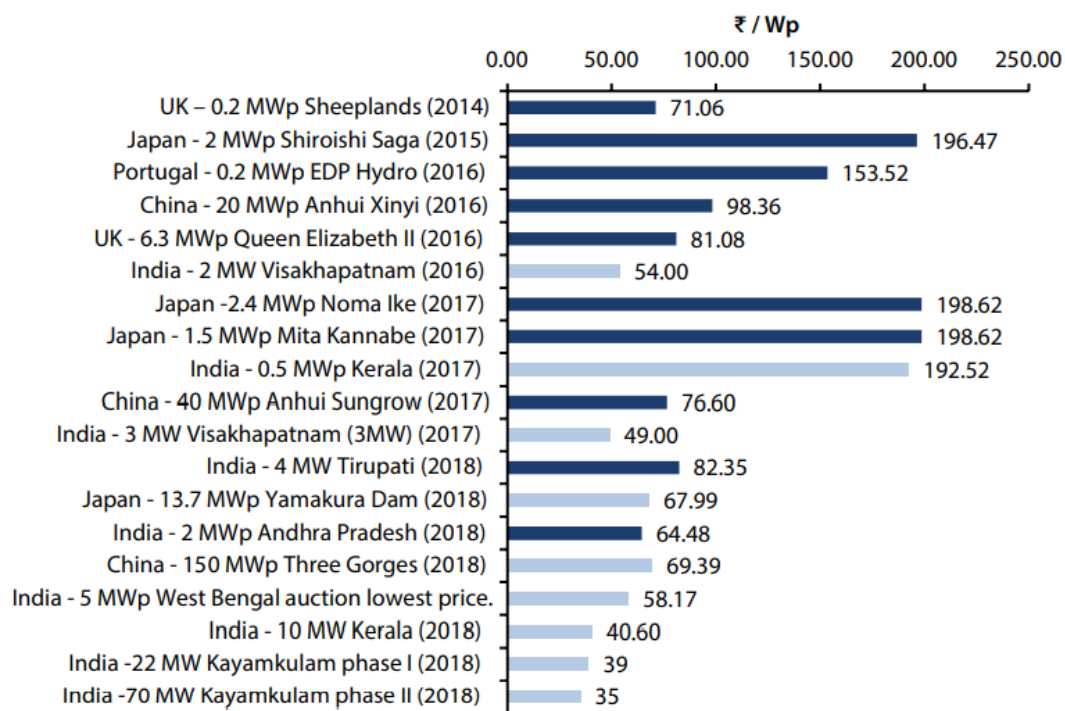


Fig. 32 - Global investment cost for floating solar PV plants [32]

1 YEN (¥) = 0.0076 EUR (€) (verified in 18/02/2022)

## SUBMERGED PV SYSTEMS

The utilization of water as the operating ambient for PV arrays has come a step further when researchers developed the first submerged PV system studies.

The integration of PV modules in a swimming pool was introduced with the least environmental impact. Cleaning problems are mitigated and low operating temperatures are easily assured, resulting in increased efficiency. Water also behaves as a filter that blocks the long-wavelength photons and transmits lights within the visible spectrum, the optimum condition for PV cells [26].

In this concept, a part of the PV panels was installed on the pool edge and the others were positioned on the pool floor, as shown in Figure 33. The modules can be easily integrated in existing swimming pools and even contribute in an aesthetic point of view.

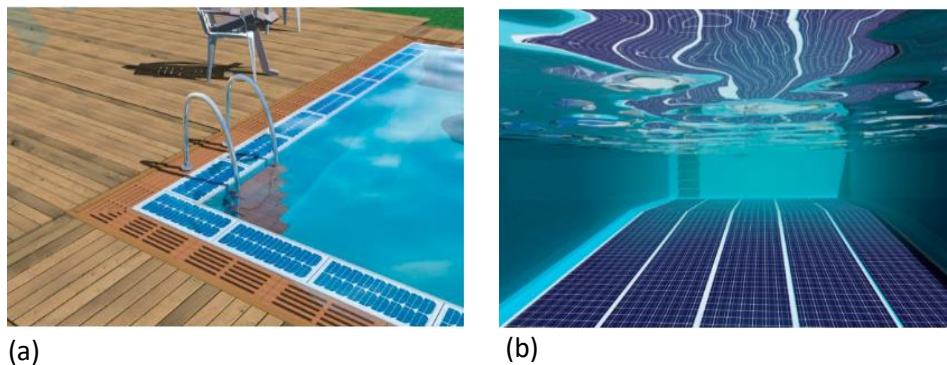


*Fig. 33 - The concept of PV integration with swimming pools: (a) PV on the pool edge, and (b) PV on the pool floor [33]*

## AGROPHOTOVOLTAIC SYSTEMS (APVs)

The idea of Agrophotovoltaic (APV) was first proposed by Goetzberger and Zastrow [34] in 1982 and it consists in the coproduction of electricity using solar energy and agricultural products on the same area. The proposed concept involves the installation of PV panels a couple of meters above the ground, as shown in Figure 34. Nowadays, this technology is also known as an agrivoltaic.

Results from various studies confirmed that using APV systems increases land-use efficiency by raising farm revenues more than 30%, but only if yield losses due to shading effects are kept down by a selection of proper crops [35]. Additionally, the agrivoltaic systems decrease water evaporation rates, ensuring that crops have more accessible water than crops cultivated in regular lands fully exposed to sun, which results in stable crop yields [36, 37].





(a)



(b)

*Fig. 34 - (a) APV system installed in Italy [38], and (b) APV facility installed above the potato farm (RESOLA project), Heggelbach, Germany [35]*

As an off-grid type of approach, numerous researchers have studied various applications of solar PV systems in agricultural practices. Solar PV energy possesses huge potential to power agricultural facilities and farm equipment, including: PV-powered water pumping and irrigation systems, PV-powered desalination systems, PV-powered solar dryers, PV-powered greenhouses, PV-powered livestock and dairy farming systems, PV-powered crop protection systems, etc. [39].



### 3. CASE STUDY

The conducted study aims to evaluate the solar potential of non-conventional PV application sites alongside highways and railways in the region of Maia, Portugal. This section gives an overview of the methodology followed to collect the data and achieve the results of this work.

#### 3.1 Area of Study

The selected area for this study (41,2°N 8,6°W) is situated in the northern coastline of Portugal and is part of the Porto district, as shown in Figure 35. It covers the Maia County and some sections of other neighbouring counties, namely Matosinhos and Valongo, totalling 489.32 km<sup>2</sup>.

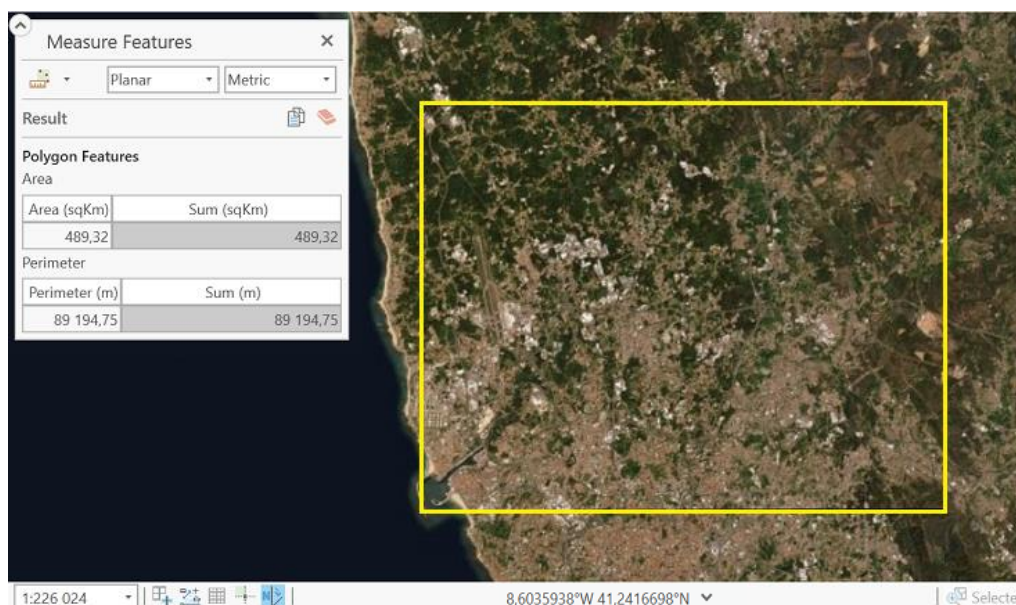


Fig. 35 – Selected study area (ArcGIS)

The proposed area is characterized by a semi-urban environment with a significant number of highways and railways with different orientations.

#### 3.2 Site Selection

Within the delimited region, various sites alongside highways and railways were identified according to solar potential and feasibility to install solar modules. Solar potential was assessed in a preliminary way by considering highway/railway orientation and the existence of tree/building shading. Feasibility was appraised based on location access, visual impact, and structural viability (most sites comprise pre-existing structures where it is easy to mount PV modules).

Taking into account the referred criteria, the first approach to pinpoint these sites was by using a very accessible and useful tool: Google Earth Pro. In total, 30 sites were selected, being 20 alongside highways (blue pins) and 10 alongside railways (red pins), represented in Figure 36.

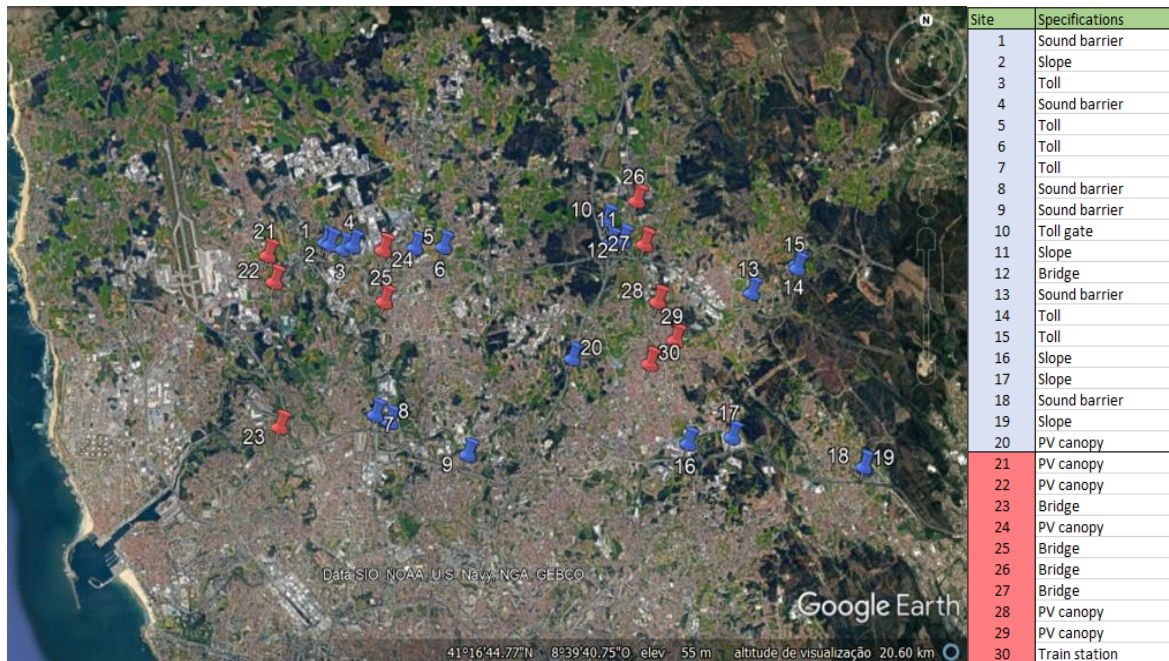


Fig. 36 - Selected sites (Google Earth Pro) and their specifications (Table)

As specified in the table of Figure 36, 7 types of structures were selected, including: sound barriers, slopes (alongside the highway/railway), electronic and non-electronic tolls (non-electronic: toll gate), bridges, PV canopies (potential roof structures that can be built over the highway/railway to accommodate PV modules), and a train station.

The following Google Earth images (Figures 37 to 66) display the 30 selected sites.



Fig. 37 – Site 1, sound barrier



Fig. 38 – Site 2, slope



Fig. 39 – Site 3, toll



Fig. 40 - Site 4, sound barrier



*Fig. 41 - Site 5, toll*



*Fig. 42 - Site 6, toll*



*Fig. 43 - Site 7, toll*



*Fig. 44 - Site 8, sound barrier*



*Fig. 45 - Site 9, sound barrier*



*Fig. 46 - Site 10, toll gate*



*Fig. 47 - Site 11, slope*



*Fig. 48 - Site 12, bridge*



*Fig. 49 - Site 13, sound barrier*



*Fig. 50 - Site 14, toll*



*Fig. 51 - Site 15, toll*



*Fig. 52 - Site 16, slope*



*Fig. 53 - Site 17, slope*



*Fig. 54 - Site 18, sound barrier*



*Fig. 55 - Site 19, slope*

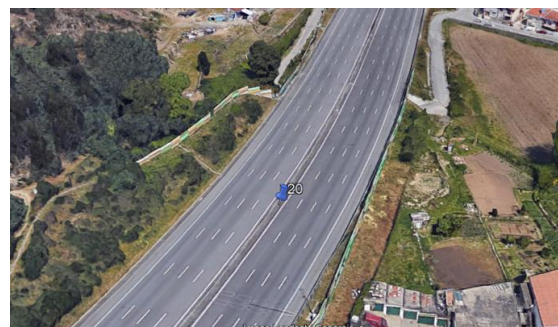


*Fig. 56 - Site 20, PV canopy*

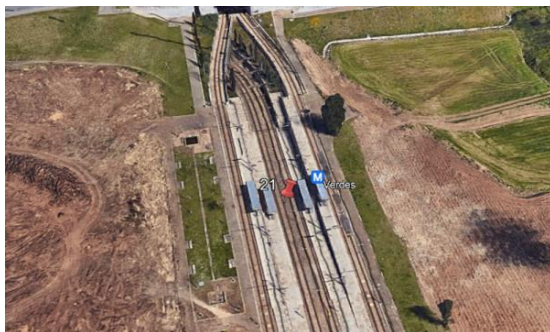


*Fig. 57 - Site 21, PV canopy*

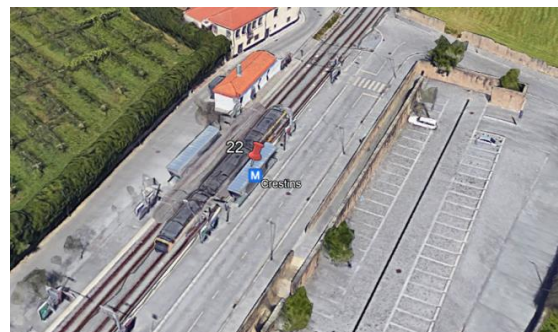


*Fig. 58 - Site 22, PV canopy*

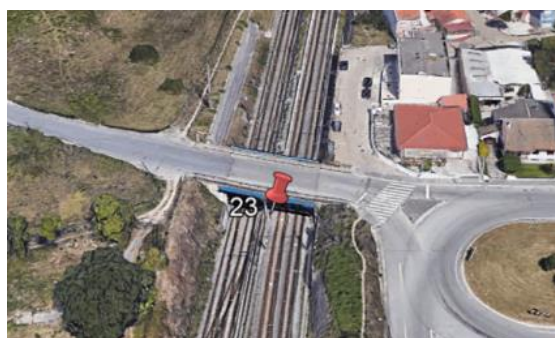


*Fig. 59 - Site 23, bridge*



*Fig. 60 - Site 24, PV canopy*



*Fig. 61 - Site 25, bridge*



*Fig. 62 - Site 26, bridge*



*Fig. 63 - Site 27, bridge*

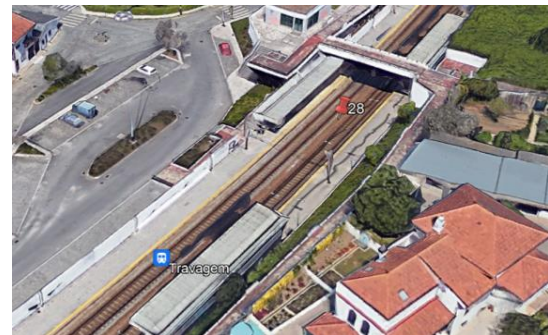


*Fig. 64 - Site 28, PV canopy*



*Fig. 65 - Site 29, PV canopy*

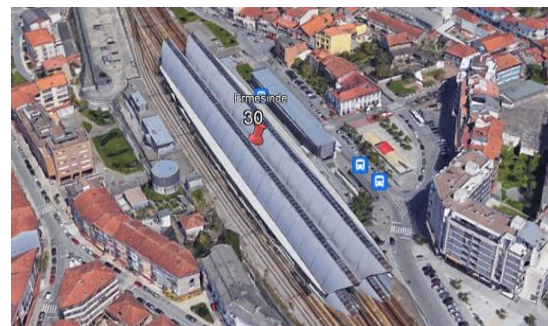


*Fig. 66 - Site 30, train station*

After selection, the sites were carefully examined according to qualitative standards and compared amongst each other. A primary group of 8 sites was identified as least favourable for PV module installation and were thus excluded:

- Site 19 may potentiate glare and was considered not aesthetically tolerable given the fact it is close to a residential area. It is also very prone to vandalism because of its easy access;
- Site 20 was considered for a PV canopy above the highway but there is too much tree shading and housing nearby, which may suffer from the highway noise that can reflect on the modules above and is amplified to the nearby homes;
- Sites 26 and 27 reveal an apparently small feasible area to install the modules compared to the other locations;
- Site 30 was eliminated due to structural constraints. Although with good orientation, the train station's roof was considered too complex to install PV modules.

The remaining 25 sites were analysed using a Geographic Information System (GIS) and a simulation software (PVSyst), which are explained in detail in the following chapter.





## 4. MODELLING

### 4.1 ArcGIS Analysis

A Geographic Information System (GIS) is a system that creates, manages, analyses, and maps all types of data. GIS connects data to a map, integrating location data (where things are) with all types of descriptive information (what things are like). This provides a foundation for mapping and analysis that is used in science and almost every industry. GIS helps users understand patterns, relationships, and geographic context [40].

ArcGIS Pro software is the latest professional desktop GIS application developed by the *Environmental Systems Research Institute (ESRI)* [40], which is the global market leader in geographic information systems. It processes geographical data by organizing it into discrete georeferenced layers which are displayed, combined, and analysed in common topographical space.

Before starting a project, it is important to define a key framework which assures the common ground of analysis in the geographic scene – the coordinate system. This is a fundamental step in order to guarantee correct and coherent relations between the layers.

The *ArcGIS Pro 2.9 Geographic and Vertical Coordinate System Tables* [41] were used as a guideline to define the Geographic Coordinate System (GCS). Being the only Portuguese mainland coordinate reference available, *Cascais* (GCS Name) was used both for xy and z coordinate systems, as shown in Figures 67 and 68.

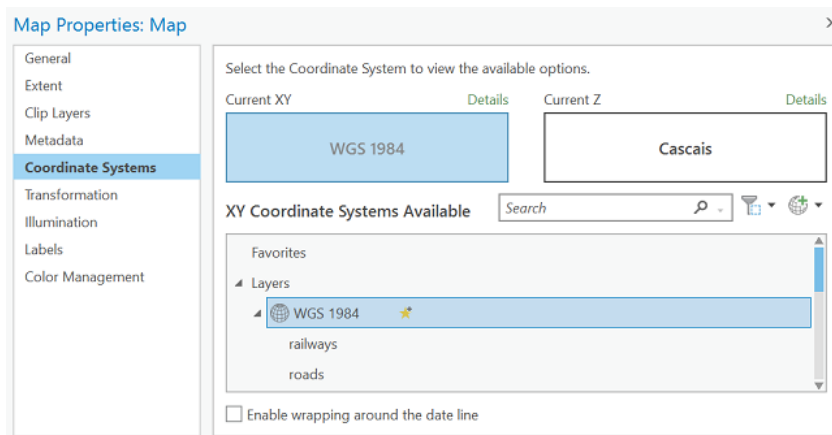


Fig. 67 – XY Coordinate System (ArcGIS)

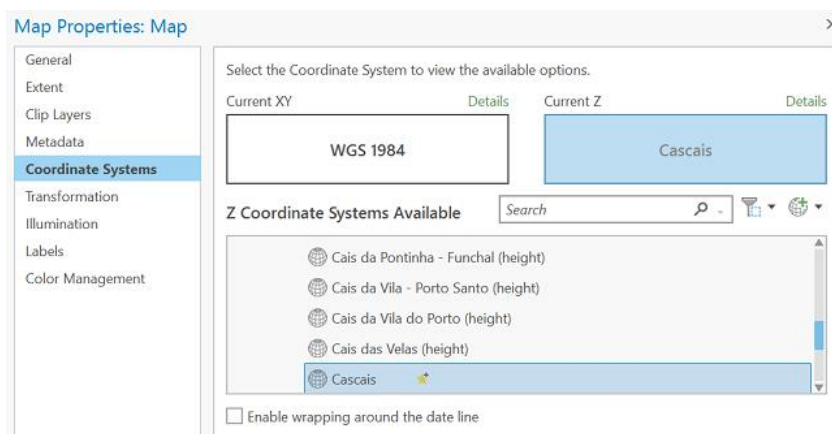


Fig. 68 – Z Coordinate System (ArcGIS)

For this project, the main input layer was a Shuttle Radar Topography Mission (SRTM) data file from NASA servers. The SRTM was an international research effort that obtained digital elevation models on a near-global scale from 56°S to 60°N, to generate a complete high-resolution digital topographic database of Earth. The elevation models are arranged into tiles, each covering one degree of latitude and one degree of longitude, named according to their south western corners. N41W009 was the used model in this work (Figure 69). It stretches from 41°N 9°W to 42°N 8°W.

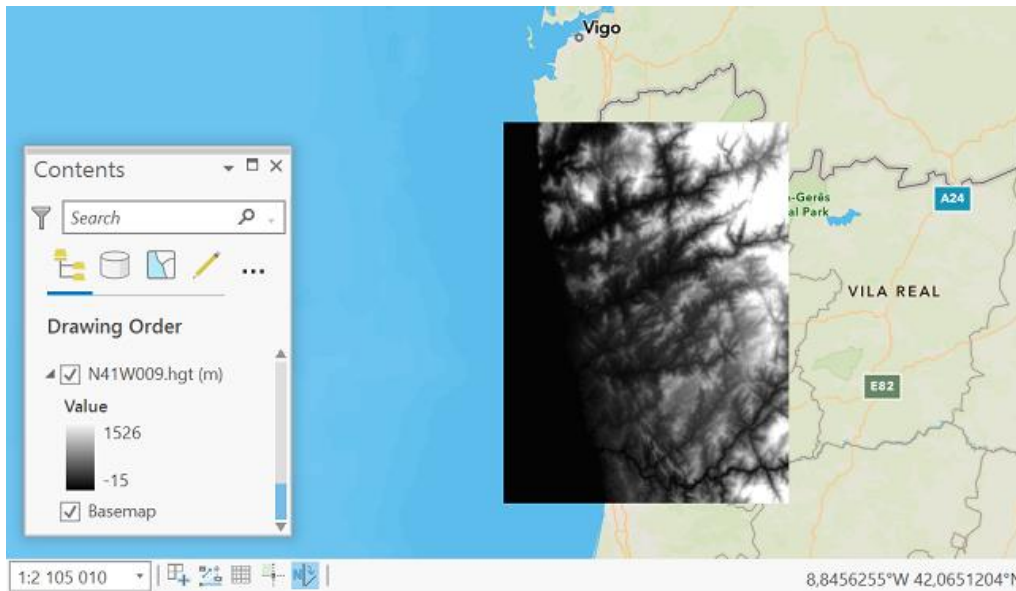


Fig. 69 - N41W009 layer (ArcGIS)

Two other layers were used as input for a better understanding of the local geography, namely: the roads and railways of Portugal (Figure 70). This data was obtained from *Forest GIS database* [42] and can be observed in the figure below.

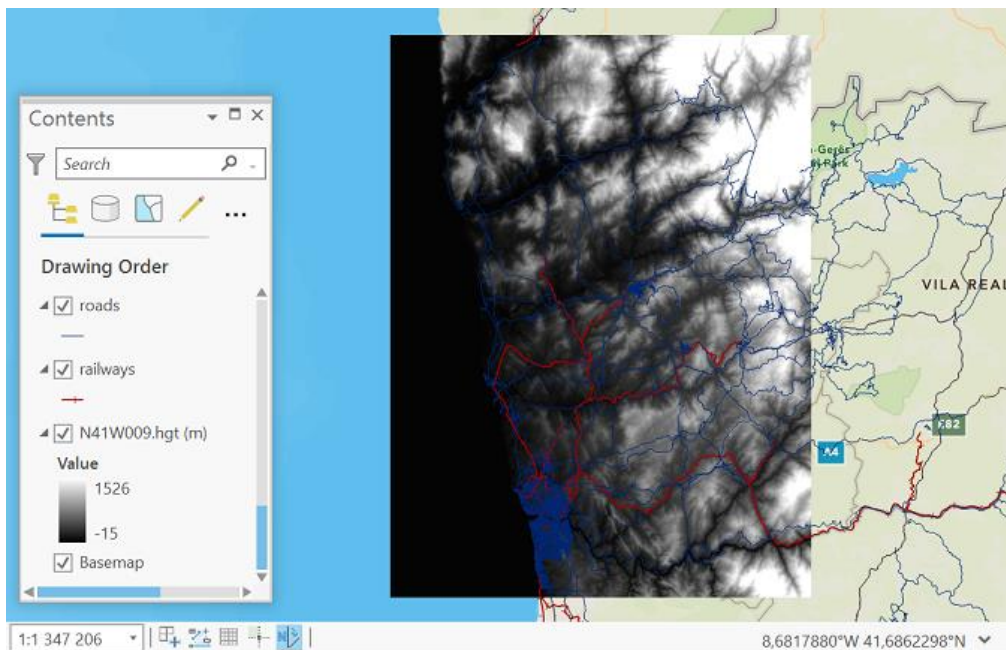


Fig. 70 - N41W009, roads, and railways of Portugal layers (ArcGIS)

As shown, the described layers go beyond the previously mentioned area of study. To minimize computational effort, constraining methods were applied. Using the *Polygon Tool*, the shape of interest was created (Figure 71) and the peripheral area was extracted from the raster dataset by applying the *Clip Raster* from the *Data Management* toolbox. Figure 72 shows the outcome of this process.

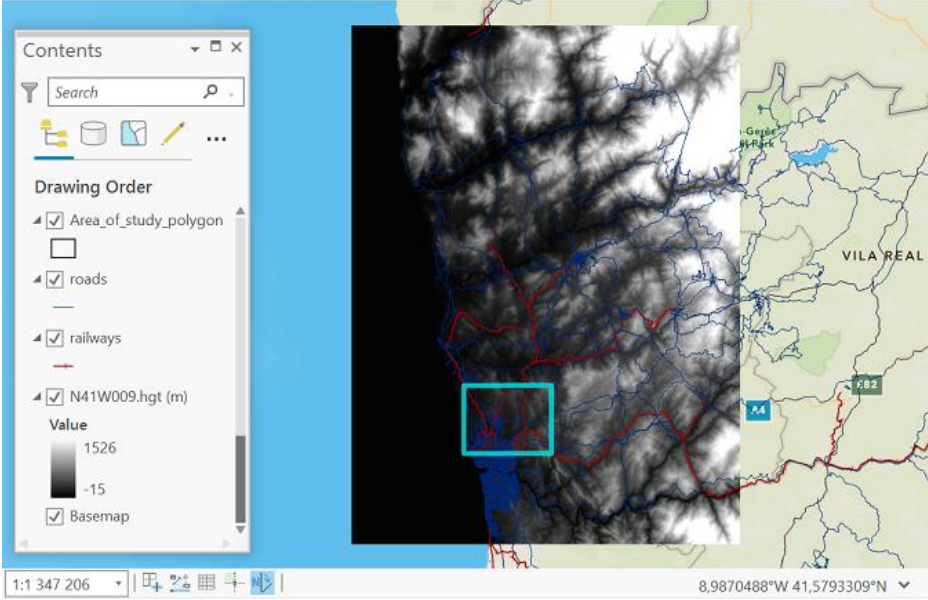


Fig. 71 - N41W009, roads, railway layers, and the polygon representative of the area of interest (ArcGIS)

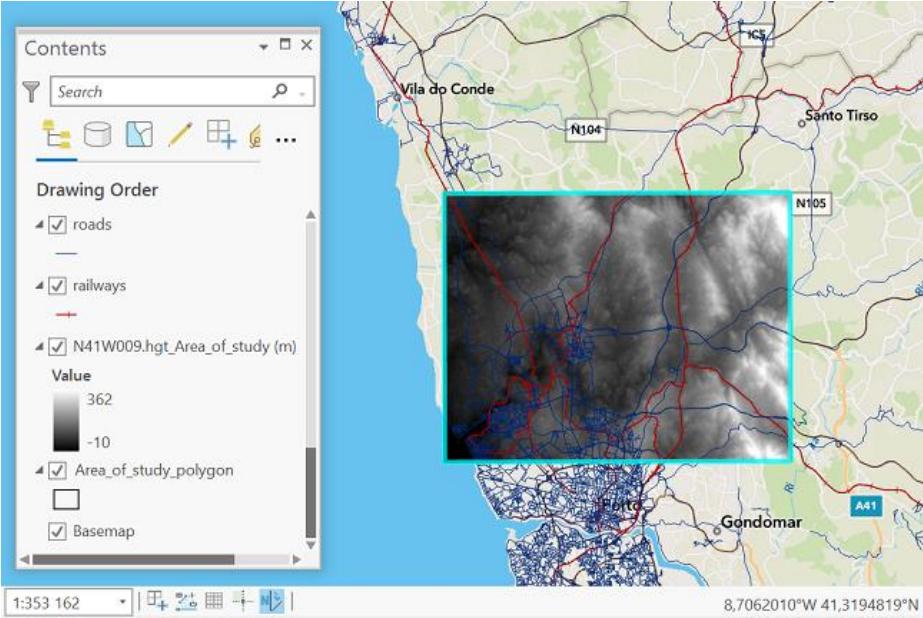


Fig. 72 - Roads layer, railways layer, and N41W009 layer confined to the area of study (ArcGIS)

Having the input data confined to the area of study, conditions are met to start analysing and modelling an incident solar radiation outline of the geographic scene.

Firstly, the *Hillshade function* was used. It produces a grayscale 3D representation of the terrain surface taking into account the sun's relative position for image shading. It is a qualitative topography method and provides two options for hillshade generation: *traditional*, which calculates the hillshade using a light source from one direction using altitude and azimuth to specify the sun's position; and *multidirectional*, which combines illumination from multiple sources to represent the hillshaded terrain.

*Traditional Hillshade* was used because the only light source that was considered was the direct sun radiation. The location of the light source was set with an azimuth of  $315^\circ$ , which is from the northwest (default), and an altitude degree of  $45^\circ$  above the horizon. The *Z factor* was set as 1. This parameter adjusts the number of ground x,y units for each surface z unit. The resulting layer can be observed in Figure 73.

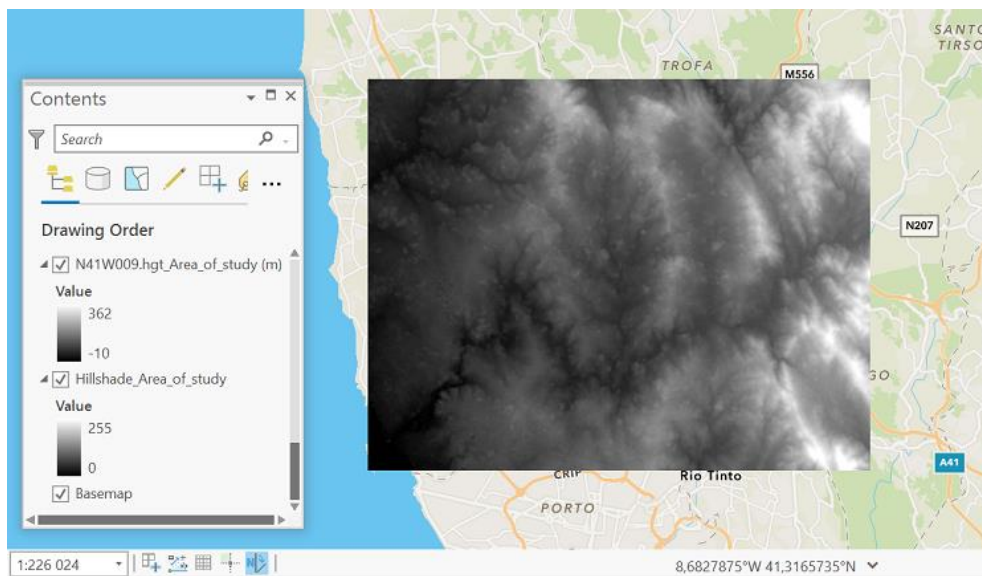


Fig. 73 - Hillshade layer overlapped by N41W009 layer with 40 % transparency (ArcGIS)

After obtaining a representation of the terrain's influence on light and shading, *Area Solar Radiation (Spatial Analyst)* was applied. The solar radiation analysis tools calculate insolation across a landscape or for specific locations, based on methods from the hemispherical viewshed algorithm developed by Rich et al. (Rich 1990, Rich et al. 1994) and further developed by Fu and Rich (2000, 2002) [43]. The total amount of radiation calculated for a particular area is given as global radiation.

*Sky resolution* was maintained as a default raster of 200 by 200 cells and *time configuration* as a whole year with monthly intervals for calculations. The *hour interval*, which is used to calculate sky sectors for the sun map, was set for 0.25 (15 min.) and the *Z factor* as 1. The number of azimuth directions used when calculating the viewshed were 32 (considered adequate for complex topography). Zenith and azimuth divisions (used to create the sky sectors in the sky map) were maintained 8 each (default). The diffuse model type was *Uniform overcast sky*, in which incoming diffuse radiation is the same from all sky directions, with a *diffuse proportion* (proportion of global normal radiation flux that is diffuse) of 0.3 and *transmissivity* (fraction of radiation that passes through the atmosphere) of 0.5 (default for clear sky conditions).

The model of the incident global solar radiation over the course of one year in the area of study was obtained and is shown in Figure 74.

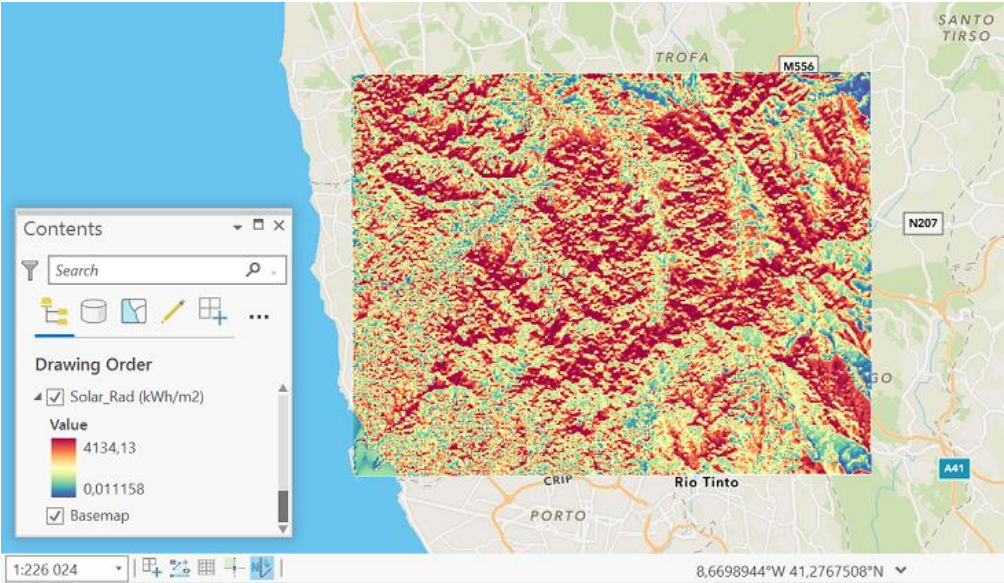


Fig. 74 - Solar Radiation layer (ArcGIS)

Having a clear image of the annual incident global solar radiation in the area, the next step was to evaluate the local incident solar radiation, that is, the incident solar radiation in each selected site. To do that, the *Polygon Tool* was used once more and the designated locations were pinpointed and drawn according to their individual shape (in blue), as shown in Figure 75.

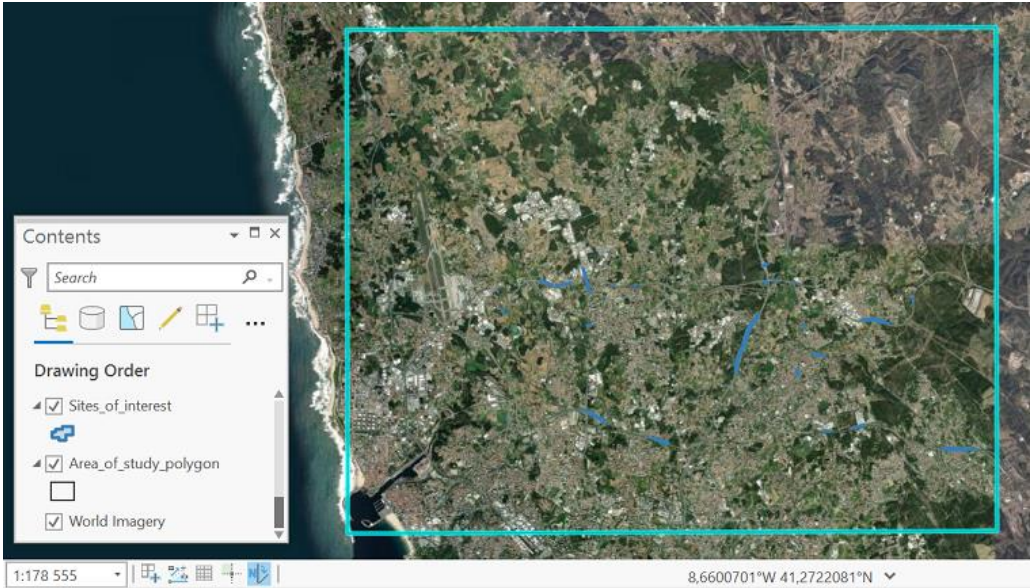


Fig. 75 - Sites of interest (ArcGIS)

Figure 76 displays the annual incident global solar radiation overlapped by the layer containing the sites of interest. This way it is possible to visualize each site’s solar potential.

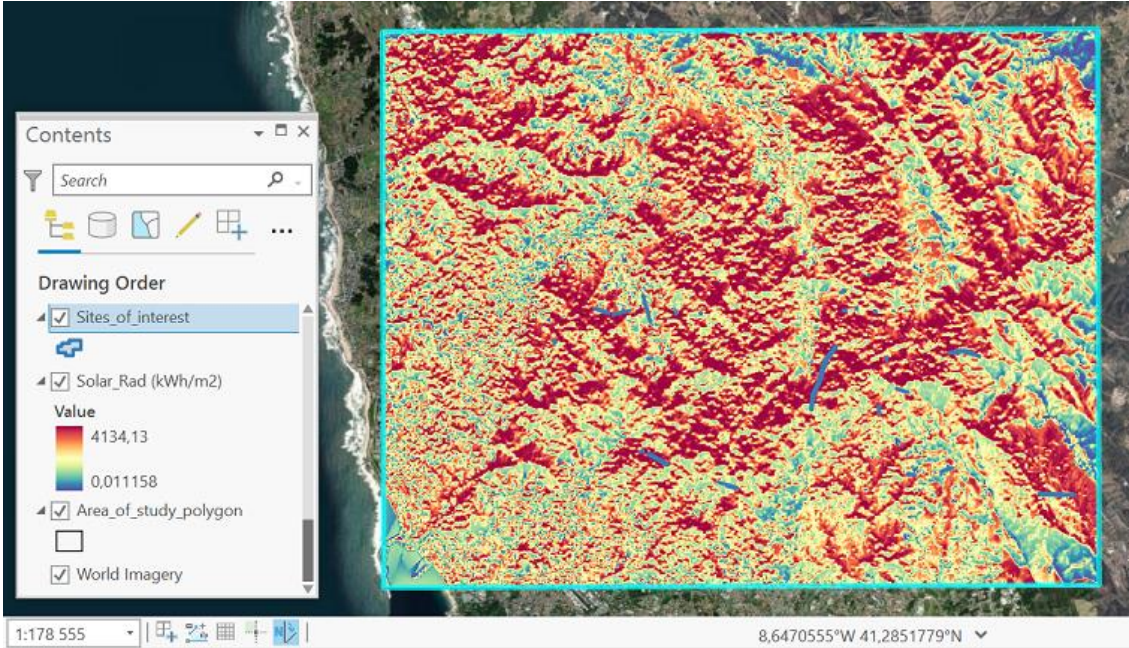


Fig. 76 - Sites of interest and solar radiation layer (ArcGIS)

It is important to note that the obtained incident solar radiation has its main reference on the terrain, i.e., it represents the global incident solar radiation on the ground. Thus, it does not consider trees, buildings, or other structures. Therefore, in the case of noise barriers, for instance, the incident solar radiation is a horizontal one. This issue will be treated in the next section, where PVsyst software is explained in detail as it played a big role in module orientation analysis.

Table 5 shows each site’s specifications, location (latitude, longitude, and altitude), and an incident solar radiation classification, derived from the ArcGIS results. This classification is based on the annual average incident global horizontal solar radiation on each site and was established as follows:

- A: 2250 kWh/m<sup>2</sup> or more
- B: 1500 – 2250 kWh/m<sup>2</sup>
- C: 750 – 1500 kWh/m<sup>2</sup>
- D: 0 – 750 kWh/m<sup>2</sup>

As mentioned before, blue represents highway sites and red represents railway sites.

Table 5 – Numbered sites and respective specification, location, and classification

Site	Specifications	Latitude	Longitude	Altitude (m)	Classification
1	Sound barrier	41°14'26.62"N	8°38'33.84"W	70	A
2	Slope	41°14'24.95"N	8°38'29.31"W	65	A
3	Toll	41°14'22.03"N	8°38'15.76"W	76	B
4	Sound barrier	41°14'23.95"N	8°38'6.66"W	79	C
5	Toll	41°14'22.75"N	8°37'5.47"W	96	A
6	Toll	41°14'23.38"N	8°36'37.55"W	86	C
7	Toll	41°12'25.52"N	8°37'44.26"W	88	A
8	Sound barrier	41°12'20.55"N	8°37'29.79"W	67	C
9	Sound barrier	41°11'57.83"N	8°36'13.62"W	78	C
10	Toll gate	41°14'41.68"N	8°33'56.52"W	121	B
11	Slope	41°14'25.68"N	8°33'53.59"W	112	B
12	Bridge	41°14'27.62"N	8°33'40.73"W	181	B
13	Sound barrier	41°13'50.80"N	8°31'34.92"W	98	B
14	Toll	41°14'10.58"N	8°30'50.48"W	138	B
15	Toll	41°14'7.61"N	8°30'49.78"W	139	A
16	Slope	41°12'5.67"N	8°32'38.60"W	134	D
17	Slope	41°12'10.21"N	8°31'56.23"W	184	D
18	Sound barrier	41°11'48.90"N	8°29'47.33"W	148	B
21	PV canopy	41°14'17.45"N	8°39'29.87"W	75	D
22	PV canopy	41°13'58.88"N	8°39'23.76"W	63	C
23	Bridge	41°12'17.06"N	8°39'17.59"W	75	D
24	PV canopy	41°14'21.21"N	8°37'36.44"W	109	C
25	Bridge	41°13'45.00"N	8°37'35.59"W	89	D
28	PV canopy	41°13'44.66"N	8°33'6.55"W	97	A
29	PV canopy	41°13'18.16"N	8°32'48.97"W	102	C

Sites with D classification (16, 17, 21, 23 and 25) were discarded. The remaining 20 locations (1 to 15, 18, 22, 24, 28, and 29) were analysed in detail with the PVsyst software, explained in the following section.

## 4.2 PVsyst Simulation

PVsyst 7.2 is a PC software developed for the study, sizing, and data analysis of complete PV systems. It deals with grid-connected, stand-alone, pumping and DC-grid (public transportation) PV systems, and includes extensive meteorological and PV systems components databases, as well as general solar energy tools [44]. This section gives an overview of the steps taken to execute the PVsyst simulation.

### GENERAL PARAMETERS

When starting a project in PVsyst, it is important to define a few general parameters which remain constant for all sub-projects in a particular region. These assure that the simulations are inherently accurate and coherent amongst each other. General parameters include: albedo, reference temperatures, and detailed losses.

Albedo values were set uniformly throughout the year with a value of 0.2, which is adequate for a semi-urban environment.

### Reference Temperatures

The design conditions, namely reference temperatures, were defined as follows:

- Lower temperature for absolute voltage limit:  $-10^{\circ}\text{C}$ . This value represents the minimum temperature that the systems may experience;
- Winter operating temperature:  $10^{\circ}\text{C}$ . This represents the mean winter ambient temperature;
- Usual operating temperature under  $1000\text{ W/m}^2$ :  $15^{\circ}\text{C}$ . This represents the mean ambient temperature throughout the year;
- Summer operating temperature:  $45^{\circ}\text{C}$ . This represents the maximum temperature that the systems may experience.

These are relatively conservative temperature values established after a careful analysis of the local meteorological data in Porto ( $41.15^{\circ}\text{N}$   $8.61^{\circ}\text{W}$ ) in the year 2021. This information was brought out by *Metoblue database* [45].

### Detailed losses

Detailed losses were specified as such:

- Limit overload loss for design: 3%. This represents the loss that may occur during the year due to potential oversized PV array with respect to the inverter;



- Loss fraction at STC (Standard Test Conditions): 1.5%. This represents the array ohmic wiring losses between the power available from the modules and the power at the terminals of the sub-array.

Additional defined losses are shown on Figure 77:

The figure shows four panels from the PVsyst software interface for defining losses:

- Module quality:** Module efficiency loss is set to -0.8%. Description: Deviation of the average effective module efficiency with respect to manufacturer specifications. (negative value indicates over-performance).
- Module mismatch losses:** Power Loss at MPP is 2.0%, Loss when running at fixed voltage is 2.5%. Description: Not relevant when MPPT operation.
- LID - Light Induced Degradation:** LID loss factor is 0.0%. Description: Degradation of crystalline silicon modules in the first operating hours with respect to the manufacturing flash test STC values.
- Strings voltage mismatch:** Power Loss at MPP is 0.1%. Description: (None).

Fig. 77 - Module quality, LID, and mismatch losses (PVsyst)

## SITE-SPECIFIC PARAMETERS

Site-specific parameters are unique for each sub-project and are highly contingent on location. These include: Meteorological data, orientation, shading, module choice, and inverter choice.

### Meteorological data

Although the selected sites are relatively close to each other, it is important to gather meteorological data for each location, in the same way as radiation data was with the GIS simulation. The collected meteorological was obtained from *Meteonorm 8.0* [10]. It includes monthly temperature values, sun paths, as well as monthly radiation, which is later compared with the data obtained by ArcGIS.

### Orientation

Orientation parameters, namely tilt and azimuth, are very site-dependant. The surface azimuth is an intrinsic characteristic of the site and amongst the selected locations varied between  $-20^\circ$  and  $15^\circ$  in respect to south orientation. Sub-arrays were contemplated in some sites where more than one surface azimuth angle was registered. Each array is associated to a certain orientation (tilt and azimuth).

Conversely, the tilt angle can be calculated and defined for optimal performance (the more perpendicular a module is to the sun's rays, the better). In general, literature agrees that the tilt angle should not vary more than  $10^\circ$  from the local latitude value. That is, a PV module installed in a latitude of  $41^\circ\text{N}$  should have a tilt angle between  $31^\circ$  for the summer and  $51^\circ$  for the winter.

PVsyst is very helpful for PV orientation design as it shows graphically the optimum tilt angle. Since the latitude amongst sites varies no more than  $0.1^\circ$ , the tilt angle was defined as  $35^\circ$  for every site with exception for PVNBs (PV noise barriers), which were set for  $90^\circ$ , and for determined slopes with a particular inclination where the arrays were designed to lay on the ground.

Figure 78 shows an example of the PVsyst layout for orientation analysis on site number 3.

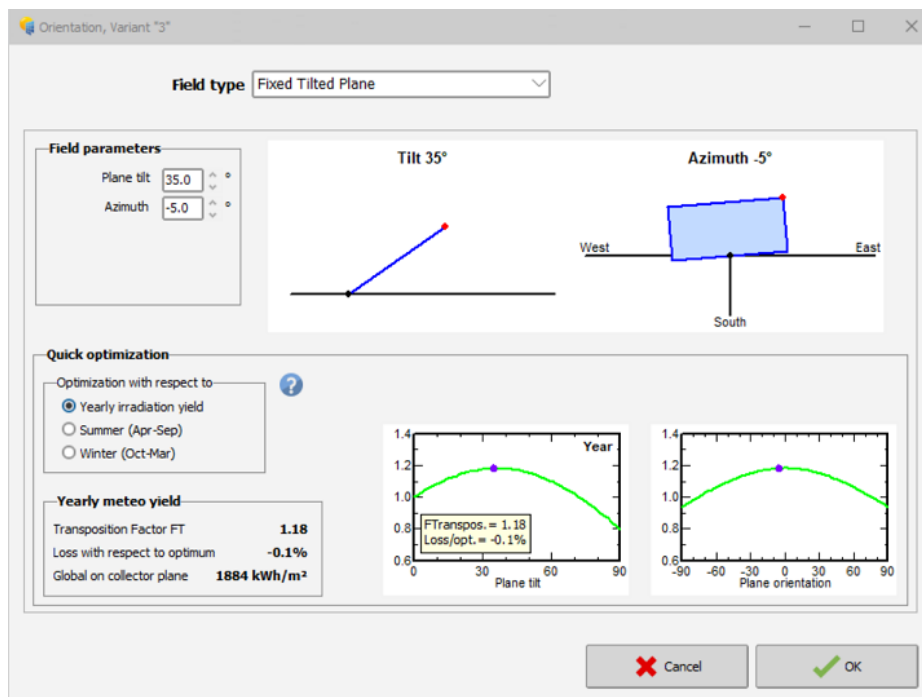


Fig. 78 - Orientation analysis of site number 3 (PVsyst)

## Shading

Shading analysis was done in a similar way as orientation analysis. In each location, PVNBs were sufficiently far from each other (on each side of large highways) to not cause significant shading on each other. Therefore, shading analysis on PVNBs was reserved for those where trees or buildings are close. For the remaining sites, row spacing was calculated to avoid shadowing and nearby trees or buildings were also considered when necessary.

To better understand shading influence, 3D models were built for every site except for 1, 2, 4, 8, and 18, which had no risk of shading. In each model, solstice simulations for 12 o'clock of 21/12/2021 were computed in order to visualize the sun's beams at this time of the year, since it is when the north hemisphere experiences less daily sunlight (because the sun is low) and thus more shading impact. The following image (Figure 79) shows an example of the computed 3D scene for site number 6. The remaining 3D modules can be found in Appendix B.

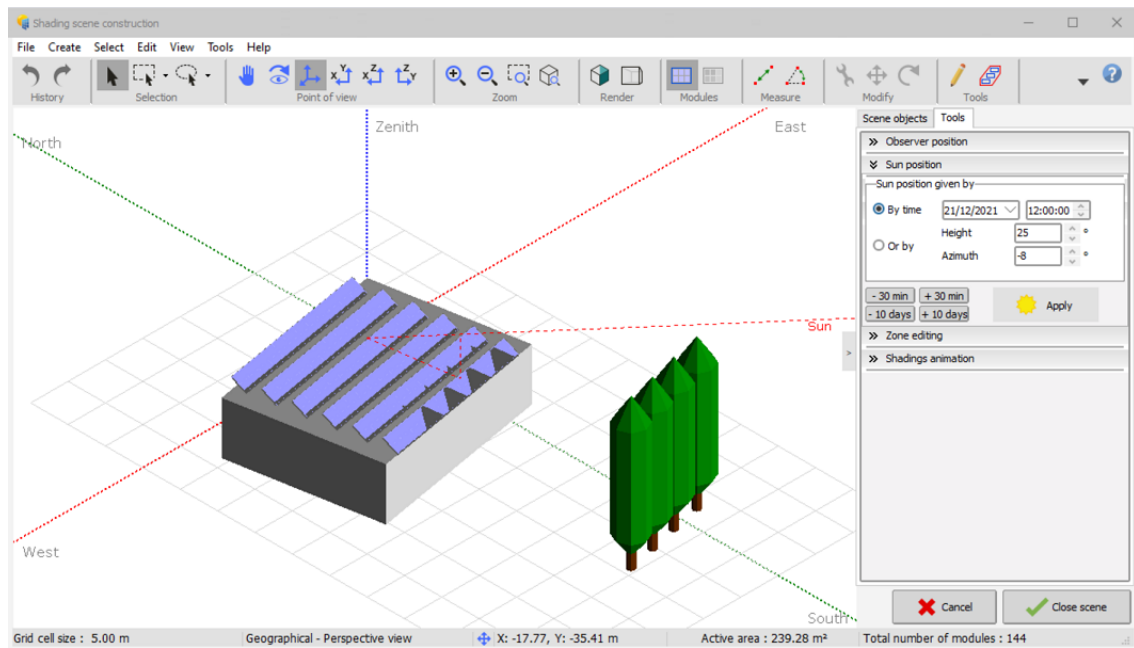


Fig. 79 - 3D shading model of site number 6 (PVsyst)

## Module choice

Various manufactures and technologies are available to be chosen. In this thesis, all modules are generic PV units with monocrystalline (Mono) silicon cells. Depending on the required total module area for each site, three different types were considered. The characteristics of each module are displayed in the table below (Table 6).

Table 6 – Module characteristics

Nominal Power at STC (Wp)	Number of Cells	Area (m <sup>2</sup> )	Voc (V)	Vmpp (V)	Isc (A)	Impp (A)	Max. Efficiency
250	60	1.627	37.40	30.70	8.63	8.14	15.36 %
300	60	1.627	37.90	31.50	9.90	9.52	18.45%
400	72	2.242	47.00	38.40	11.10	10.41	17.83%

Voc - Open circuit voltage

Vmpp - Max. power point voltage

Isc - Short-circuit current

Impp - Max. power point current

## Inverter choice

To choose the most suitable inverter for each case the following aspects were considered:

- Peak power of the PV array: the maximum amount of DC power that the inverter can convert to AC is usually lower than the maximum PV array power due to losses in the system before the inverter. The output power limits the number of modules that can be connected to it;
- Voltage: since voltage is highly influenced by temperature, values must be checked for extreme temperatures. The  $V_{mpp}$  (maximum power point voltage) has to be between the inverter operating voltage limits and the  $V_{oc}$  (open circuit voltage) needs to be lower than the input maximum voltage;
- Current: the number of strings in parallel determines the output current. This current must not exceed the maximum input current of the inverter.

Several types of inverters are available to be chosen. Table 7 shows characteristics of the chosen inverters.

*Table 7 – Inverter characteristics*

Input side (DC PV array)				Output side (AC grid)			Max. Efficiency
Power Threshold (W)	MPPT Range (V)	Absolute Max. PV voltage (V)	Max. PV current (A)	Nominal AC Power (kWac)	Max. AC current (A)	Frequency	
60	150 - 750	900	38.0	7.5	20.0	50/60 Hz	98.50%
60	150 – 750	900	38.0	9.0	20.0	50/60 Hz	98.50%
60	350 – 600	800	38.0	12.0	22.0	50/60 Hz	98.00%
200	450 – 700	900	40.0	30.0	30.0	50 Hz	94.00%
297	500 – 1450	1500	88.0	60.0	48.0	50/60 Hz	98.50%
5000	320 – 700	1000	N/A	500	800	50 Hz	97.50%

The following table (Table 8) shows each site's specifications, location, sub-arrays, orientation, as well as the modules and inverters used. As mentioned before, blue represents sites alongside highways and red represent sites alongside railways.

Table 8 – Specifications, location, sub-arrays, orientation, modules, and inverters used in each site

Site	Specifications	Location	Nbr. of arrays	Orientations (Tilt / Azimuth)	PV Module	Nbr. of Modules	Nbr. of Strings	Inverter	Nbr. of Inverters
1	Sound barrier	41°14'26.62"N 8°38'33.84"W	1	90 / 15°	Mono 400 Wp	96	6	30 kWac	1
2	Slope	41°14'24.95"N 8°38'29.31"W	1	45 / 15°	Mono 400 Wp	2375	95	60 kWac	13
3	Toll	41°14'22.03"N 8°38'15.76"W	2	35 / -5°	Mono 250 Wp	144	12	9 kWac	3
				35 / -5°	Mono 250 Wp	144	12	9 kWac	3
4	Sound barrier	41°14'23.95"N 8°38'6.66"W	1	90 / -10°	Mono 400 Wp	330	22	30 kWac	4
5	Toll	41°14'22.75"N 8°37'5.47"W	1	35 / 15°	Mono 250 Wp	144	12	9 kWac	3
6	Toll	41°14'23.38"N 8°36'37.55"W	1	35 / -10°	Mono 250 Wp	144	12	9 kWac	3
7	Toll	41°12'25.52"N 8°37'44.26"W	2	35 / 10°	Mono 250 Wp	144	12	9 kWac	3
				35 / 10°	Mono 250 Wp	144	12	9 kWac	3
8	Sound barrier	41°12'20.55"N 8°37'29.79"W	2	90 / 30°	Mono 300 Wp	680	34	30 kWac	6
				90 / 30°	Mono 300 Wp	600	30	30 kWac	6
9	Sound barrier	41°11'57.83"N 8°36'13.62"W	4	90 / 10°	Mono 300 Wp	416	26	30 kWac	4
				90 / 10°	Mono 300 Wp	140	7	30 kWac	1
				90 / 10°	Mono 300 Wp	480	24	30 kWac	4
				90 / 10°	Mono 300 Wp	28	4	7.5 kWac	1
10	Toll gate	41°14'41.68"N 8°33'56.52"W	4	18 / -20°	Mono 250 Wp	400	20	30 kWac	4
				35 / -20°	Mono 250 Wp	108	12	7.5 kWac	3
				35 / -20°	Mono 250 Wp	108	12	7.5 kWac	3
				35 / -20°	Mono 250 Wp	144	8	30 kWac	1

11	Slope	41°14'25.68"N 8°33'53.59"W	3	35 / 0°	Mono 400 Wp	1456	112	500 kWac	1
				35 / 0°	Mono 400 Wp	1280	517	500 kWac	1
				35 / 0°	Mono 400 Wp	1890	126	500 kWac	2
12	Bridge	41°14'27.62"N 8°33'40.73"W	1	35 / 0°	Mono 300 Wp	80	4	9 kWac	2
13	Sound barrier	41°13'50.80"N 8°31'34.92"W	7	90 / -10°	Mono 300 Wp	126	7	30 kWac	1
				90 / -15°	Mono 300 Wp	126	7	30 kWac	1
				90 / 0°	Mono 300 Wp	240	12	30 kWac	2
				90 / 10°	Mono 300 Wp	160	8	30 kWac	2
				90 / -10°	Mono 300 Wp	200	10	30 kWac	2
				90 / 0°	Mono 300 Wp	200	10	30 kWac	2
				90 / 10°	Mono 300 Wp	240	12	30 kWac	2
14	Toll	41°14'10.58"N 8°30'50.48"W	1	35 / 0°	Mono 250 Wp	108	12	7.5 kWac	3
15	Toll	41°14'7.61"N 8°30'49.78"W	1	35 / -5°	Mono 250 Wp	108	12	7.5 kWac	3
18	Sound barrier	41°11'48.90"N 8°29'47.33"W	3	90 / 0°	Mono 300 Wp	1700	85	500 kWac	1
				90 / 0°	Mono 250 Wp	160	8	30 kWac	1
				90 / 0°	Mono 300 Wp	800	40	30 kWac	6
22	PV canopy	41°13'58.88"N 8°39'23.76"W	2	35 / -15°	Mono 300 Wp	252	14	30 kWac	2
				35 / -15°	Mono 300 Wp	324	18	30 kWac	3
24	PV canopy	41°14'21.21"N 8°37'36.44"W	1	35 / -15°	Mono 400 Wp	2090	209	500 kWac	2
28	PV canopy	41°13'44.66"N 8°33'6.55"W	1	35 / 0°	Mono 300 Wp	1148	82	12 kWac	22
29	PV canopy	41°13'18.16"N 8°32'48.97"W	1	35 / 15°	Mono 300 Wp	1720	86	500 kWac	1

## 5. RESULTS AND DISCUSSION

The results obtained from the reported study are exposed and discussed in this chapter. Software comparison is firstly presented and is followed by a detailed analysis of the simulation results. Finally, a brief economic analysis is conducted.

### 5.1 ArcGIS and PVsyst Comparison

It is important to carry out a brief comparison between the two used softwares in terms of data collection. ArcGIS and PVsyst are applied with different purposes, as it is known. However, in this study, they shared the common ground of solar radiation data gathering.

ArcGIS results were already presented earlier in the study and served as a location assessment. In essence, they confirmed the solar potential of the studied sites. On the other hand, PVsyst radiation data, obtained via *Meteonorm 8.0* [10], were used for calculations within system simulation. Radiation data from each of these sources are compared in Table 9.

As mentioned in section 3.2, the ArcGIS classification used in this work was based on the annual average incident global horizontal solar radiation on each site and was established as follows:

- A: 2250 kWh/m<sup>2</sup> or more
- B: 1500 – 2250 kWh/m<sup>2</sup>
- C: 750 – 1500 kWh/m<sup>2</sup>
- D: 0 – 750 kWh/m<sup>2</sup>

Blue represents highway sites and red represents railway sites.

*Table 9 – Numbered sites and respective specification, location, and classification*

Site	Location	ArcGIS Classification	PVsyst Global Horizontal Annual Radiation (kWh/m <sup>2</sup> )
1	41°14'26.62"N 8°38'33.84"W	A	1596.1
2	41°14'24.95"N 8°38'29.31"W	A	1595.6
3	41°14'22.03"N 8°38'15.76"W	B	1595.7
4	41°14'23.95"N 8°38'6.66"W	C	1596.7
5	41°14'22.75"N 8°37'5.47"W	A	1597.3
6	41°14'23.38"N 8°36'37.55"W	C	1597.0

7	41°12'25.52"N 8°37'44.26"W	A	1601.7
8	41°12'20.55"N 8°37'29.79"W	A	1599.8
9	41°11'57.83"N 8°36'13.62"W	C	1602.0
10	41°14'41.68"N 8°33'56.52"W	C	1596.8
11	41°14'25.68"N 8°33'53.59"W	B	1597.2
12	41°14'27.62"N 8°33'40.73"W	B	1597.2
13	41°13'50.80"N 8°31'34.92"W	B	1597.6
14	41°14'10.58"N 8°30'50.48"W	B	1594.8
15	41°14'7.61"N 8°30'49.78"W	A	1594.8
18	41°11'48.90"N 8°29'47.33"W	B	1597.3
22	41°13'58.88"N 8°39'23.76"W	C	1594.3
24	41°14'21.21"N 8°37'36.44"W	C	1597.1
28	41°13'44.66"N 8°33'6.55"W	A	1598.8
29	41°13'18.16"N 8°32'48.97"W	C	1599.0

At first sight, the results plainly differ. Yet if we take into consideration certain aspects, the presented values can have a clearer explanation.

PVsyst gave rather constant values as oppose to ArcGIS. However, these values revolve around 1600 kWh/m<sup>2</sup>. This corresponds closely to the 1500 kWh/m<sup>2</sup> limit between classifications B and C. Given the strong and almost equal presence of these two classifications (6 sites with B classification and 7 sites with C) it is reasonable to assume that most of ArcGIS radiation values may also be distributed around the B and C limit, that is around 1500 kWh/m<sup>2</sup>. This way, results do not seem so diverse.

Nevertheless, some results are far from close. The 7 sites with A classification obtained from ArcGIS have far different radiation values than the ones obtained from PVsyst.

The global horizontal incident radiation obtained from ArcGIS was mainly based on terrain/elevation data and the results obtained from PVsyst were based on meteorological data, having more than 8000 weather stations around the world as well as 5 geostationary satellites. The following simulation results were obtained with PVsyst software and using its' radiation values.



## 5.2 Simulation Results

In this section, simulation results are presented and discussed. Yearly recorded parameters, explained in section 2.2.4, were documented for each site and are listed below:

- *Module area;*
- *Produced energy;*
- *Specific production;*
- *System losses;*
- *PV conversion efficiency at STC;*
- *Performance ratio (PR).*

The sites were grouped into structure type categories for better result comparison.

### TOLLS

Table 10 shows the results obtained for PV toll applications.

*Table 10 – Results of PV toll sites*

Site	Module Area (m <sup>2</sup> )	Produced Energy (MWh)	Specific Production (kWh/kWp)	System Losses (kWh/kWp)	PV Conversion Efficiency at STC	PR
3	469	108.6	1508	29.2	15.36%	0.818
5	234	54.04	1501	29.2	15.36%	0.818
6	234	53.94	1498	29.2	15.36%	0.812
7	469	108.8	1511	29.2	15.36%	0.821
10	1236	262.5	1381	84.0	15.36%	0.768
14	176	40.54	1501	29.2	15.36%	0.815
15	176	40.53	1501	29.2	15.36%	0.816

### Module Area

Module area is not quite an outcome of the PVsyst simulation, yet it is a very important parameter that helps comprehend certain results of this study.

In the listed sites, module area is directly related with the number of tolls. Sites 3 and 7 have practically double module area of 5 and 6 because they also comprise double the number of tolls (2 tolls as oppose to 1 in each site). Site number 10 has a much bigger module area since even more structures were considered. (2 electronic tolls, 1 toll gate, and a small toll office).

Sites 14 and 15 have far less module area because the individual tolls are located in a north-south oriented highway. Since tolls are not squared shape (length is numerically different from width), the module layout is different according to highway orientation, and so is module area.

## **Produced Energy**

The produced energy is directly related to module area, hence the results of these two parameters are very much in accordance. Slight differences amongst equal module area sites are registered only due to near shadings. Sites 5 and 6, for example, are identical in terms of module area and very similar in terms of what is considered favourable orientation ( $15^\circ$  and  $-10^\circ$  surface azimuth angles in relation to south orientation respectively), but differ on the existence of near shadings. Site 6 has nearby trees which were computed in the simulation and therefore offer small undesired shading. For this reason, site 6 produces slightly less energy during the year than site 5.

## **Specific Production**

Specific production follows a similar pattern to energy production, since it is the ratio between this parameter and the solar installed capacity. After discussing the energy production outcome, it is easy to understand the specific production's results by simply analysing its' denominator, i.e., the solar installed capacity. This parameter depends fundamentally on module type and given that the listed toll sites were set to use the same module type (Mono 250 Wp), specific production depends mainly on its numerator, that is, energy production. This is why specific production is registered to be much in accordance with the produced energy of each site. Numbers 14 and 15, for instance, reveal basically the same value of MWh produced and virtually the same specific production.

## **System Losses**

System losses are related to a number of factors, being inverter efficiency the most influential one. The first 4 sites listed in Table X were projected to use inverters of the same type (9 kWac inverter) in each system, as were sites 14 and 15 (7.5 kWac inverter).

On the other hand, site number 10 uses two types of inverters in its system (7.5 kWac and 30 kWac inverters). This potentiates mismatch losses. Furthermore, 30 kWac inverters are the least efficient inverters considered in this study (94.00% efficiency). Even though inverters are extremely efficient components, their efficiency highly influences system losses.

Despite its vast module area, site 10 is also the most influenced by shading, which results both in a loss of output and in an increased mismatch between shaded and unshaded modules. Hence the big system loss difference between site 10 and the remaining locations.

## **Conversion Efficiency**

Conversion efficiency is the percentage of electrical power that can be produced from the solar irradiance received under standard test conditions (STC). This parameter depends on the utilized solar modules. Since all toll sites used the same module type (Mono 250 Wp), the conversion efficiency was verified equal in all cases.

## Performance Ratio (PR)

Performance ratio compares the actual produced energy with the energy which would be produced in an ideal scenario, i.e., if a system was continuously working at its nominal STC. Essentially, the PR depends only on the effectively produced energy and on the overall system losses. Since system losses are the same for all the tabled sites, except for number 10, the PR analysis can be made by simply examining the produced energy column: the more energy produced, the bigger the PR. This is true for every site in the table. In addition, the system which experienced the most losses is also the one with the smallest performance ratio, that is, site number 10.

## SLOPES

The following table (Table 11) shows the results obtained for the PV systems applied in slopes alongside highways.

*Table 11 – Results of PV slope sites*

Site	Module Area (m <sup>2</sup> )	Produced Energy (MWh)	Specific Production (kWh/kWp)	System Losses (kWh/kWp)	PV Conversion Efficiency at STC	PR
2	5324	1481	1559	29.2	17.83%	0.864
11	10371	2749	1485	113.15	17.83%	0.803

## Module Area

Immediately, it is clear that the module area of each of these sites is completely different. Site 11 has almost double the module area of site 2 and this is reflected especially on energy production.

## Produced Energy

As expected, the energy produced in site 11 is much greater compared to site number 2. However, the difference is not almost double, as it is with the area. It is slightly less. The energy produced in site 11 is approximately 1.86 times higher than the produced in site 2. This proves that energy production is not only function of module area, since it is also highly influenced by system losses. Site 11 experiences much higher system losses than site 2, so energy production in site 11 is high, but is not as high as anticipated by simple module area analysis.

## Specific Production

Despite the difference in produced energy, the specific production of site 2 is actually larger than site 11. Specific production is the ratio between the effectively produced energy and the solar installed capacity, which depends essentially on PV module type. Since the two sites were equipped with the

same module type (Mono 400 Wp), this means that the energy production played a big role in this result. Proportionally, site 2 produced more effectively than site 11 so specific production was registered greater in site 2.

### System Losses

Site 11 experienced more system losses than site 2 because in the latter modules were designed to be attached to the slope. The slope in site 2 has a 45° tilt angle which is fairly acceptable for PV modules installed at the given latitude (approximately 41.2°N). Since the modules were intended to be directly mounted onto the slope, they do not create shade between them.

Conversely, in site 11 the terrain is practically flat, so modules were projected with a 35° tilt and 3.5 m distance between rows computed in the 3D shading scene. This distance was calculated to minimize shading yet they still experience some row shading, depending on the time of the year and day. This is why system losses in site 11 are higher than in site 2.

In any case, both sites experience system losses due to operation temperature, as can be seen in the system loss diagrams of Appendix C.

### Conversion Efficiency

As mentioned before, conversion efficiency depends on the efficiency of the used PV modules. In this case, both sites were projected to use the same module type (Mono 400 Wp with 17.83% efficiency) so conversion efficiency is equal.

### Performance Ratio (PR)

The performance ratio depends on the effectively produced energy and on the overall system losses. Despite high levels of energy production, site 11 also experienced very large system losses, as explained. Consequently, its PR is lower than PR of site number 2.

## BRIDGE

Table 12 shows the results obtained for the PV bridge system.

*Table 12 – Results of PV bridge site*

Site	Module Area (m <sup>2</sup> )	Produced Energy (MWh)	Specific Production (kWh/kWp)	System Losses (kWh/kWp)	PV Conversion Efficiency at STC	PR
12	130	37.39	1558	113.15	18.45%	0.842

In terms of module area, this is the smallest simulated system. Nevertheless, the produced energy is quite reasonable, mainly due to good orientation (35° tilt and 0° surface azimuth).

Specific production is rather high largely because of the powerful PV modules used (Mono 300 Wp), which ensure a good solar installed capacity.

In spite the good specific production result, system losses are evident mainly due to operating temperatures and small shadings between modules. These losses are detailly presented in the system loss diagrams, Appendix C.

PV conversion efficiency is effectively high due to the quality of the utilized modules (Mono 300 Wp).

Finally, the performance ratio is good despite the verified losses. This was due to the solid energy production result.

## SOUND BARRIERS

The following table (Table 13) shows the results obtained for the PVNBs (PV noise barriers).

*Table 13 – Results of PVNB sites*

Site	Module Area (m <sup>2</sup> )	Produced Energy (MWh)	Specific Production (kWh/kWp)	System Losses (kWh/kWp)	PV Conversion Efficiency at STC	PR
1	215	38.17	994	80.3	17.83%	0.814
4	740	130.9	992	80.3	17.83%	0.812
8	2082	384.6	1002	83.95	18.45%	0.816
9	1731	294.6	923	76.65	18.45%	0.756
18	4328	804.9	1019	29.2	18.26%	0.836

### Module Area

The module area of the listed locations varies significantly because of the different extension and hight of each sound barrier site. This is reflected directly on the produced energy.

### Produced Energy

As mentioned, produced energy depends highly on module area. Site 18 has more than 20 times bigger module area than site 1. In the same way, the energy produced by site 18 is also more than 20 times larger.

## **Specific Production**

Despite the big differences on module area and produced energy amongst the sites, specific production results are rather similar, around 1000 kWh/kWp. As known, specific production represents the ratio between the produced energy and the solar installed capacity, which depends on the used solar modules.

The simulations computed for sites 8, 9, and 18 used Mono 300 Wp modules. Site 10 used some additional Mono 250 Wp modules. For this reason, the solar installed capacity of these sites can be considered rather similar. In this sense, the specific production is simply determined by energy production. Amongst these three sites, number 18 shows the highest energy production, followed by number 8 and lastly number 9. As can be observed, specific production follows the same rule.

On the other hand, sites 1 and 4 were designed to use Mono 400 Wp. These sites register the lowest energy production in general. However, for their installed capacity, which is bigger than the remaining sites, the produced energy is somewhat high. This explains why sites 1 and 4 show similar specific production values to sites 8, 9, and 10, even though these sites had much higher energy production.

## **System Losses**

System losses are related to a number of aspects. Firstly, the angle of solar radiation incidence. In the case of these noise barriers, this angle is quite unfavourable given that modules were projected to be attached to the walls of the noise barriers, that is, with a 90° tilt. This explains common losses amongst the listed sites.

Furthermore, the surface azimuth also influences solar radiation incidence and consequently system losses. The less south-oriented site is number 8 with a surface azimuth of 30°, therefore it is also the site where more system losses are experienced. Conversely, site 18 is the best oriented one with a surface azimuth of 0°, which explains its overall small losses.

Despite the high efficiency of inverters in general, inverter efficiency deeply influences system losses. All the listed locations were projected to use 30 kWac inverters. From the listed types of inverters considered in this work, this one is the least efficient, with 94.00% max. efficiency. Sites 9 and 18 used additional more efficient inverters: 7.5 kWac with 98.50% efficiency and 500 kWac with 97.50%, respectively. This clarifies why sites 1, 4, and 8 had higher losses than sites 9 and 18.

In turn, site 9 shows more losses than 18 due to nearby trees and building shadings, which were considered in its 3D model.

## **Conversion Efficiency**

Conversion efficiency depends entirely on the utilized solar modules. Sites 1 and 4 used Mono 400 Wp modules with 17.83% efficiency, while sites 8, 9, and 10 used Mono 300 Wp modules with 18.45% efficiency. Site 10 used some additional Mono 250 Wp modules with a lower efficiency. This is why sites 8 and 9, which used more efficient modules, registered better conversion efficiency values than the remaining sites.

### Performance Ratio (PR)

The PR depends on the effectively produced energy and on the overall system losses. Site 18 experienced by far the lowest system losses and the most produced energy, therefore it presents the highest PR.

On the other hand, site 8, which registered the largest system losses, has the second highest PR value in the table. However, since the PR evaluates a system's quality and highly depends on energy output, the efficiency of the models highly influences this parameter. As mentioned before, sites 8 and 9 were equipped with the more efficient models (Mono 300 Wp with 18.45%). Given that site 8 had more energy production, it presents also a higher PR.

Site 9 registers the lowest PR possibly due to shading, since this site had many trees and houses nearby. Shading blocks part of the solar irradiation received which significantly reduces the systems' output, therefore lowering its' PR.

### PV CANOPIES

Table 14 shows the results obtained for the PV canopy systems applied in railways.

*Table 14 – Results of PV canopy sites*

Site	Module Area (m <sup>2</sup> )	Produced Energy (MWh)	Specific Production (kWh/kWp)	System Losses (kWh/kWp)	PV Conversion Efficiency at STC	PR
22	937	247.9	1434	109.5	18.45%	0.783
24	4685	1227	1468	29.2	17.83%	0.799
28	1868	517.2	1502	113.15	18.45%	0.811
29	2798	771.8	1496	29.2	18.45%	0.814

#### Module Area

Once again, module area differs quite substantially between sites. Site 24 has exactly 5 times the module area of site 22.

#### Produced Energy

As it is known, the produced energy highly depends on module area and the two parameters are much in accordance, as it was expected.

## **Specific Production**

Specific production is rather similar amongst the listed locations. As mentioned before, this parameter represents the ratio between the produced energy and the solar installed capacity, which highly depends on module type.

Sites 22, 28 and 29 were designed to use Mono 300 Wp modules. This means that the solar installed capacity is fairly similar. Thus, what determines specific production in these sites is their energy production. As observed, the more energy produced, the higher the specific production.

Conversely, the modules used in site 24 were Mono 400 Wp. This means that the solar installed capacity in site 24 is higher than in the other locations. Even though this site registers the higher energy production, it is not that high when compared to its installed capacity. That is why this site has lower specific production than sites 28 and 29, even though these sites have lower energy production.

## **System Losses**

System losses are most dependent on the type of inverter used, despite their overall high efficiency when compared to other system components. Site 22 registered high system losses mainly because it used the least efficient type of inverter from the list of inverters considered in this study: the 30 kWac with an efficiency of 94.00%.

Site 28, however, registered the higher losses. Although the type of inverter used was very efficient (12 kWac with 98.00% efficiency), its low threshold power (60 W) and MPPT range required the use of lots of inverters to fulfil the systems' necessities. 22 inverters were used in this site. This number of inverters potentiates mismatch and wire losses.

Significant operation temperature losses were also identified in all four sites, as shown in the system loss diagrams in Appendix C.

## **Conversion Efficiency**

The conversion efficiency was overall good. This parameter depends exclusively on the utilized solar modules. All tabled sites used Mono 300 Wp modules with 18.45% efficiency, with exception of site 24, which used Mono 400 Wp modules with 17.83% efficiency.

## **Performance Ratio (PR)**

As mentioned earlier, the PR depends on the effectively produced energy and on the overall system losses.

Sites 24 and 29 experienced the least system losses. Site 29 registered the highest PR even though it was the second largest energy producer, after site 24. In turn, site 24 has the second lowest PR, despite its' impressive energy production. This might be explained by near shadings (computed in the site's 3D model), which influence the solar irradiation received, which reduces the systems' output. The lower the output, the lower the PR.



Although site 28 registered the highest system losses, site 22 (which also experienced high losses) is the one with the lowest PR. This is simply clarified by observing site's 22 energy production. It is by far the lowest in the list.

### **5.3 Selection**

After discussing the results, the sites were once more subjected to a selection. Since the PR is the ultimate quality assessing parameter, the 5 sites with the lowest PR were excluded (9 to 11, 22, and 24).

The remaining 15 sites (1 to 8, 12, 13, 14, 15, 18, 28, and 29) are economically analysed in the following section.



## 6. Economic Analysis

In this section, a brief economic analysis is explained. This serves as complement of the results obtained earlier and helps point out the sites with not only better solar potential but also more economically viable.

This analysis started with a price data gathering in regard to the components used in the simulations, namely PV modules and inverters. As mentioned in section 3.3.2, generic components were used and do not correspond to any particular type of brand or model. This way, the PV modules and inverters used in the simulations were associated to real models, taking in consideration their specifications. The specifications of the generic components used in the simulations are listed in section 3.3.2 and the datasheets of the real models in Appendix D.

Thanks to this association, it was possible to set adequate market prices to the PV modules and inverters used in the simulations. Table 15 shows the established correlations. Price information was obtained via *Europe Solar Store* [46].

*Table 15 – Correlations established between generic components used in the simulations, real component models, and component prices*

PV Modules		
Generic PV Module (used in simulations)	Real PV Module Model	Price per module
Mono 250 Wp	Victron 260W-20V Poly	138.00 €
Mono 300 Wp	LG MonoX Plus LG300S1C-A5	172.00 €
Mono 400 Wp	SunPower SPR-MAX3-400	334.00 €
Inverters		
Generic Inverter (used in simulations)	Real Inverter Model	Price per inverter
7.5 kWac	Fronius Primo 8.2-1	1,381.00 €
9.0 kWac	Solax X3-9.0-T	1,243.00 €
12.0 kWac	Sungrow SG12RT	1,472.00 €
30.0 kWac	GoodWe GW30K-MT	1,992.00 €
60.0 kWac	GoodWe GW60KN-MT	2,968.00 €
500 kWac	EFASOLAR 500	4,630.28 €

Using the notions of PV economics, it was possible to calculate the *initial investment* as well as estimate the *annual return* and *payback time* for each site.

In this study, the initial investment accounts only for PV module and inverter costs. Other dismissed incumbencies in this analysis include costs of capital and annual operating costs.

The price of energy was considered to be 0.21 €/kWh, including taxes. This value was consulted in the official website of EDP – *Energias de Portugal* [47].

The following table (Table 16) shows each site’s initial investment, annual return, and payback time.

*Table 16 – Initial investment, annual return, and payback time for each site*

Site	Initial Investment	Annual Return (€/year)	Payback Time (years)
1	34,056.00 €	8015.7	4.25
2	831,834.00 €	311010	2.67
3	47,202.00 €	22806	2.07
4	118,188.00 €	27489	4.30
5	23,601.00 €	11348.4	2.08
6	23,601.00 €	11327.4	2.08
7	47,202.00 €	22848	2.07
8	244,064.00 €	80766	3.02
12	16,246.00 €	7851.9	2.07
13	246,128.00 €	80703	3.05
14	19,047.00 €	8513.4	2.24
15	19,047.00 €	8511.3	2.24
18	470,654.28 €	169029	2.78
28	229,840.00 €	108612	2.12
29	300,470.28 €	162078	1.85

After careful observation of these results, it is possible to perform one final site selection. Since payback time expresses the relation between the other two parameters, a few sites can be considered less economically fitting, namely sites 1, 4, 8, 13, and 18, which present higher payback time. This way, the 10 sites which can be considered as the ones with more solar potential and more economical feasibility are: 2, 3, 5, 6, 7, 12, 14, 15, 28, and 29.

The obtained economic results are obviously very optimistic given the considerations mentioned before. Nevertheless, this brief economic analysis allows a different perspective on what one might consider as suitable sites for non-conventional highway/railway PV applications.

## 7. CONCLUSION AND FUTURE WORKS

The conducted study reached its primary objective of selecting the 10 sites for non-conventional highway and railway grid-connected PV applications with the most solar potential and economic viability out of the 30 initially proposed locations in the designated area.

Different subject fields were interconnected throughout this work. From the fundamentals of solar technologies and PV systems to the non-conventional applications of those systems. From the geographical data processing and analysis with ArcGIS software to the 3D model creation and PV simulation with PVsyst software, as well as an economic overview. The collectiveness of knowledge covered in this study allowed a wide and wholesome perspective on the latest PV technologies and their integration on a semi-urban environment.

The final result represents a positive standpoint of non-conventional PV applications with one slope site (2), six toll sites (3, 5, 6, 7, 14, 15), one bridge (12), and two PV canopies (28, 29) as the most promising locations in the area both in solar potential and in economic feasibility.

From all the studied sites, the slope site (2) registered the uppermost PR value of 0.864 as well as a paramount high electricity production of 1481 MWh, with rather low system losses. Therefore, it proves to be the most promising of all sites in terms of electricity generation.

Clearly, toll sites also represent an excellent PV application and should be considered for practical installation, since out of the 7 toll sites only one was discarded. Although considered for a grid-connected implementation, this application may even be considered for charging electronic tolls with solar power and the surplus energy production being delivered to the grid.

While not economically viable, most of the proposed PV noise barriers (1, 4, 8, 13, and 18) showed great solar potential despite their unfavourable tilt angle of 90° compared to other applications. The energy production results could have been even better if the considered area contained north-south oriented highways with noise barriers. This way, bifacial modules could have been considered, harnessing energy on one side during half of the day and on the other side during the other half of the day, which would maximize energy production.

In this sense, future works may be considered both on the optimization of the PV noise barriers and tolls as well as on the geographical expansion of this type of study. Portugal has indisputable potential in terms of solar exposition when compared to other European countries. Moreover, it has an extensive highway and railway network for its size. For these reasons, similar studies should be furtherly considered on a national scale.

All in all, this study validates the potential of non-conventional grid-connected PV applications in highways and railway with a few limitations, namely in the ArcGIS analysis section. Although the input data is correct, it lacks on tree and building mapping, since it is purely based on terrain elevation (SRTM data). This influences the subsequent incident solar radiation calculation results. The second major limitation of this work is related to the economic analysis. As mentioned before, only module and inverter costs were considered, which makes it a slightly narrow economic standpoint.

In conclusion, the present work demonstrates that the described PV applications can be not only environmentally friendly and convenient for the selected location but also economically attractive.



## 8. REFERENCES

1. Zhong, T., et al., *Assessment of solar photovoltaic potentials on urban noise barriers using street-view imagery*. *Renewable Energy*, 2021. **168**: p. 181-194.
2. *Renewables 2021 - Global Status Report*. REN 21, 2021.
3. Ministros, P.d.C.d., *Decreto-Lei n.º 162/2019*. 2019: Diário da República, 1.ª série. p. 45.
4. *Direção-Geral de Energia e Geologia* (via [www.dgeg.gov.pt](http://www.dgeg.gov.pt)).
5. *National Geographic Society* (via [www.nationalgeographic.org](http://www.nationalgeographic.org)).
6. John A. Duffie, W.A.B., *Solar Engineering of Thermal Processes*. 2013.
7. Kalogirou, S., *Solar Energy Engineering: Processes and Systems*. 1st ed. 2009.
8. Jäger, K., *Solar Energy - Fundamentals, Technology and Systems*. 2014.
9. Martin Kaltschmitt, W.S., Andreas Wiese, *Renewable Energy, Technology, Economics and Environment*. 2007.
10. *Meteonorm 8.0 software* (via [www.meteonorm.com](http://www.meteonorm.com)).
11. *Green Rhino Energy* (via [www.greenrhinoenergy.com](http://www.greenrhinoenergy.com)).
12. David Tan, A.K.S., *Handbook for Solar PV Systems*. 2009.
13. *Florida Solar Energy Center - FSEC* (via <https://energyresearch.ucf.edu/>).
14. Rabindra Kumar Satpathy, V.P., *Solar PV Power: Design, Manufacturing and Applications from Sand to Systems*. 2021.
15. Pearsall, N.M., *Introduction to photovoltaic system performance*, in *The Performance of Photovoltaic (PV) Systems*. 2017. p. 1-19.
16. Angèle Reinders, P.V., Wilfried van Sark, Alexandre Freundlich, *Photovoltaic Solar Energy (From Fundamentals to Applications) - The Economics of PV Systems*. 2017.
17. Jordan, D.C. and S.R. Kurtz, *Photovoltaic Degradation Rates-an Analytical Review*. *Progress in Photovoltaics: Research and Applications*, 2013. **21**(1): p. 12-29.
18. Henemann, A., *BIPV Built-in solar energy*. 2008.
19. Petter Jelle, B., C. Breivik, and H. Drolsum Røkenes, *Building integrated photovoltaic products: A state-of-the-art review and future research opportunities*. *Solar Energy Materials and Solar Cells*, 2012. **100**: p. 69-96.
20. U.S. Department of Transportation, F.H.A., Office of Natural Environment, , *Highway Renewable Energy: Photovoltaic Noise Barriers*. 2017.
21. De Schepper, E., et al., *Combining photovoltaics and sound barriers – A feasibility study*. *Renewable Energy*, 2012. **46**: p. 297-303.
22. Harinarayana, P.S.a.T., *Solar energy generation potential along national highways*. Sharma and Harinarayana *International Journal of Energy and Environmental Engineering* 2013.
23. [www.solar-panel-mounting.com](http://www.solar-panel-mounting.com).
24. A. Coutu, R., et al., *Engineering Tests to Evaluate the Feasibility of an Emerging Solar Pavement Technology for Public Roads and Highways*. *Technologies*, 2020. **8**(1).
25. Akbari H, R.L., *Characterizing the Fabric of the Urban Environment - A Case Study of Metropolitan Chicago, Illinois*. 2001.
26. Aghaei, M., et al., *New concepts and applications of solar PV systems*, in *Photovoltaic Solar Energy Conversion*. 2020. p. 349-390.
27. Zhou, B., et al., *A review on solar pavement and photovoltaic/thermal (PV/T) system*. *Transportation Research Part D: Transport and Environment*, 2021. **93**.
28. Radziemska, E., *The effect of temperature on the power drop in crystalline silicon solar cells*. 2003.
29. Hai-feng Jiang, Y.-q.C., Xu-dong Zha, Qi-sen Zhang, *Current Situation and Development Trend of Solar Pavement Technology*. 2018.
30. *The Green Optimistic Journal* (via [www.greenoptimistic.com](http://www.greenoptimistic.com)).

31. *Solar Energy Research Institute of Singapore (SERIS) at the National University of Singapore (NUS)* (via <https://www.seris.nus.edu.sg/>).
32. Mohit Acharya, S.D., *Floating Solar Photovoltaic (FSPV) A Third Pillar to Solar PV Sector?* 2019: The Energy and Resources Institute (TERI).
33. Clota, M.R. and P.R.-C. , Giuseppe Marco Tina, *Submerged PV solar panel for swimming pools: SP3*. 2017.
34. Goetzberger, A. and A. Zastrow, *On the Coexistence of Solar-Energy Conversion and Plant Cultivation*. International Journal of Solar Energy, 2007. **1**(1): p. 55-69.
35. Weselek, A., et al., *Agrophotovoltaic systems: applications, challenges, and opportunities. A review*. Agronomy for Sustainable Development, 2019. **39**(4).
36. Horst, R.R.v.d., *Solar farms on agricultural land: a partial equilibrium analysis*. 2019.
37. Jessica Owley, A.W.M., *The New Agriculture: From Food Farms to Solar Farms*. 2019.
38. Trommsdorff, M., *An economic analysis of agrophotovoltaics opportunities, risks and strategies toward a more efficient land use*. 2016.
39. Gorjian, S., et al., *On-farm applications of solar PV systems*, in *Photovoltaic Solar Energy Conversion*. 2020. p. 147-190.
40. *Environmental Systems Research Institute (ESRI)* (via [www.esri.com](http://www.esri.com)).
41. *ArcGIS Pro 2.9 Geographic and Vertical Coordinate System Tables*
42. *Forest GIS database* (via [www.forest-gis.com](http://www.forest-gis.com)).
43. *ArcGIS Pro software* (via [www.pro.arcgis.com](http://www.pro.arcgis.com)).
44. *PVsyst software* (via [www.pvsyst.com](http://www.pvsyst.com)).
45. *Meteoblue database* ([www.meteoblue.com](http://www.meteoblue.com)).
46. *Europe Solar Store* (via [www.europe-solarstore.com](http://www.europe-solarstore.com)).
47. *EDP - Energias de Portugal* (via [www.edp.pt](http://www.edp.pt)).



## APPENDIX A – ArcGIS Global Radiation Calculation

### Global radiation calculation

Global radiation ( $G_{\text{Global}_{\text{tot}}}$ ) is calculated as the sum of direct ( $D_{\text{Dir}_{\text{tot}}}$ ) and diffuse ( $D_{\text{Dif}_{\text{tot}}}$ ) radiation of all sun map and sky map sectors, respectively.

$$G_{\text{Global}_{\text{tot}}} = D_{\text{Dir}_{\text{tot}}} + D_{\text{Dif}_{\text{tot}}}$$

### Direct solar radiation

Total direct insolation ( $D_{\text{Dir}_{\text{tot}}}$ ) for a given location is the sum of the direct insolation ( $D_{\text{Dir}_{\theta,\alpha}}$ ) from all sun map sectors:

$$D_{\text{Dir}_{\text{tot}}} = \sum D_{\text{Dir}_{\theta,\alpha}} \quad (1)$$

The direct insolation from the sun map sector ( $D_{\text{Dir}_{\theta,\alpha}}$ ) with a centroid at zenith angle ( $\theta$ ) and azimuth angle ( $\alpha$ ) is calculated using the following equation:

$$D_{\text{Dir}_{\theta,\alpha}} = S_{\text{Const}} * \beta^{m(\theta)} * \text{SunDur}_{\theta,\alpha} * \text{SunGap}_{\theta,\alpha} * \cos(\text{AngIn}_{\theta,\alpha}) \quad (2)$$

■ where:

- $S_{\text{Const}}$  — The solar flux outside the atmosphere at the mean earth-sun distance, known as solar constant. The solar constant used in the analysis is 1367 W/m<sup>2</sup>. This is consistent with the World Radiation Center (WRC) solar constant.
- $\beta$  — The transmissivity of the atmosphere (averaged over all wavelengths) for the shortest path (in the direction of the zenith).
- $m(\theta)$  — The relative optical path length, measured as a proportion relative to the zenith path length (see equation 3 below).
- $\text{SunDur}_{\theta,\alpha}$  — The time duration represented by the sky sector. For most sectors, it is equal to the day interval (for example, a month) multiplied by the hour interval (for example, a half hour). For partial sectors (near the horizon), the duration is calculated using spherical geometry.
- $\text{SunGap}_{\theta,\alpha}$  — The gap fraction for the sun map sector.
- $\text{AngIn}_{\theta,\alpha}$  — The angle of incidence between the centroid of the sky sector and the axis normal to the surface (see equation 4 below).

Relative optical length,  $m(\theta)$ , is determined by the solar zenith angle and elevation above sea level. For zenith angles less than 80°, it can be calculated using the following equation:

$$m(\theta) = \text{EXP}(-0.000118 * \text{Elev} - 1.638 * 10^{-9} * \text{Elev}^2) / \cos(\theta) \quad (3)$$

■ where:

- $\theta$  — The solar zenith angle.
- $\text{Elev}$  — The elevation above sea level in meters.

The effect of surface orientation is taken into account by multiplying by the cosine of the angle of incidence. Angle of incidence ( $\text{AngIn}_{\text{Sky}_{\theta,\alpha}}$ ) between the intercepting surface and a given sky sector with a centroid at zenith angle and azimuth angle is calculated using the following equation:

$$\text{AngIn}_{\theta,\alpha} = \text{acos}(\cos(\theta) * \cos(G_z) + \sin(\theta) * \sin(G_z) * \cos(\alpha - G_a)) \quad (4)$$

■ where:

- $G_z$  — The surface zenith angle.  
Note that for zenith angles greater than 80°, refraction is important.
- $G_a$  — The surface azimuth angle.

## APPENDIX B – 3D Shading Models (PVsyst)

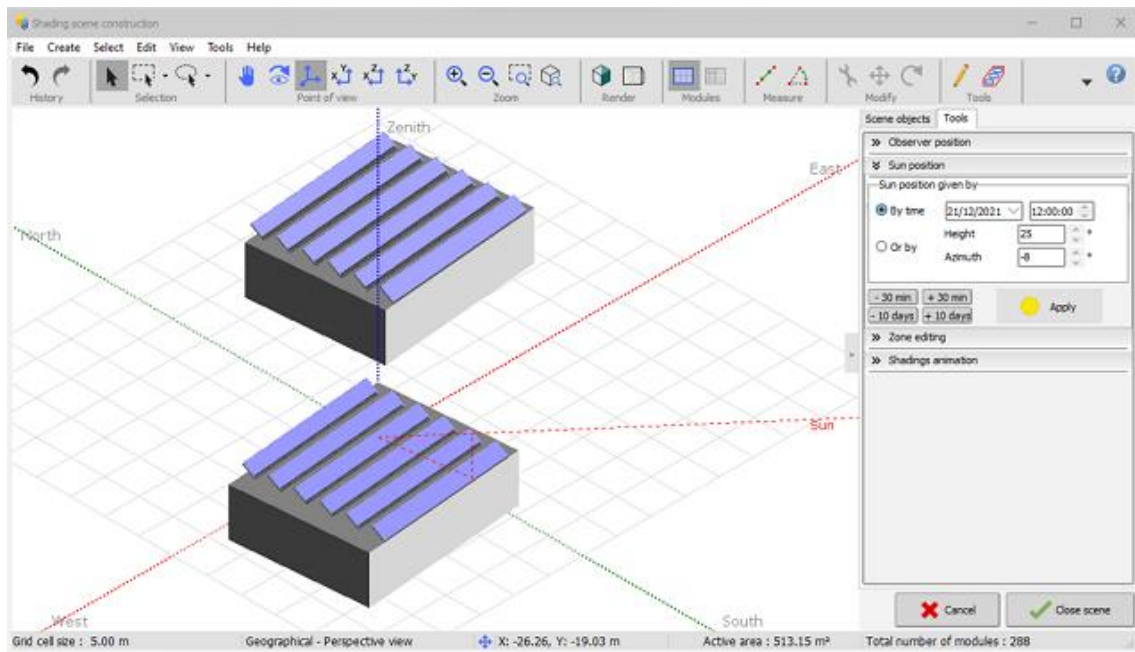


Fig. B.1 – 3D Shading Model of site 3

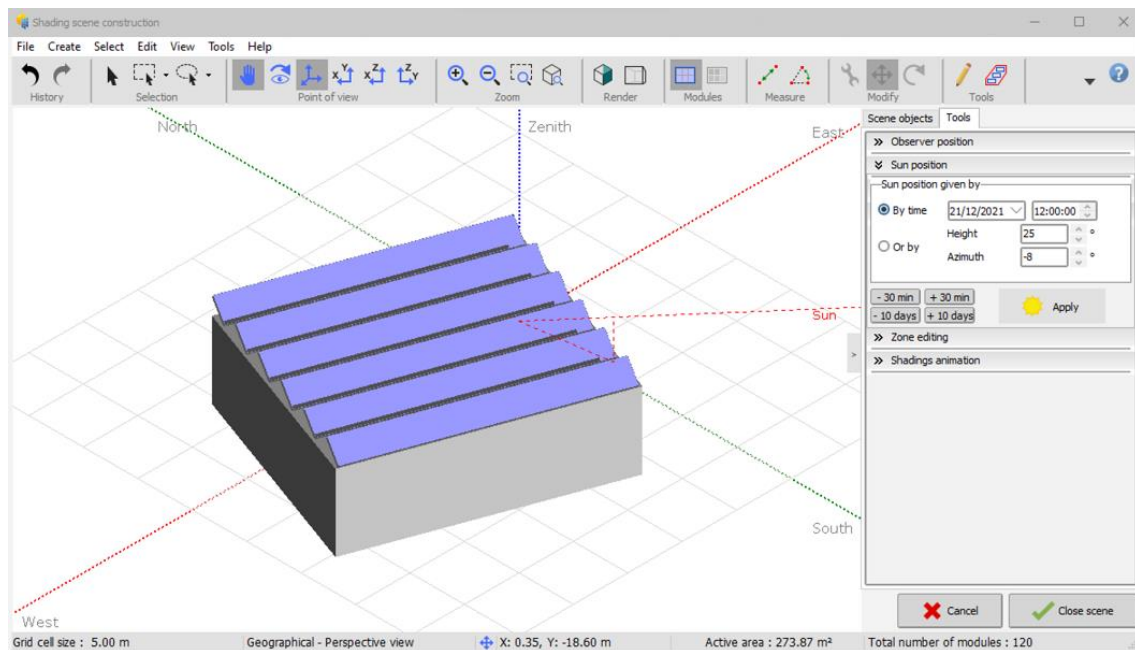


Fig. B.2 – 3D Shading Model of site 5

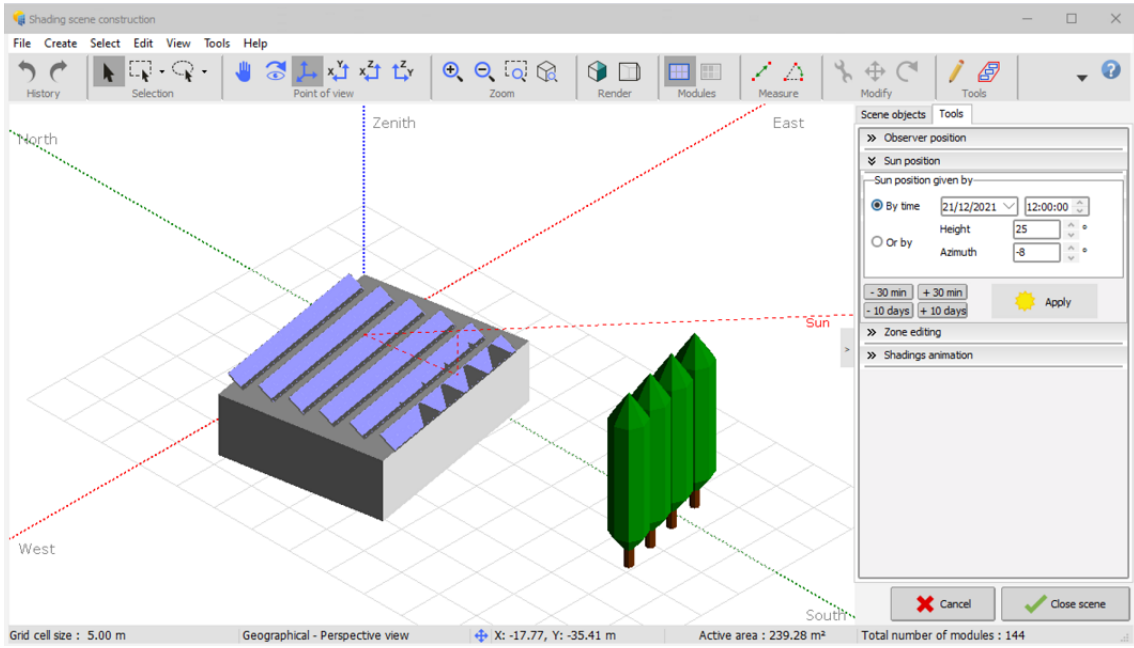


Fig. B.3 – 3D Shading Model of site 6

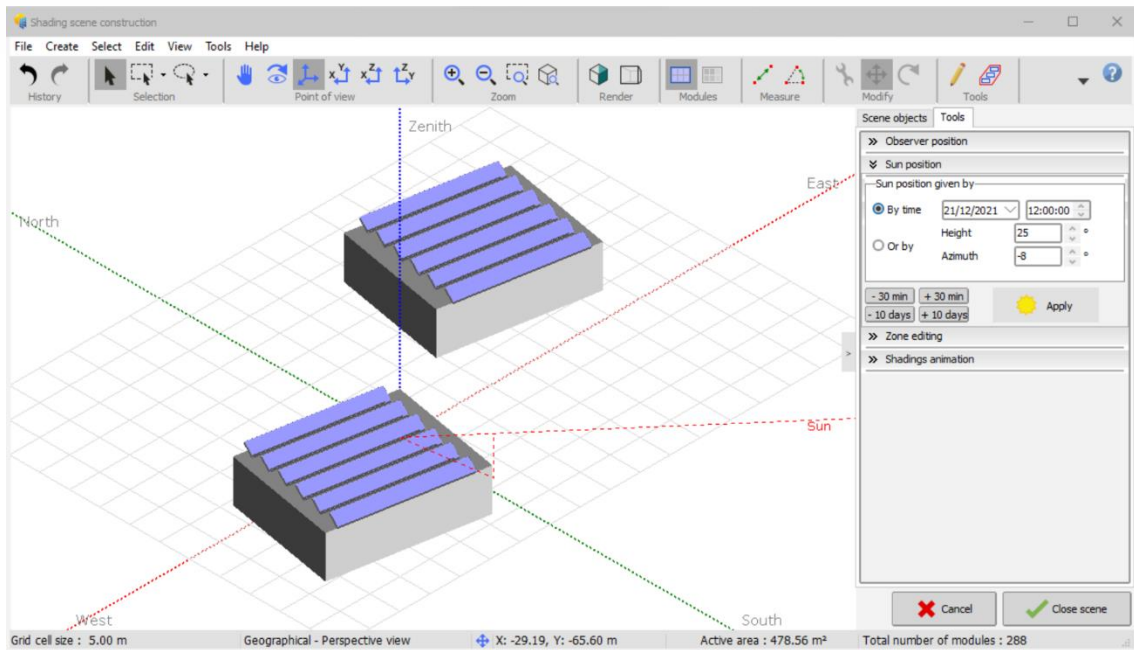


Fig. B.4 – 3D Shading Model of site 7

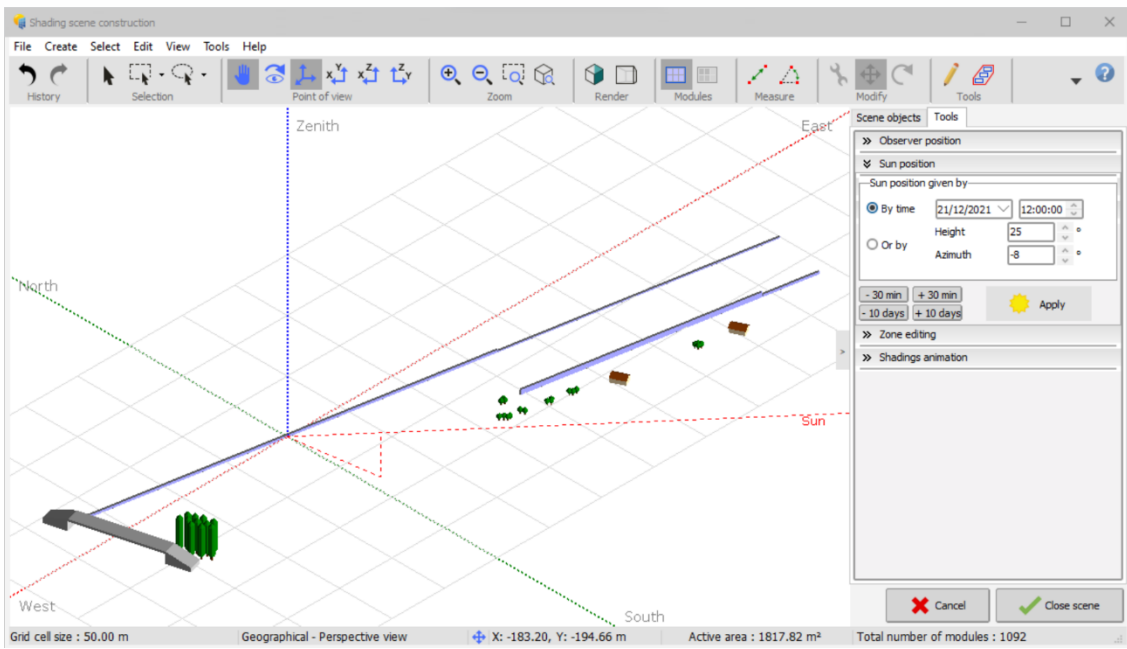


Fig. B.5 – 3D Shading Model of site 9

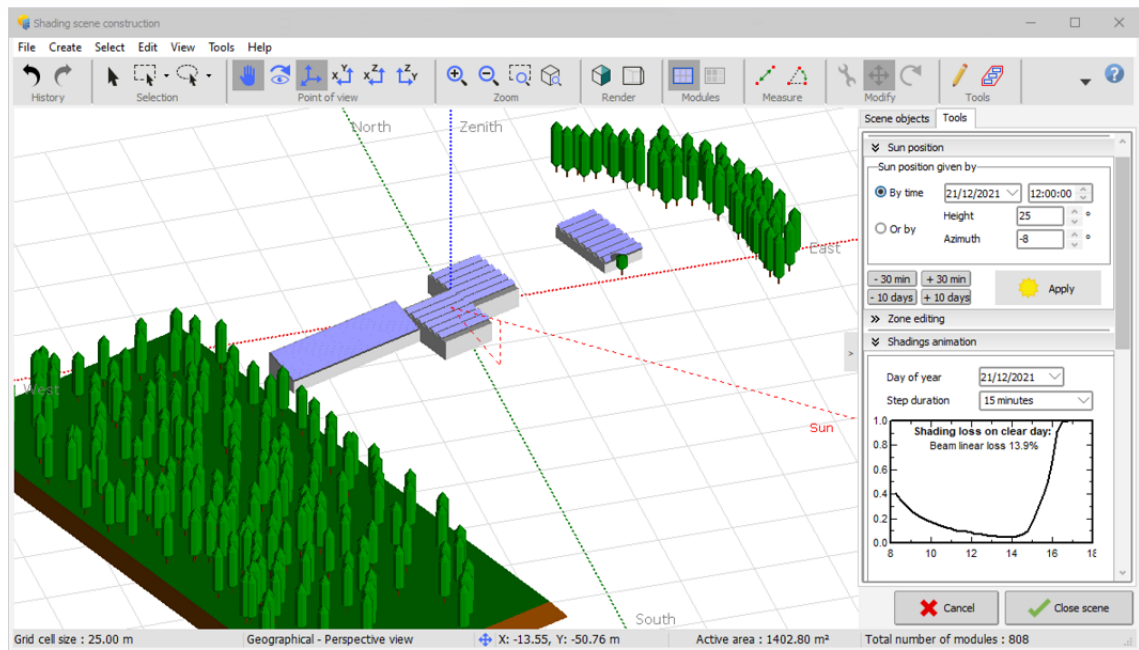


Fig. B.6 – 3D Shading Model of site 10

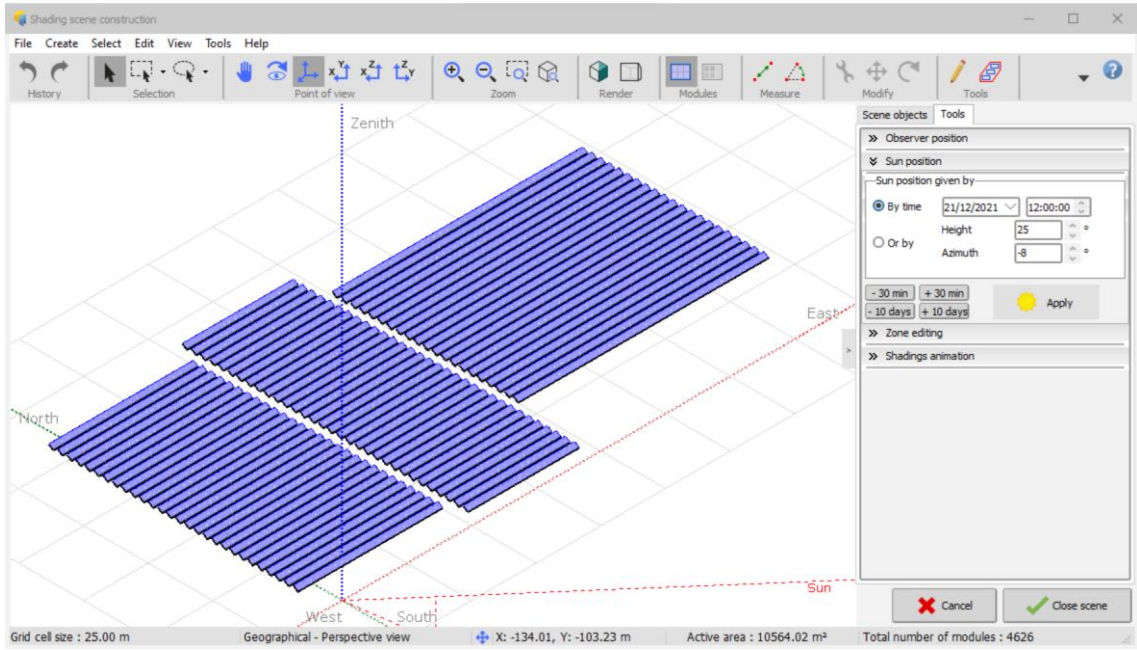


Fig. B.7 – 3D Shading Model of site 11

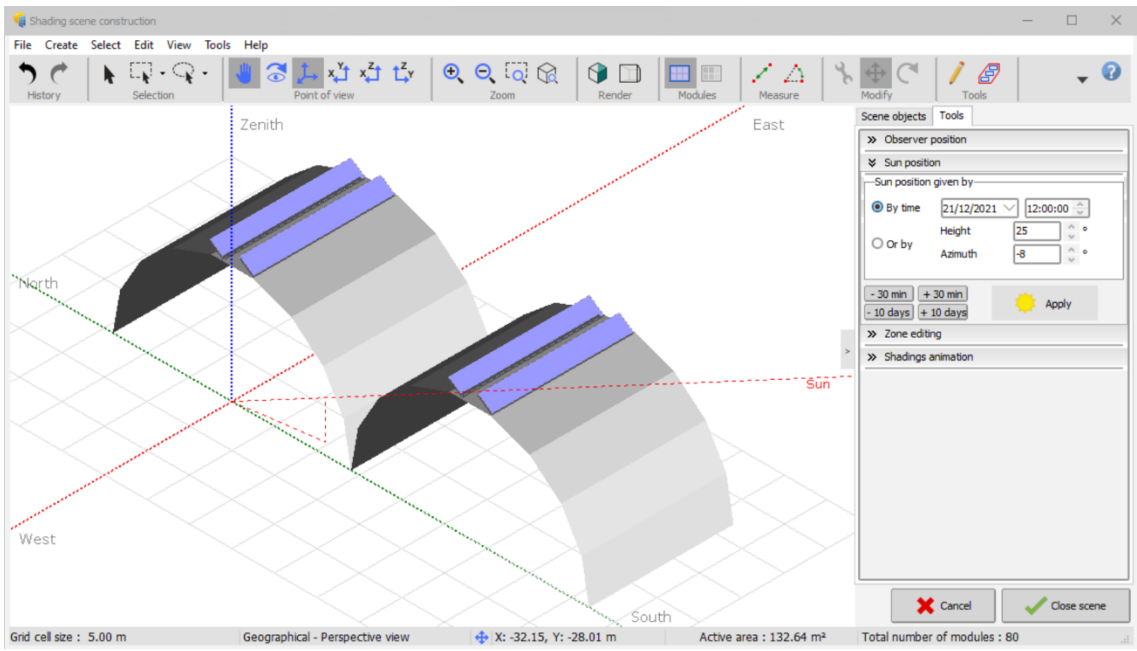


Fig. B.8 – 3D Shading Model of site 12

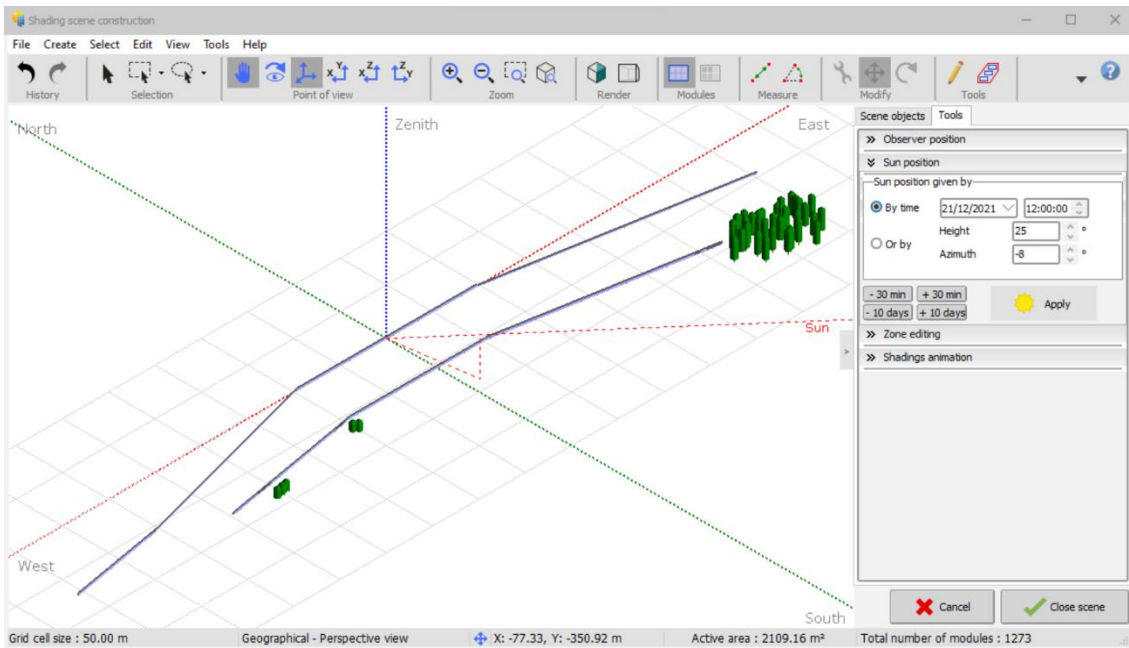


Fig. B.9 – 3D Shading Model of site 13

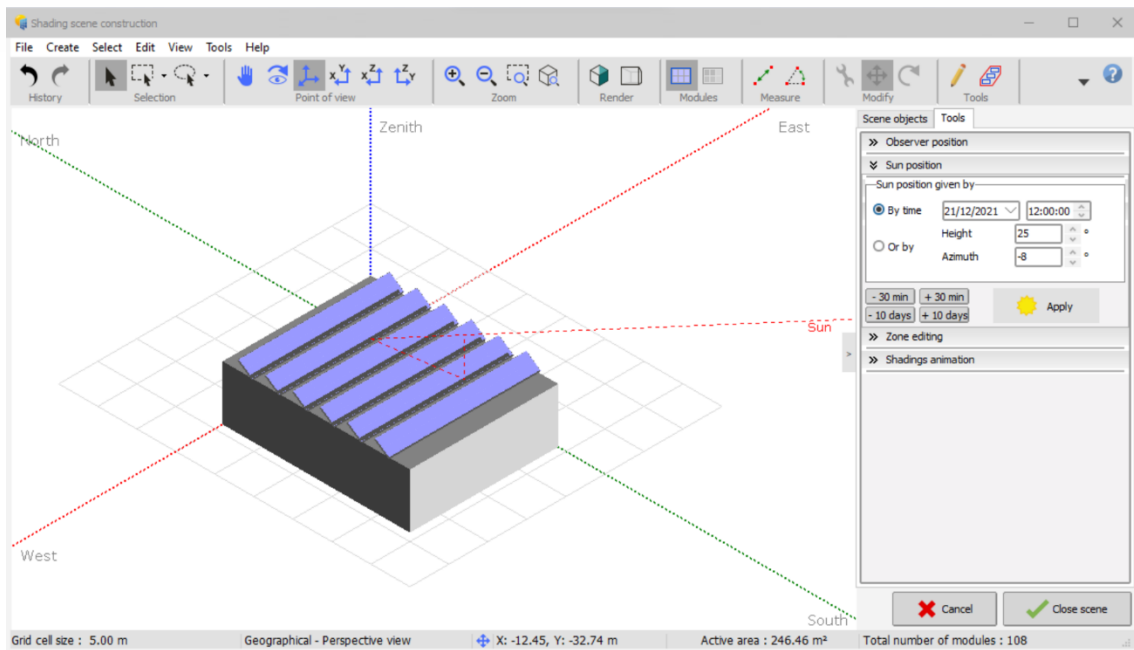


Fig. B.10 – 3D Shading Model of site 14

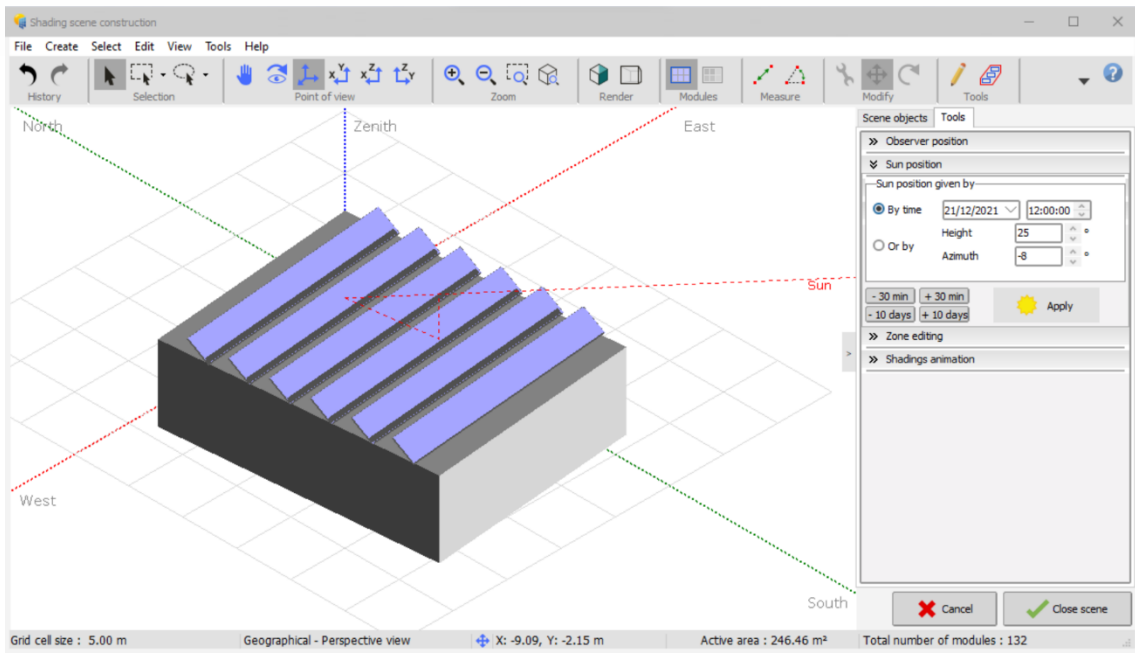


Fig. B.11 – 3D Shading Model of site 15

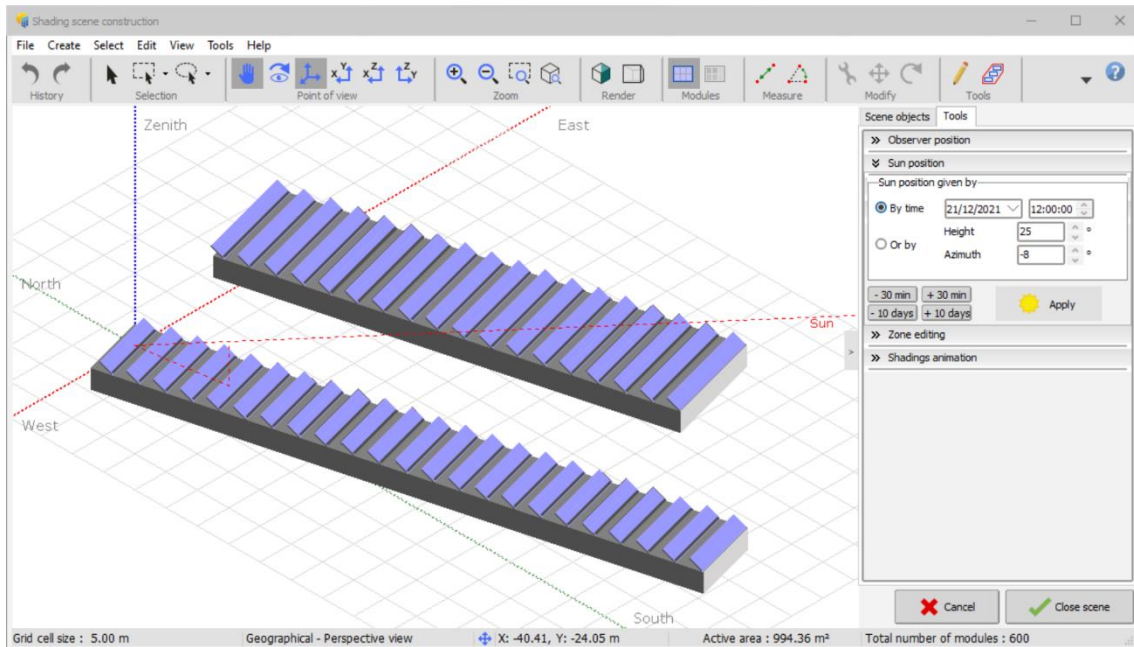


Fig. B.12 – 3D Shading Model of site 22

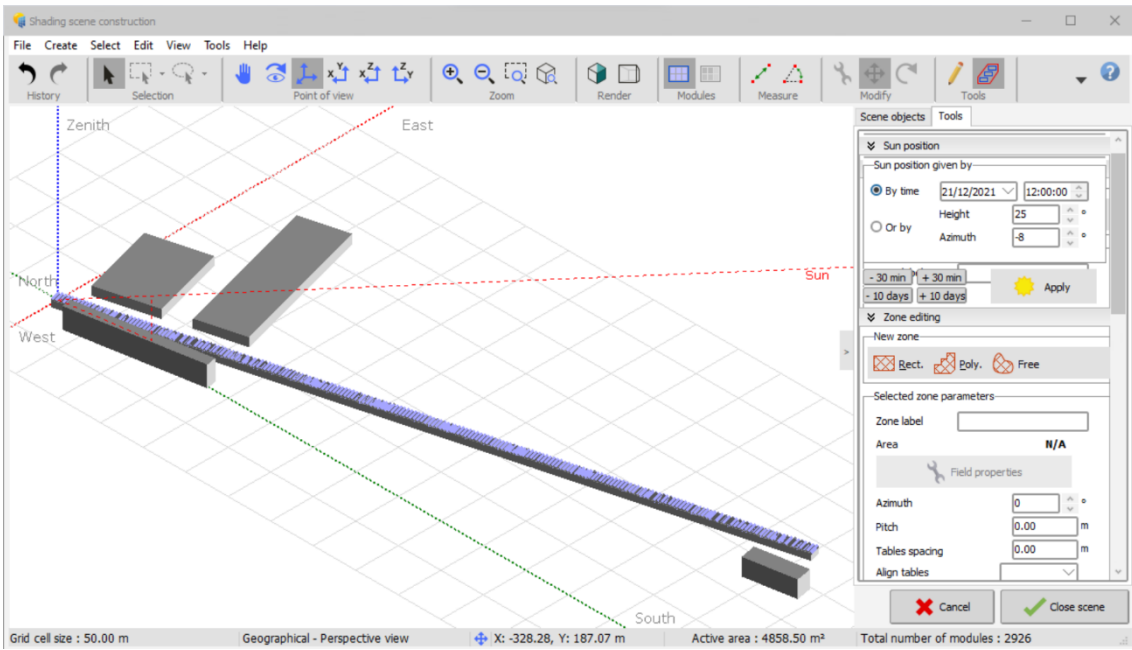


Fig. B.13 – 3D Shading Model of site 24

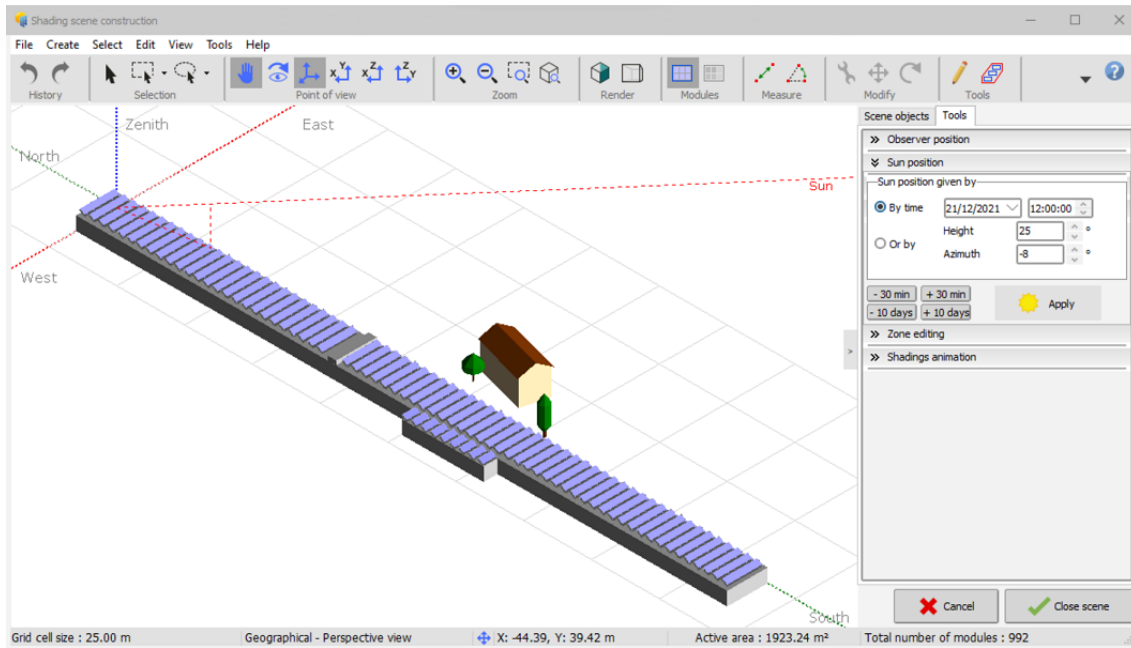


Fig. B.14 – 3D Shading Model of site 28



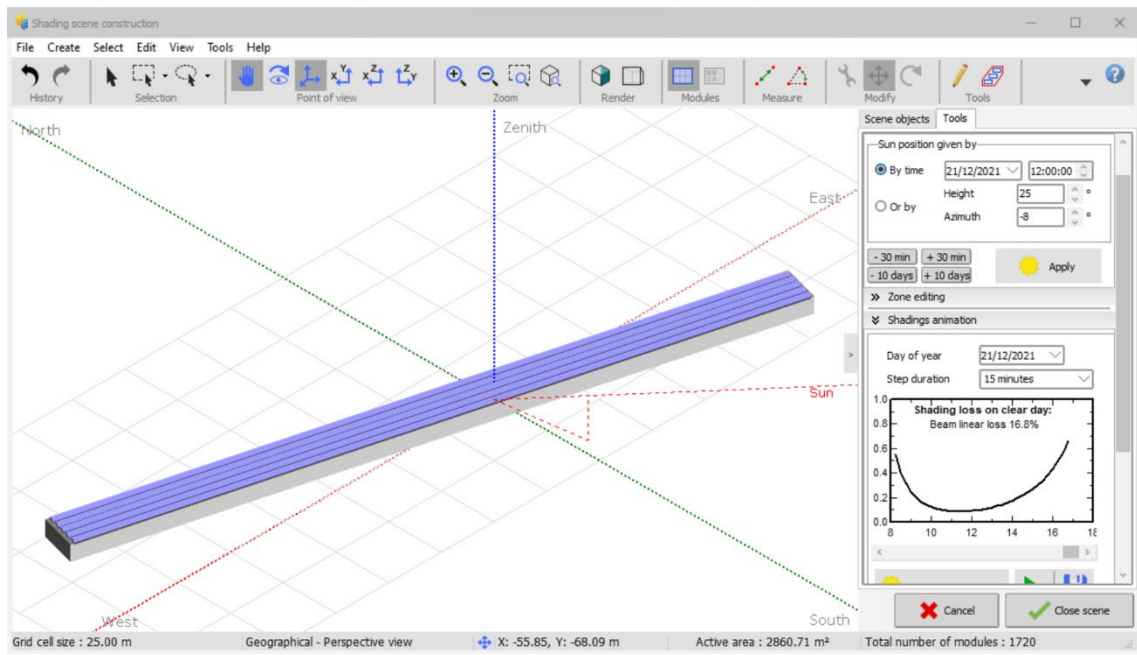


Fig. B.15 – 3D Shading Model of site 29

## APPENDIX C – Loss Diagrams (PVsyst)

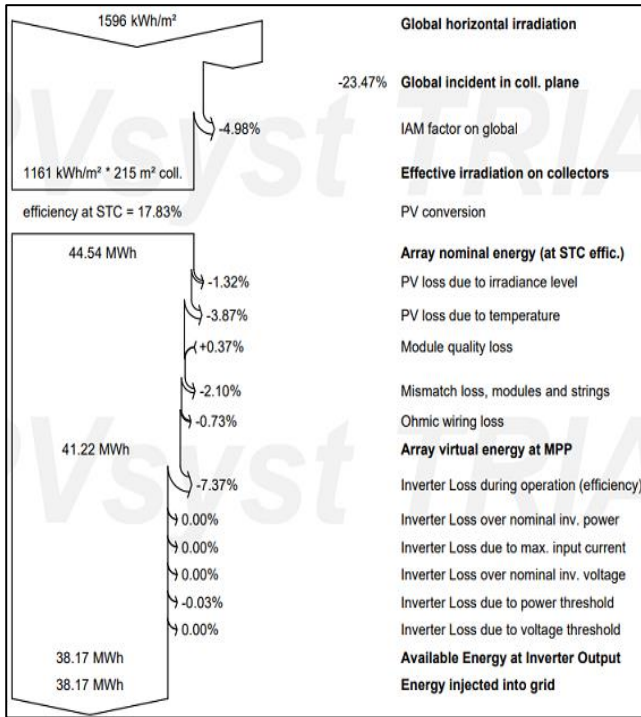


Fig. C.1 – Loss diagram of site 1

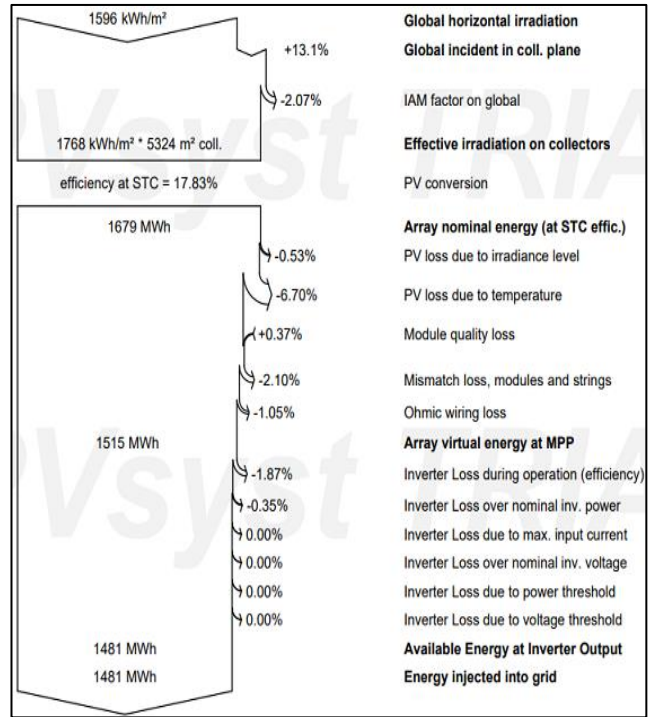


Fig. C.2 – Loss diagram of site 2

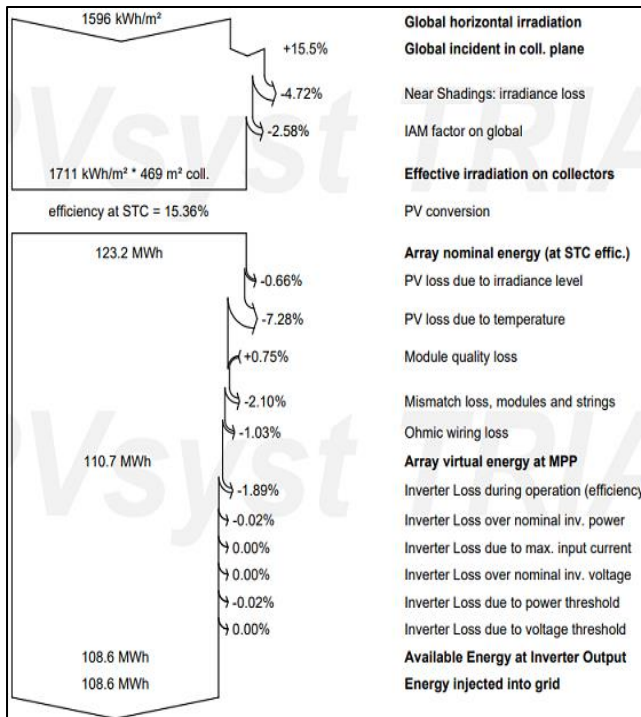


Fig. C.3 – Loss diagram of site 3

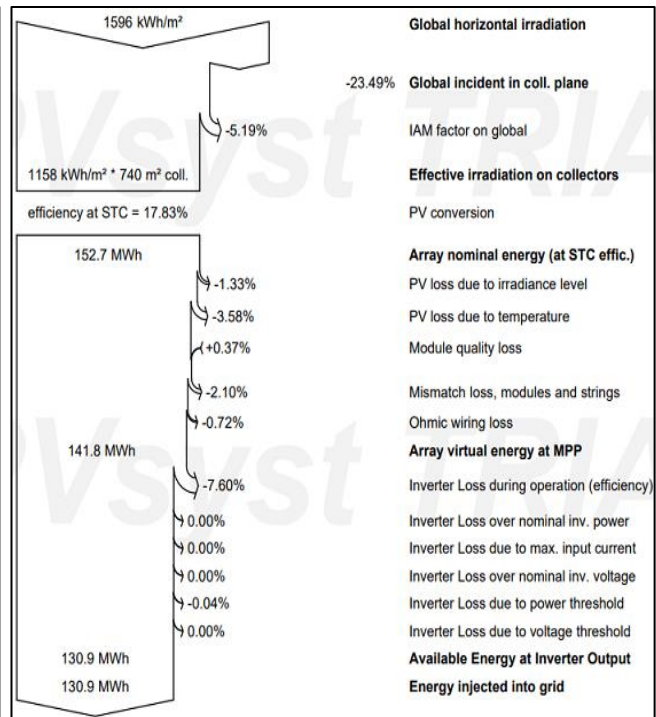


Fig. C.4 – Loss diagram of site 4

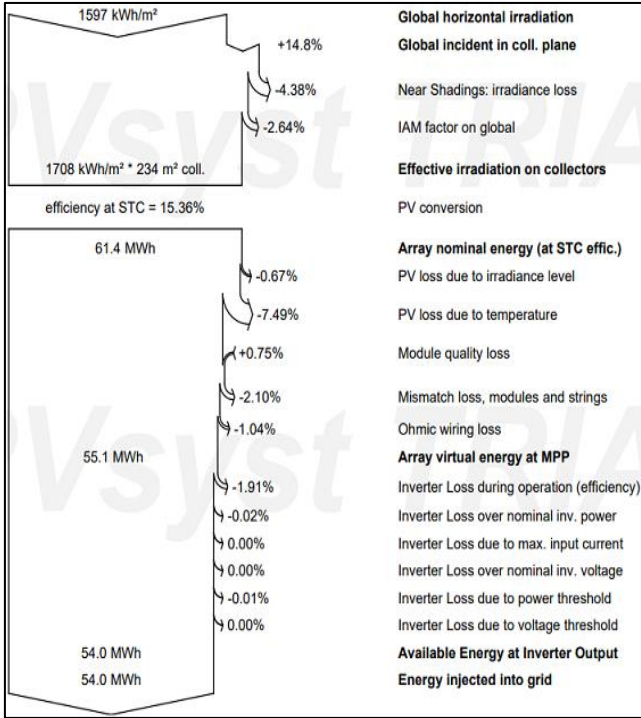


Fig. C.5 – Loss diagram of site 5

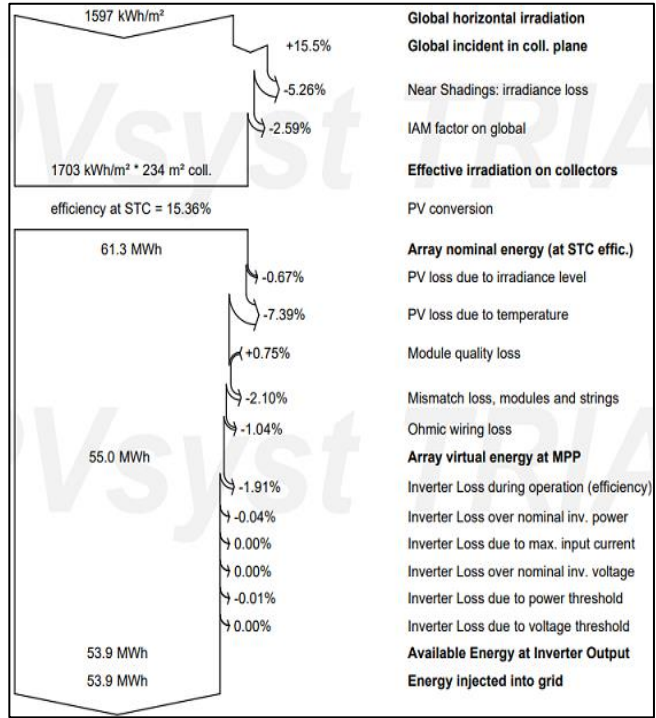


Fig. C.6 – Loss diagram of site 6

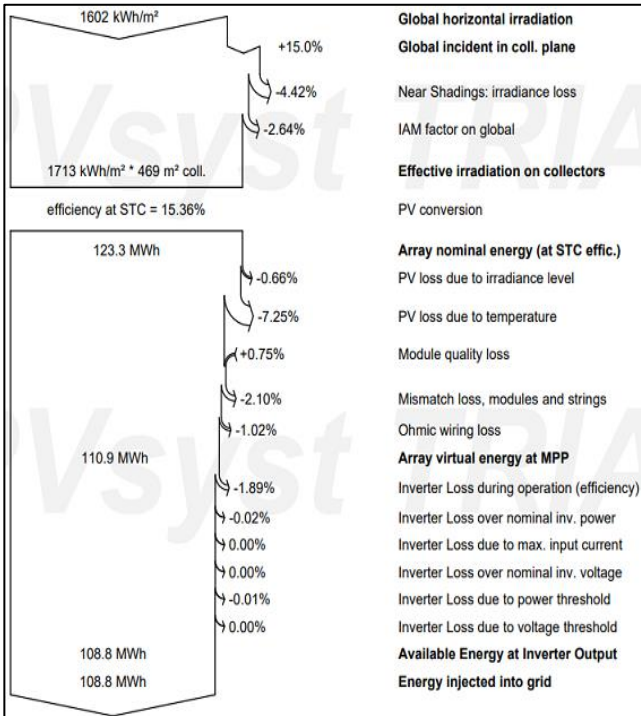


Fig. C.7 – Loss diagram of site 7

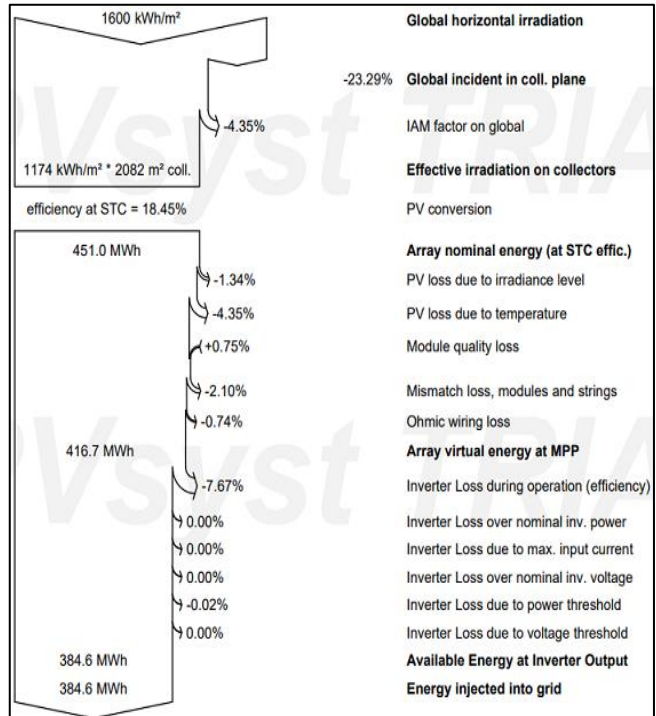


Fig. C.8 – Loss diagram of site 8

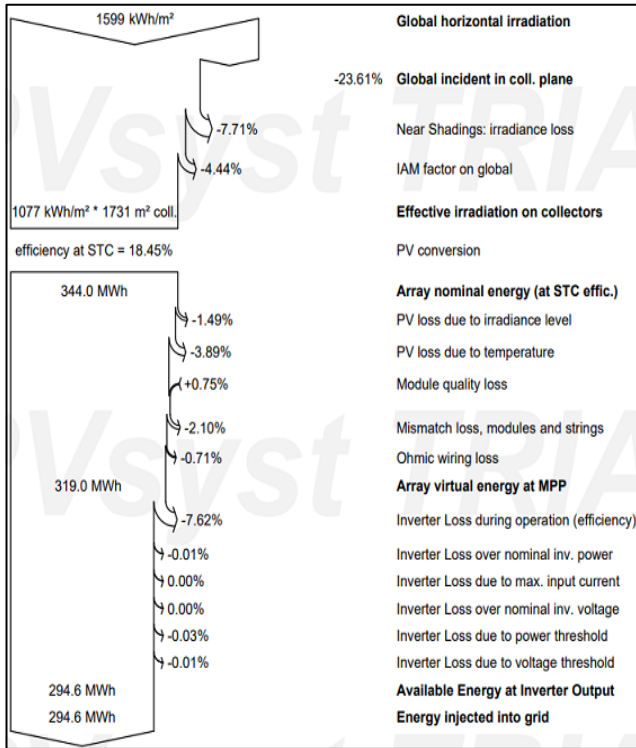


Fig. C.9 – Loss diagram of site 9

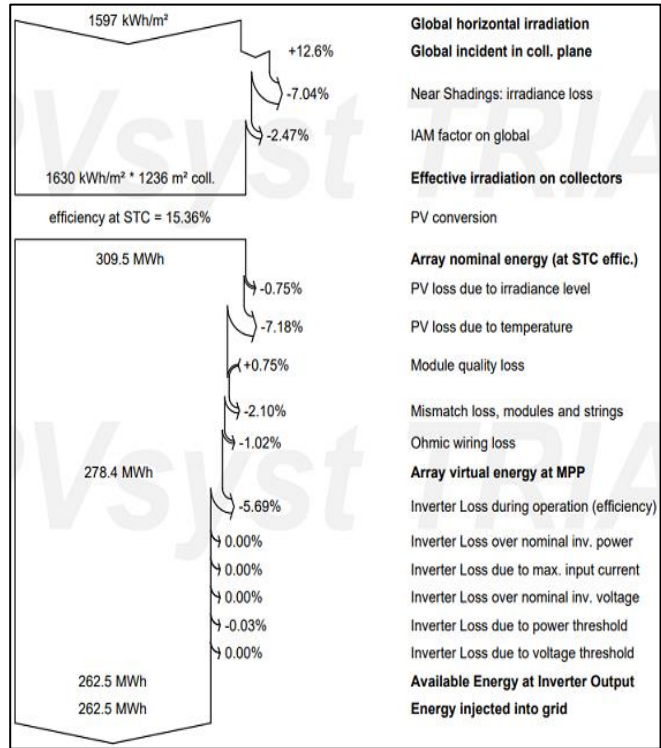


Fig. C.10 – Loss diagram of site 10

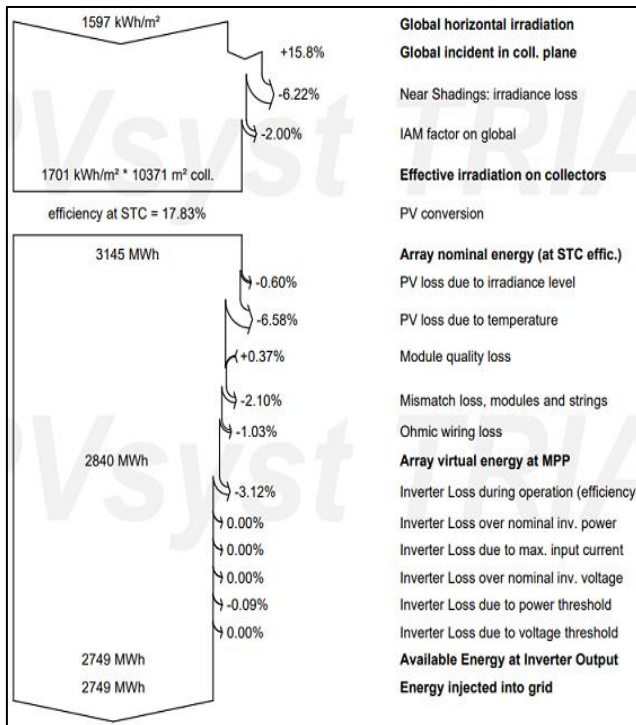


Fig. C.11 – Loss diagram of site 11

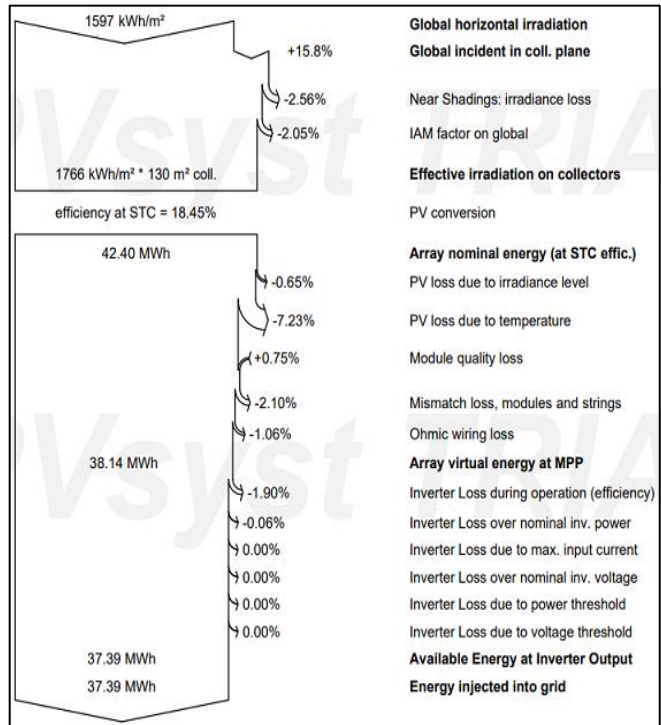


Fig. C.12 – Loss diagram of site 12

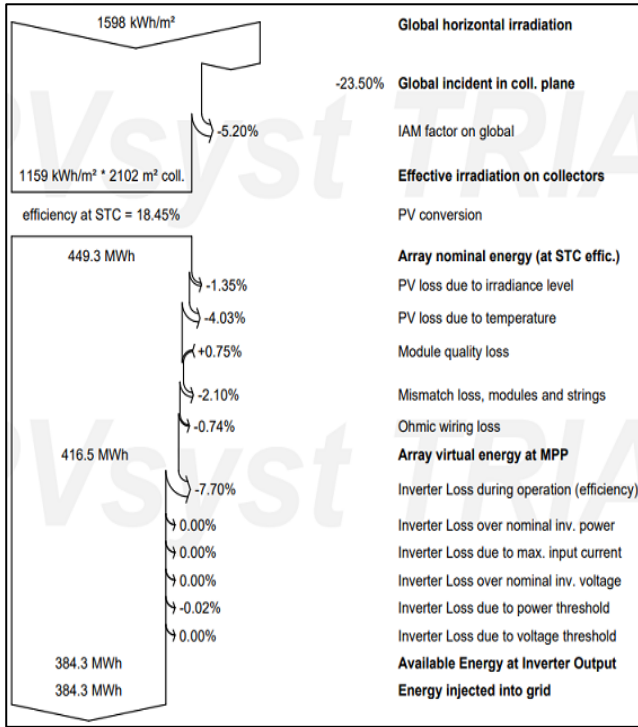


Fig. C.13 – Loss diagram of site 13

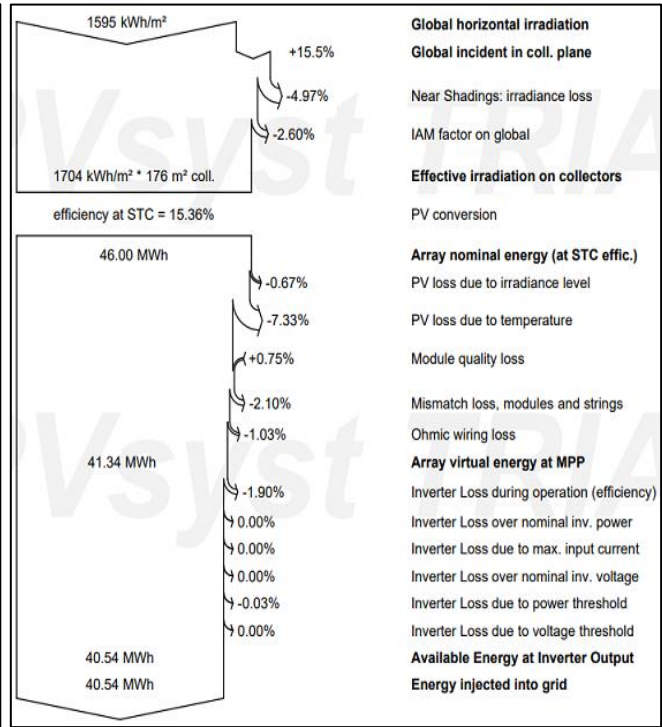


Fig. C.14 – Loss diagram of site 14

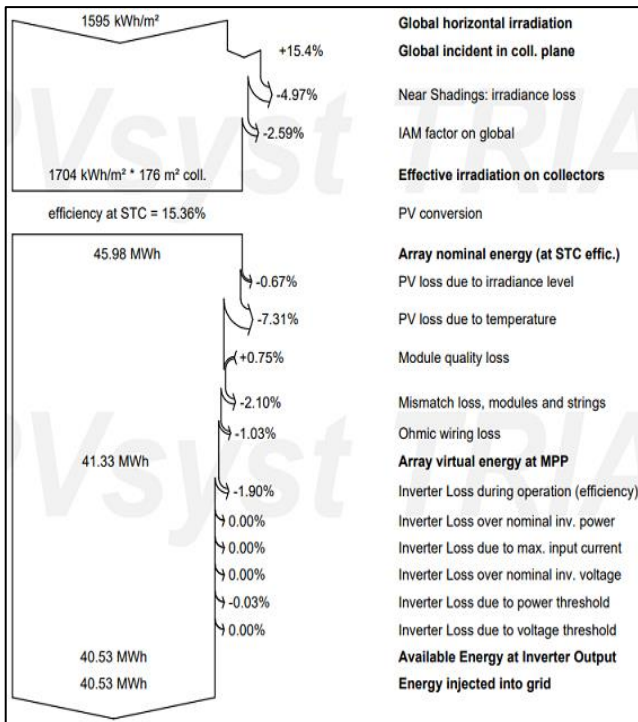


Fig. C.15 – Loss diagram of site 15

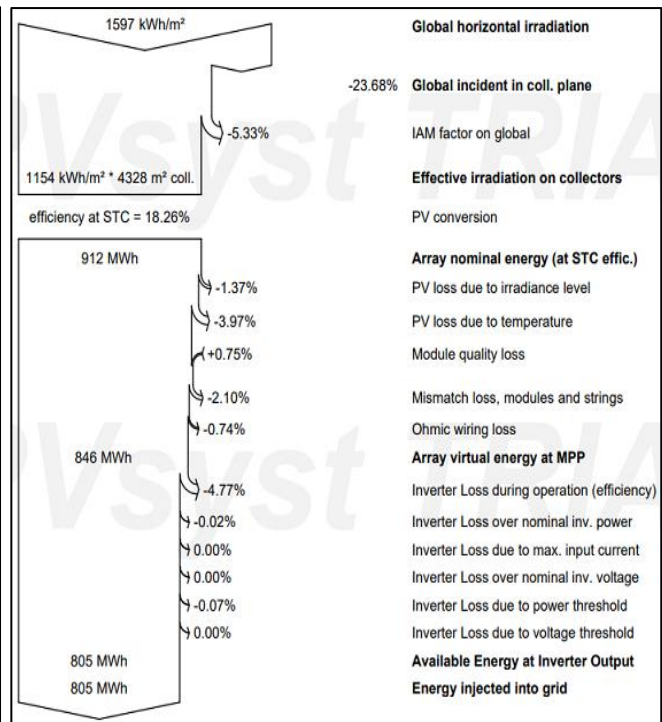


Fig. C.16 – Loss diagram of site 18

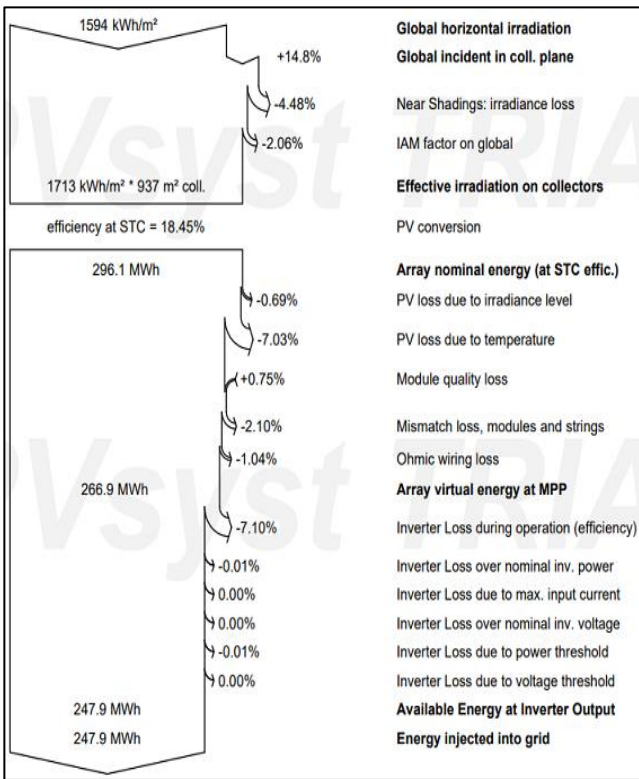


Fig. C.17 – Loss diagram of site 22

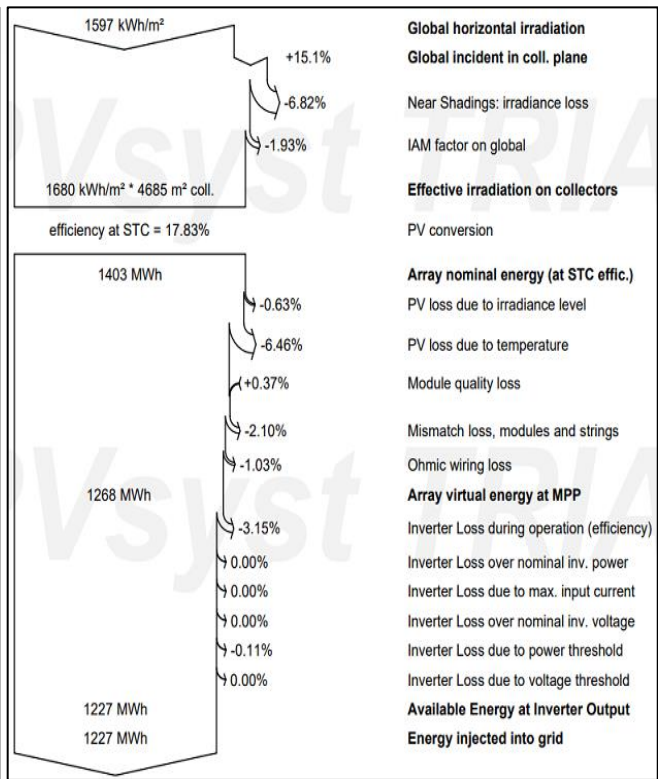


Fig. C.18 – Loss diagram of site 24

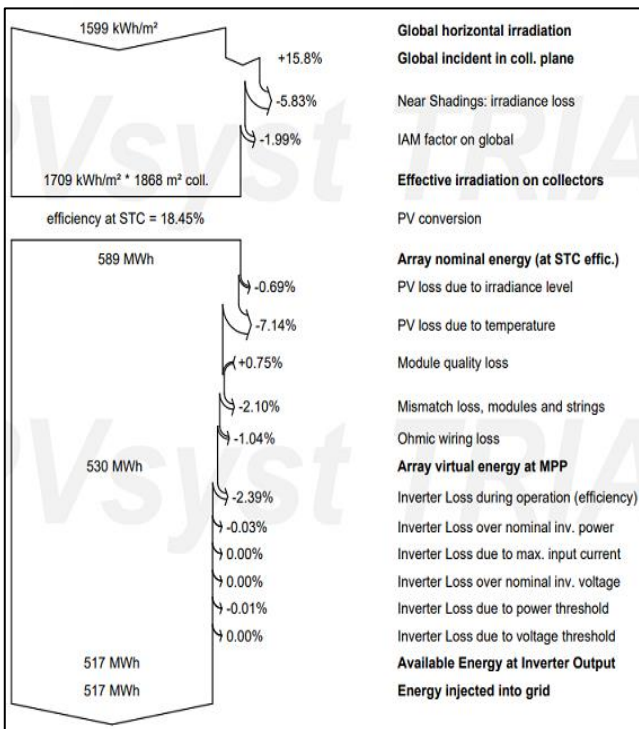


Fig. C.19 – Loss diagram of site 28

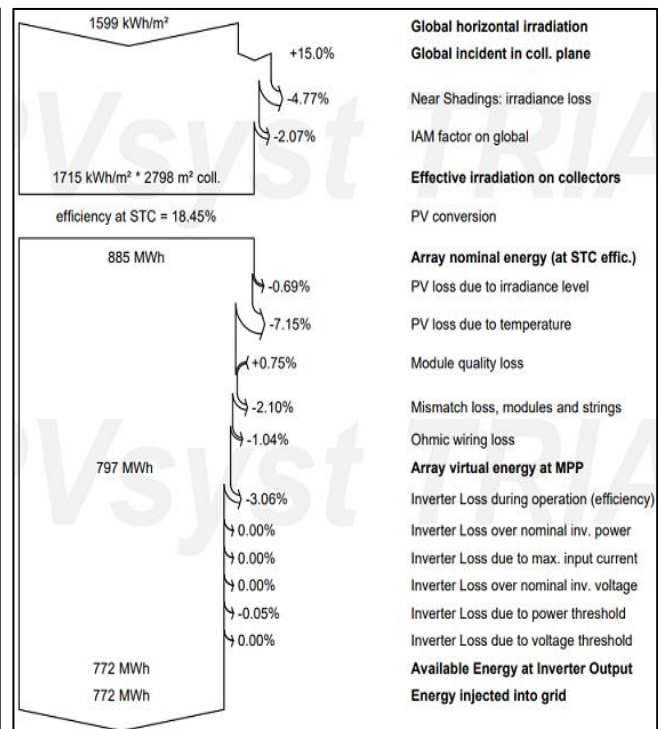


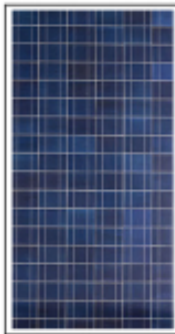
Fig. C.20 – Loss diagram of site 29

# APPENDIX D – PV Module Datasheets



## BlueSolar Polycrystalline Panels

www.victronenergy.com



BlueSolar Polycrystalline 175W

- Low voltage-temperature coefficient enhances high-temperature operation.
- Exceptional low-light performance and high sensitivity to light across the entire solar spectrum.
- 25-Year limited warranty on power output and performance.
- 5-Year limited warranty on materials and workmanship.
- Sealed, waterproof, multi-functional junction box gives high level of safety.
- High performance bypass diodes minimize the power drop caused by shade.
- Advanced EVA (Ethylene Vinyl Acetate) encapsulation system with triple-layer back sheet meets the most stringent safety requirements for high-voltage operation.
- A sturdy, anodized aluminium frame allows modules to be easily roof-mounted with a variety of standard mounting systems.
- Highest quality, high-transmission tempered glass provides enhanced stiffness and impact resistance.
- High power models with pre-wired quick-connect system with MC4 (PV-ST01) connectors.



MC4 connectors

Article Number	Description	Net weight	Electrical data under STC (1)				
			Nominal Power	Max-Power Voltage	Max-Power Current	Open-Circuit Voltage	Short-Circuit Current
			P <sub>nom</sub>	V <sub>mp</sub>	I <sub>mp</sub>	V <sub>oc</sub>	I <sub>sc</sub>
		Kg	W	V	A	V	A
SPP040201200	20W-12V Poly 440 x 350 x 25mm series 4a	1.9	20	18.4	1.09	21.96	1.18
SPP040301200	30W-12V Poly 655 x 350 x 25mm series 4a	2.8	30	18.2	1.66	21.80	1.80
SPP040451200	45W-12V Poly 425 x 668 x 25mm series 4a	3.1	45	19.1	2.36	22.90	2.55
SPP040601200	60W-12V Poly 545 x 668 x 25mm series 4a	4	60	19.3	3.12	23.10	3.37
SPP040901200	90W-12V Poly 780 x 668 x 30mm series 4a	6.1	90	19.5	4.61	23.44	4.98
SPP041151200	115W-12V Poly 1015 x 668 x 30mm series 4a	8	115	18.94	6.08	22.73	6.56
SPP041751200	175W-12V Poly 1485 x 668 x 30mm series 4a	12	175	18.3	9.56	21.9	10.24
SPP032602000	260W-20V Poly 1640 x 992 x 40mm series 3a	17	260	30	8.66	36.75	9.30
SPP042702000	270W-20V Poly 1640 x 992 x 35mm series 4a	18.4	270	31.7	8.52	38.04	9.21
SPP043302400	330W-24V Poly 1956 x 992 x 40mm series 4a	22.5	330	37.3	8.86	44.72	9.57

Module	SPP 040201200	SPP 040301200	SPP 040451200	SPP 040601200	SPP 040901200	SPP 041151200	SPP 041751200	SPP 032601200	SPP 042702000	SPP 043302400
Nominal Power (± 3% tolerance)	20W	30W	45W	60W	90W	115W	175W	260W	270W	330W
Cell type	Polycrystalline									
Number of cells in series	36						60	60	72	
Maximum system voltage (V)	1000V									
Temperature coefficient of P <sub>MP</sub> (%)	-0.45/°C	-0.45/°C	-0.45/°C	-0.45/°C	-0.45/°C	-0.45/°C	-0.45/°C	-0.45/°C	-0.47/°C	-0.45/°C
Temperature coefficient of V <sub>oc</sub> (%)	-0.35/°C	-0.35/°C	-0.35/°C	-0.35/°C	-0.35/°C	-0.35/°C	-0.35/°C	-0.35/°C	-0.34/°C	-0.35/°C
Temperature coefficient of I <sub>sc</sub> (%)	+0.04/°C	+0.04/°C	+0.04/°C	+0.04/°C	+0.04/°C	+0.04/°C	+0.04/°C	+0.04/°C	+0.045/°C	+0.04/°C
Temperature Range	-40°C to +85°C									
Surface Maximum Load Capacity	200 kg/m <sup>2</sup>									
Allowable Hail Load	23 m/s, 7.53 g									
Junction Box Type	PV-LH805	PV-LH806			PV-LH801	PV-LH808			PV-8002	
Length of Cable / connector	No cable				900 mm / MC4					
Output tolerance	± 3%									
Frame	Aluminium									
Product warranty	5 years									
Warranty on electrical performance	10 years 90% + 25 years 80% of power output									
Smallest packaging unit	1 panel									
Quantity per pallet	380	240	180	140	90	80	36	20	32	37

1) STC (Standard Test Conditions) 1000 W/m<sup>2</sup>, 25°C, AM (Air Mass) 1.5

## Mechanical Properties

Cells	6 x 10
Cell Vendor	LG
Cell Type	Monocrystalline / P-type
Cell Dimensions	161.7 x 161.7 mm / 6 inches
# of Busbar	4
Dimensions (L x W x H)	1686 x 1016 x 40 mm 66.38 x 40 x 1.57 inch
Front Load	6000Pa
Rear Load	5400Pa
Weight	18 kg
Connector Type	MC4
Junction Box	IP67 with 3 Bypass Diodes
Cables	1000 mm x 2 ea / 39.37 in x 2 ea
Glass	High Transmission Tempered Glass
Frame	Anodized Aluminium

## Certifications and Warranty

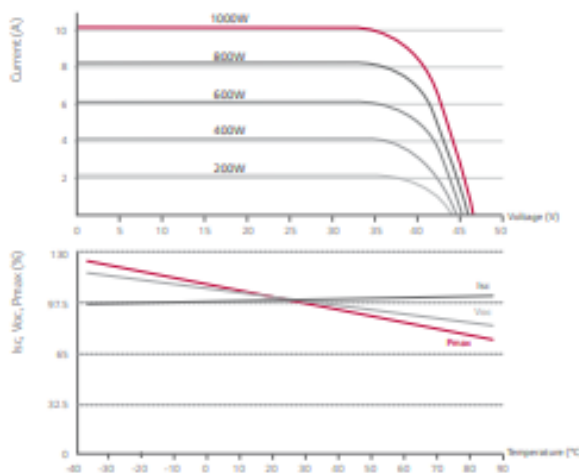
Certifications	IEC 61215, IEC 61730-1/-2 UL 1703 IEC 61701 (Salt mist corrosion test) IEC 62716 (Ammonia corrosion test) ISO 9001
Module Fire Performance (USA)	Type 1
Fire Rating (CANADA)	Class C (ULC / ORD C1703)
Product Warranty	12 years
Output Warranty of P <sub>max</sub>	Linear warranty**

\*\* 1) 1st year - 98%, 2) After 2nd year - 0.55% annual degradation, 3) 25 years - 84.8%

## Temperature Characteristics

NOCT	45 ± 3 °C
P <sub>mpp</sub>	-0.41%/°C
V <sub>oc</sub>	-0.30%/°C
I <sub>sc</sub>	0.03%/°C

## Characteristic Curves



## Electrical Properties (STC \*)

Module	300W	295W	290W
Maximum Power (P <sub>max</sub> )	300	295	290
MPP Voltage (V <sub>mpp</sub> )	31.6	31.3	31.0
MPP Current (I <sub>mpp</sub> )	9.50	9.43	9.36
Open Circuit Voltage (V <sub>oc</sub> )	38.9	38.6	38.3
Short Circuit Current (I <sub>sc</sub> )	10.07	10.02	9.97
Module Efficiency	17.5	17.2	16.9
Operating Temperature	-40 ~ +90		
Maximum System Voltage	1000		
Maximum Series Fuse Rating	20		
Power Tolerance (%)	0 ~ +3		

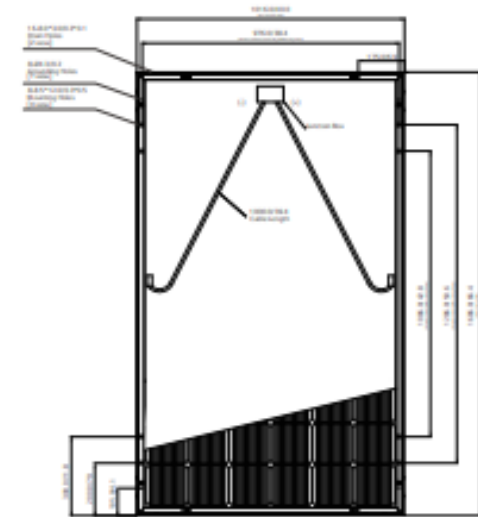
\* STC (Standard Test Condition) Irradiance 1000 W/m<sup>2</sup>, Ambient Temperature 25 °C, AM 1.5  
\* The nameplate power output is measured and determined by LG Electronics at its sole and absolute discretion.

## Electrical Properties (NOCT\*)

Module	300W	295W	290W
Maximum Power (P <sub>max</sub> )	220	216	212
MPP Voltage (V <sub>mpp</sub> )	29.1	28.7	28.4
MPP Current (I <sub>mpp</sub> )	7.56	7.53	7.47
Open Circuit Voltage (V <sub>oc</sub> )	36.0	35.7	35.4
Short Circuit Current (I <sub>sc</sub> )	8.10	8.06	8.02

\* NOCT (Nominal Operating Cell Temperature) Irradiance 800W/m<sup>2</sup>, ambient temperature 20 °C, wind speed 1m/s

## Dimensions (mm/in)



\* The distance between the center of the mounting/grounding holes.



North America Solar Business Team  
 LG Electronics U.S.A. Inc.  
 1000 Sylvan Ave, Englewood Cliffs, NJ 07632  
 Contact: lg.solar@lge.com  
 www.lgsolarusa.com

Product specifications are subject to change without notice.

Copyright © 2017 LG Electronics. All rights reserved.  
 01/01/2017

Innovation for a Better Life



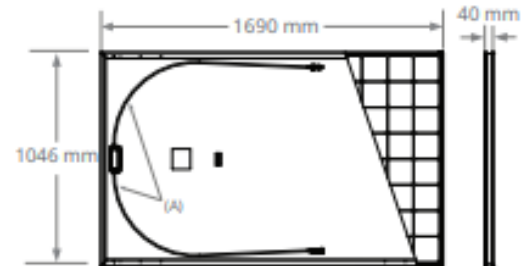


## MAXEON<sup>®</sup> 3 | 400 W Residential Solar Panel

Electrical Data			
	SPR-MAX3-400	SPR-MAX3-390	SPR-MAX3-370
Nominal Power (P <sub>nom</sub> ) <sup>7</sup>	400 W	390 W	370 W
Power Tolerance	+5/0%	+5/0%	+5/0%
Panel Efficiency	22.6%	22.1%	20.9%
Rated Voltage (V <sub>mpp</sub> )	65.8 V	64.5 V	61.8 V
Rated Current (I <sub>mpp</sub> )	6.08 A	6.05 A	5.99 A
Open-Circuit Voltage (V <sub>oc</sub> )	75.6 V	75.3 V	74.7 V
Short-Circuit Current (I <sub>sc</sub> )	6.58 A	6.55 A	6.52 A
Max. System Voltage	1000 V IEC		
Maximum Series Fuse	15 A		
Power Temp Coef.	-0.29% / °C		
Voltage Temp Coef.	-176.8 mV / °C		
Current Temp Coef.	2.9 mA / °C		

Tests And Certifications	
Standard Tests <sup>8</sup>	IEC 61215, IEC 61730 Class 1 fire rated per UNI 9177
Quality Management Certs	ISO 9001:2015, ISO 14001:2015
EHS Compliance	RoHS (Pending), OHSAS 18001:2007, lead free, REACH SVHC-163 (Pending)
Sustainability	Cradle to Cradle Certified™ (Pending)
Ammonia Test	IEC 62716
Desert Test	10.1109/PVSC.2013.6744437
Salt Spray Test	IEC 61701 (maximum severity)
PID Test	1000 V: IEC 62804, PVEL 600 hr duration
Available Listings	TUV <sup>9</sup>

Operating Condition And Mechanical Data	
Temperature	-40° C to +85° C
Impact Resistance	25 mm diameter hail at 23 m/s
Solar Cells	104 Monocrystalline Maxeon Gen III
Tempered Glass	High-transmission tempered anti-reflective
Junction Box	IP-65, Stäubli (MC4), 3 bypass diodes
Weight	19 kg
Design Load	Wind: 2660 Pa, 274 kg/m <sup>2</sup> front & back Snow: 4000 Pa, 408 kg/m <sup>2</sup> front
Max. Load <sup>10</sup>	Wind: 4000 Pa, 408 kg/m <sup>2</sup> front & back Snow: 6000 Pa, 611 kg/m <sup>2</sup> front
Frame	Class 1 black anodized (highest AAMA rating)



FRAME PROFILE



A. Cable Length: 1200 mm +/-10 mm  
B. LONG SIDE: 32 mm  
SHORT SIDE: 24 mm

Please read the safety and installation guide.

1 SunPower 400 W, 22.6% efficient, compared to a Conventional Panel on same-sized arrays (260 W, 16% efficient, approx. 1.6 m<sup>2</sup>), 7% more energy per watt (based on PVsyst pan files for avg EU climate), 0.5%/yr slower degradation rate (Jordan, et. al. "Robust PV Degradation Methodology and Application." PVSC 2018).

2 DNV "SunPower Shading Study." 2013. Compared to a conventional front contact panel.

3 #1 rank in "Fraunhofer PV Durability Initiative for Solar Modules: Part 3". PVTech Power Magazine, 2015.

4 SunPower is rated #1 on Silicon Valley Toxics Coalition's Solar Scorecard.

5 Cradle to Cradle Certified is a multi-attribute certification program that assesses products and materials for safety to human and environmental health, design for future use cycles, and sustainable manufacturing.

6 Maxeon2 and Maxeon3 panels additionally contribute to LEED Materials and Resources credit categories.

7 Standard Test Conditions (1000 W/m<sup>2</sup> irradiance, AM 1.5, 25° C). NREL calibration Standard SOMS current, LACCS FF and Voltage.

8 Class C fire rating per IEC 61730.

9 Also certified under names SPR-XXX-XXX.

10 Calculated with a 1.5 Safety Factor.

Designed in USA

Made in Philippines (Cells)

Modules Assembled in Mexico

Visit [www.sunpowercorp.co.uk](http://www.sunpowercorp.co.uk) for more information.

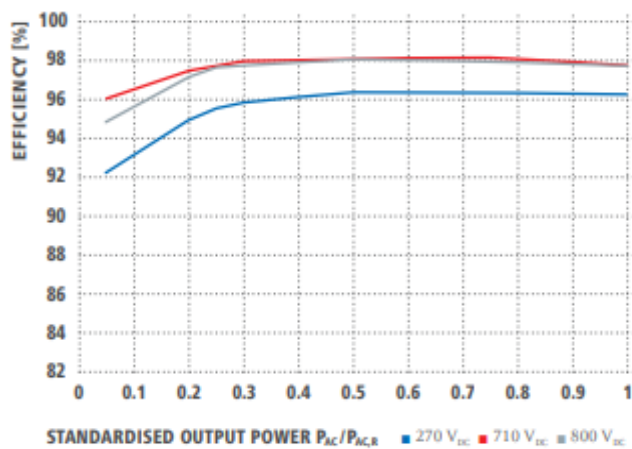
Specifications included in this datasheet are subject to change without notice.

©2019 SunPower Corporation. All rights reserved. SUNPOWER, the SUNPOWER logo and MAXEON are trademarks or registered trademarks of SunPower Corporation. Cradle to Cradle Certified™ is a certification mark licensed by the Cradle to Cradle Products Innovation Institute.

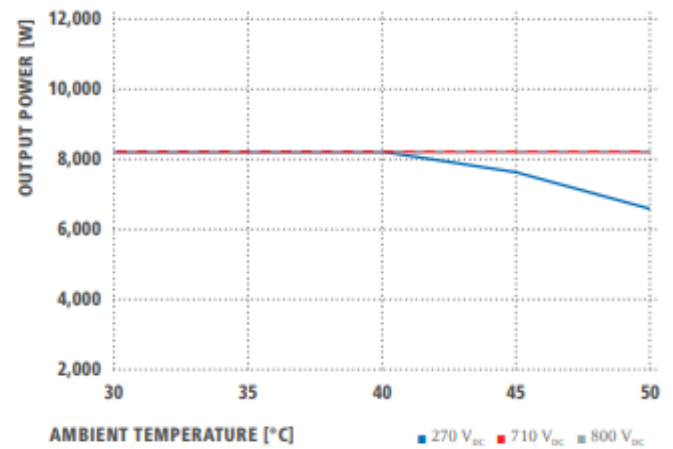
**SUNPOWER<sup>®</sup>**  
MAXEON<sup>®</sup>

## APPENDIX E – Inverter Datasheets

### FRONIUS PRIMO 8.2-1 EFFICIENCY CURVE



### FRONIUS PRIMO 8.2-1 TEMPERATURE DERATING



### TECHNICAL DATA FRONIUS PRIMO (5.0-1, 5.0-1 AUS, 6.0-1, 8.2-1)

INPUT DATA	PRIMO 5.0-1	PRIMO 5.0-1 AUS	PRIMO 6.0-1	PRIMO 8.2-1
Number of MPP trackers	2			
Max. input current ( $I_{DC\ max\ 1} / I_{DC\ max\ 2}$ )	12.0 A / 12.0 A		18.0 A / 18.0 A	
Max. array short circuit current (MPP1/MPP2)	18.0 A / 18.0 A		27.0 A / 27.0 A	
DC input voltage range ( $U_{DC\ min} - U_{DC\ max}$ )	80 - 1,000 V			
Feed-in start voltage ( $U_{DC\ start}$ )	80 V			
Usable MPP voltage range	80 - 800 V			
Number of DC connections	2 + 2			
Max. PV generator output ( $P_{DC\ max}$ )	7.5 kW <sub>peak</sub>	7.5 kW <sub>peak</sub>	9.0 kW <sub>peak</sub>	12.3 kW <sub>peak</sub>
OUTPUT DATA	PRIMO 5.0-1	PRIMO 5.0-1 AUS	PRIMO 6.0-1	PRIMO 8.2-1
AC nominal output ( $P_{AC,n}$ )	5,000 W	4,600 W	6,000 W	8,200 W
Max. output power	5,000 VA	5,000 VA	6,000 VA	8,200 VA
AC output current ( $I_{AC\ nom}$ )	21.7 A	21.7 A	26.1 A	35.7 A
Grid connection (voltage range)	1 ~ NPE 220 V / 230 V (180 V - 270 V)			
Frequency (frequency range)	50 Hz / 60 Hz (45 - 65 Hz)			
Total harmonic distortion	< 5 %			
Power factor ( $\cos \phi_{AC,n}$ )	0.85 - 1 ind. / cap.			
GENERAL DATA	PRIMO 5.0-1	PRIMO 5.0-1 AUS	PRIMO 6.0-1	PRIMO 8.2-1
Dimensions (height x width x depth)	645 x 431 x 204 mm			
Weight	21.5 kg			
Degree of protection	IP 65			
Protection class	1			
Overvoltage category (DC / AC) <sup>1)</sup>	2 / 3			
Night time consumption	< 1 W			
Inverter design	Transformerless			
Cooling	Regulated air cooling			
Installation	Indoor and outdoor installation			
Ambient temperature range	-40 - +55 °C			
Permitted humidity	0 - 100 %			
Max. altitude	4,000 m			
DC connection technology	4x DC+ and 4x DC- screw terminals 2.5 - 16 mm <sup>2</sup>			
AC connection technology	3-pole AC screw terminals 2.5 - 16 mm <sup>2</sup>			
Certificates and compliance with standards	DIN V VDE 0126-1-1/A1, IEC 62109-1/-2, IEC 62116, IEC 61727, AS 4777-2, AS 4777-3, G83/2, G59/3, CEI 0-21, VDE AR N 4105 <sup>2)</sup>			

<sup>1)</sup> According to IEC 62109-1.

<sup>2)</sup> Fronius Primo 5.0-1, Fronius Primo 6.0-1 and Fronius Primo 8.2-1 are not fully compliant with VDE AR N 4105. Further information regarding the availability of the inverters in your country can be found at [www.fronius.com](http://www.fronius.com).



X3-4.0-T    X3-5.0-T    X3-6.0-T    X3-7.0-T    X3-8.0-T    X3-9.0-T    X3-10.0-T

INPUT (DC)							
Max.DC power [W]	5200	6500	7800	8400	9600	10800	12000
Max.DC voltage [V]	800	800	800	1000	1000	1000	1000
Nominal DC operating voltage [V]	600	600	600	600	600	600	600
Max. input current (input A/input B) [A]	11/11	11/11	11/11	11/11	11/11	11/11	11/11
Max. short circuit current (input A/input B) [A]	14/14	14/14	14/14	14/14	14/14	14/14	14/14
Operating voltage range [V]	160-750	160-750	160-750	160-900	160-900	160-900	160-900
MPPT voltage range [V] (full load)	190-750	240-750	285-750	330-800	380-800	425-800	470-800
Start up DC voltage [V]	140	140	140	140	140	140	140
Start output DC voltage [V]	180	180	180	180	180	180	180
Shut down DC voltage [V]	100	100	100	100	100	100	100
No. of MPPT trackers	2	2	2	2	2	2	2
Strings per MPPT tracker	1	1	1	1	1	1	1
DC disconnection switch	optional	optional	optional	optional	optional	optional	optional
OUTPUT (AC)							
Nominal AC power [W]	4000	5000	6000	7000	8000	9000	10000
Max. apparent AC power [W]	4000	5000	6000	7000	8000	9000	10000
Rated grid voltage (AC voltage range) [V]	3/N/PE, 230/400(310-480)						
Rated grid Frequency [Hz]	50/60; +/-5						
Max. AC current [A]	6.4	8.0	9.6	11.2	12.8	14.4	16.0
Displacement power factor	0.8leading-0.8lagging						
THDi, rated power [%]	<2						
EFFICIENCY							
MPPT efficiency [%]	99.9	99.9	99.9	99.9	99.9	99.9	99.9
Euro-efficiency [%]	97.8	97.8	97.8	98	98	98	98
Max. efficiency [%]	98.3	98.3	98.3	98.4	98.4	98.5	98.5
POWER CONSUMPTION							
Night consumption [W]	<3						
STANDARD							
Safety	EN62109-1/-2						
EMC	EN61000-6-1;EN61000-6-2;EN61000-6-3;EN61000-3-2;EN61000-3-3						
Certification	AS4777.2-2015; VDE4105						
ENVIRONMENT LIMIT							
Protection class	IP65						
Operating temperature range [°C]	-25~+60(derating at 45)						
Humidity [%]	0~100, condensing						
Altitude[m]	4000( derating at 3000 )						
Storage temperature [°C]	-25~60						
Noise emission(typical)[dB]	<35						
Over voltage category	III(electric supply side), III(PV side)						
GENERAL							
Dimensions(WxHxD) [mm]	460*400*180						
Weight [kg]	23	23	23	26	26	26	26
DC input type	MC4						
Cooling concept	Natural						
Topology	Transformerless						
Earth fault alarm	Yes(80dB)						
Communication	Rs485 /DRM / WIFI(optional) / LAN (optional)/ USB / RF						
LED	3						
LCD display	Backlight 20*4 character						
Warranty [year]	5						

\*Can be modified without notice.(V3)

Type designation	SG5.0RT	SG6.0RT	SG7.0RT	SG8.0RT	SG10RT	SG12RT
<b>Input (DC)</b>						
Recommended max. PV input power	7.5 kWp	9.0 kWp	10.5 kWp	12 kWp	15 kWp	18 kWp
Max. PV input voltage	1100 V *					
Min. PV input voltage / Start-up input voltage	180 V					
Nominal input voltage	600 V					
MPP voltage range	160 V – 1000 V					
No. of independent MPP inputs	2					
No. of PV strings per MPPT	1/1	1/1	2/1	2/1	2/1	2/1
Max. PV input current	25 A (12.5 A / 12.5 A)		37.5 A (25 A / 12.5 A)			
Max. DC short-circuit current	32 A (16 A / 16 A)		48 A (32 A / 16 A)			
Max. current for input connector	30 A					
<b>Output (AC)</b>						
Nominal AC power (@230 V, 50 Hz)	5000 W	6000 W	7000 W***	8000 W	10000 W	12000 W
Max. AC output power	5500 VA**	6600 VA**	7700 VA**	8800 VA**	11000 VA**	13200 VA**
Max. AC output current	8.3 A	10 A	11.7 A	13.3 A	16.7 A	20 A
Nominal AC voltage	3 / N / PE, 220 / 380 V 3 / N / PE, 230 / 400 V 3 / N / PE, 240 / 415 V					
AC voltage range	180 V – 276 V / 311 V – 478 V					
Nominal grid frequency / Grid frequency range	50 Hz / 45 – 55 Hz 60 Hz / 55 – 65 Hz					
Harmonic (THD)	<3 % (at nominal power)					
Power factor at nominal power / Adjustable power factor	>0.99 / 0.8 leading – 0.8 lagging					
Feed-in phases / AC connection	3 / 3					
<b>Efficiency</b>						
Max. efficiency	98.40%	98.40%	98.40%	98.50%	98.50%	98.50%
European efficiency	97.40%	97.40%	97.70%	97.80%	97.90%	97.90%
<b>Protection</b>						
Grid monitoring	Yes					
DC reverse connection protection	Yes					
AC short-circuit protection	Yes					
Leakage current protection	Yes					
Surge Protection	DC Type II / AC Type II					
DC switch	Yes					
Arc fault circuit interrupter (AFCI)	Yes					
PID recovery function	Yes					
<b>General Data</b>						
Dimensions (W*H*D)	370*480*195 mm					
Mounting method	Wall-mounting bracket					
Weight	18 kg					
Topology	Transformerless					
Degree of protection	IP65					
Operating ambient temperature range	-25 °C to 60 °C					
Allowable relative humidity range	0% – 100%					
Cooling method	Natural cooling					
Max. operating altitude	4000 m (> 2000 m derating)					
Noise(Typical)	35 dB (A)					
Display	LED					
Communication	WLAN / Ethernet / RS485 / Di / DO					
DC connection type	MC4 (Max. 6 mm <sup>2</sup> )					
AC connection type	Plug and play					
Compliance	IEC / EN 61000-6-1/2/3/4, IEC / EN62109-1/2, IEC 61727, IEC 62116, IEC 61683, EN50530, AS/NZS 4777.2:2015, VDE-AR-N-4105, DIN VDE0126-1-1, EN50549-1					

\*: The inverter enters the standby state when the input voltage ranges between 1,000 V and 1,100 V. If the maximum DC voltage in the system can exceed 1000 V, the MC4 connectors included in the scope of delivery must not be used. In this case MC4 Evo2 connectors must be used.  
 \*\*: For Australia & Belgium & Germany, max. AC output power: SG5.0RT is 5000 VA, SG6.0RT is 6000 VA, SG8.0RT is 8000 VA, SG10RT is 10000 VA, SG12RT is 12000 VA.  
 \*\*\*: Australia: 6999 W, 6999 VA; Belgium & Germany: 7000 W, 7000 VA.



# SMT Series Datasheet



Technical Data	GW25K-MT	GW30K-MT	GW36K-MT
<b>PV String Input Data</b>			
Max. DC Input Power (Wp)	32500	39000	42900
Max. DC Input Voltage (V)	1100	1100	1100
MPPT Range (V)	200-950	200-950	200-950
Start-up Voltage (V)	180	180	180
Nominal DC Input Voltage (V)	600	600	600
Max. Input Current (A)	25/25/25	25/25/25	25/25/25
Max. Short Current (A)	31.3/31.3/31.3	31.3/31.3/31.3	31.3/31.3/31.3
No. of MPP Trackers	3	3	3
No. of Input Strings per Tracker	2/2/2	2/2/2	2/2/2
<b>AC Output Data</b>			
Nominal Output Power (W)	25000	30000	36000 <sup>1)</sup>
Max. Output Power (W)	27500 <sup>2)</sup>	33000 <sup>2)</sup>	36000 <sup>2)</sup>
Max. Output Apparent Power (VA)	27500 <sup>3)</sup>	33000 <sup>3)</sup>	36000 <sup>3)</sup>
Nominal Output Voltage (V)		400, 3L/N/PE or 3L/PE	
Nominal Output Frequency (Hz)	50/60	50/60	50/60
Max. Output Current (A)	40	48	53.3
Output Power Factor		~1 (Adjustable from 0.8 leading to 0.8 lagging)	
Output THDI (@Nominal Output)	<3%	<3%	<3%
<b>Efficiency</b>			
Max. Efficiency	98.7%	98.8%	98.8%
European Efficiency	>98.4%	>98.5%	>98.5%
<b>Protection</b>			
Anti-islanding Protection	Integrated	Integrated	Integrated
Input Reverse Polarity Protection	Integrated	Integrated	Integrated
PV String Current Monitoring	Integrated	Integrated	Integrated
Anti-PID Function for Module	Optional	Optional	Optional
Insulation Resistor Detection	Integrated	Integrated	Integrated
DC Surge Protection		Type II (Type II optional)	
AC Surge Protection		Type II (Type II optional)	
Residual Current Monitoring Unit	Integrated	Integrated	Integrated
Output Over Current Protection	Integrated	Integrated	Integrated
Output Short Protection	Integrated	Integrated	Integrated
Output Over Voltage Protection	Integrated	Integrated	Integrated
AFCI	Optional	Optional	Optional
Terminal Temperature Detection	Optional	Optional	Optional
<b>General Data</b>			
Operating Temperature Range (°C)	-30-60	-30-60	-30-60
Relative Humidity	0-100%	0-100%	0-100%
Operating Altitude (m)	≤3000	≤3000	≤3000
Cooling	Fan Cooling	Fan Cooling	Fan Cooling
User Interface		LCD & LED or APP & LED	
Communication		RS485 or WiFi or GPRS or PLC	
Weight (kg)	40	40	40
Size (Width*Height*Depth mm)	480*590*200	480*590*200	480*590*200
Protection Degree	IP65	IP65	IP65
Night Self Consumption (W)	<1	<1	<1
Topology		Transformerless	

<sup>1)</sup>: 33kW for Italy, 36kW for other countries.

<sup>2)</sup>: For Belgium Max. Output Power (W): GW25K-MT is 25000; GW30K-MT is 30000; GW36K-MT is 36000.

<sup>3)</sup>: For Belgium Max. Output Apparent Power (VA): GW25K-MT is 25000; GW30K-MT is 30000; GW36K-MT is 36000.

\*. Please visit GoodWe website for the latest certificates.

# MT Series Datasheet



Technical Data	GW50KN-MT	GW60KN-MT	GW50KBF-MT	GW60KBF-MT	GW75KBF-MT	GW80KBF-MT
<b>DC Input Data</b>						
Max. PV Power (W)	65000	80000	65000	80000	97500	104000
Max. DC Input Voltage (V)	1100	1100	1100	1100	1100	1100
MPPT Range (V)	200~1000	200~1000	200~1000	200~1000	200~1000	200~1000
Starting Voltage (V)	200	200	200	200	200	200
Min. Feed-in Voltage (V)	210	210	210	210	210	210
Nominal DC Input Voltage (V)	620	620	620	620	750	800
Max. Input Current per MPPT (A)	33/33/22/22	33	30	44	44	39
Max. Short Circuit Current per MPPT (A)	41.5/41.5/27.5/27.5	41.5	37.5	55	55	54.8
No. of MPP Trackers	4	4	4	4	4	4
No. of Input Strings per Tracker	3/3/2/2	3	2	3	3	3
<b>AC Output Data</b>						
Nominal Output Power (W)	50000	60000	50000	60000	75000	80000
Max. AC Active Power (cosφ=1)	55000;57500 @415Vac*1	66000;69000 @415Vac*1	55000;57500 @415Vac*1	66000;69000 @415Vac*1	82500*1	88000*1
Max. Output Apparent Power (VA)	55000;57500 @415Vac*2	66000;69000 @415Vac*2	55000;57500 @415Vac*2	66000;69000 @415Vac*2	82500*2	88000*2
Nominal Output Voltage (V)	400, default 3L+N+PE, 3L+PE optional in settings				500, 3L/PE	540, 3L/PE
Nominal Output Frequency (Hz)	50/60	50/60	50/60	50/60	50/60	50/60
Max. Output Current (A)	80	96	80	96	95.3	94.1
Output Power Factor	-1 (Adjustable from 0.8 leading to 0.8 lagging)					
Output THDi (@Nominal Output)	<3%	<3%	<3%	<3%	<3%	<3%
<b>Efficiency</b>						
Max. Efficiency	98.7%	98.8%	98.8%	98.8%	99.0%	99.0%
European Efficiency	98.3%	98.5%	98.3%	98.3%	98.4%	98.4%
<b>Protection</b>						
PV String Current Monitoring	Integrated	Integrated	Integrated	Integrated	Integrated	Integrated
Anti-Islanding Protection	Integrated	Integrated	Integrated	Integrated	Integrated	Integrated
Input Reverse Polarity Protection	Integrated	Integrated	Integrated	Integrated	Integrated	Integrated
Insulation monitoring	Integrated	Integrated	Integrated	Integrated	Integrated	Integrated
DC fuse	Integrated	Integrated	Integrated	Integrated	Integrated	Integrated
Anti-PID Function for Module	Optional	Optional	Optional	Optional	Optional	Optional
DC Surge Arrester	Integrated (Type II)					
AC Surge Arrester	Integrated (Type II)					
Residual Current Monitoring Unit	Integrated	Integrated	Integrated	Integrated	Integrated	Integrated
AC Over Current Protection	Integrated	Integrated	Integrated	Integrated	Integrated	Integrated
AC Short Circuit Protection	Integrated	Integrated	Integrated	Integrated	Integrated	Integrated
AC Over Voltage Protection	Integrated	Integrated	Integrated	Integrated	Integrated	Integrated
Humidity Monitoring	-	-	-	NA	NA	NA
<b>General Data</b>						
Ambient Temperature Range (°C)	-30~60	-30~60	-30~60	-30~60	-30~60	-30~60
Relative Humidity	0~100%	0~100%	0~100%	0~100%	0~100%	0~100%
Operating Altitude (m)	≤4000	≤4000	≤4000	≤4000	≤4000	≤4000
Cooling	Fan Cooling	Fan Cooling	Fan Cooling	Fan Cooling	Fan Cooling	Fan Cooling
Display	LCD or WiFi+APP			LED, WiFi+APP		
Communication	RS485 or WiFi or PLC					
Weight (kg)	59	64	60	65	65	65
Dimension (Width-Height-Depth) (mm)	586-788-264	586-788-264	586-788-264	586-788-267	586-788-267	586-788-267
Protection Degree	IP65	IP65	IP65	IP65	IP65	IP65
Night Self Consumption (W)	<1	<1	<1	<1	<1	<1
Topology	Transformerless					

\*1: For Belgium Max. Output Power (W): GW50KN-MT is 50000, GW60KN-MT is 60000, GW50KBF-MT is 50000, GW60KBF-MT is 60000, GW75KBF-MT is 75000, GW80KBF-MT is 80000.  
 \*2: For Belgium Max. Output Apparent Power (VA): GW50KN-MT is 50000, GW60KN-MT is 60000, GW50KBF-MT is 50000, GW60KBF-MT is 60000, GW75KBF-MT is 75000, GW80KBF-MT is 80000.  
 \*: Please visit GoodWe website for the latest certificates.

## Technical Data

<sup>1</sup>EFASOLAR 800 <sup>2</sup>EFASOLAR 600 <sup>3</sup>EFASOLAR 700 <sup>4</sup>EFASOLAR 900

Electrical				
<b>Input</b>				
Maximum power	575 kW	725 kW	840 kW	1035 kW
Minimum voltage	450 V	480 V	530 V	620 V
Maximum voltage			1000 V	
MPPT range	475 V - 830 V	510 V - 830 V	555 V - 830 V	635 V - 830 V
Maximum current	1200 A	1300 A	1350 A	1485 A
Number of independent MPPT inputs	1			
Number of DC inputs <sup>1</sup>	6 inputs equipped with fuses			
<b>Output</b>				
Rated power (25 °C / 50 °C)	550 kVA / 500 kVA	690 kVA / 630 kVA	790 kVA / 730 kVA	980 kVA / 900 kVA
Rated voltage <sup>2</sup>	270 V	315 V	360 V	420 V
Rated current	1070 A	1155 A	1170 A	1237 A
Frequency	50 Hz / 60 Hz			
Maximum current	1260 A	1310 A	1310 A	1370 A
THD	< 3%			
Power factor <sup>3</sup> / Displacement power factor <sup>4</sup>	1,0 / 0,8 inductive to 0,8 capacitive			
Required grid type	IT grid			
Isolation transformer	No			
<b>Efficiency</b>				
Maximum <sup>5</sup>	98,4%	98,5%	98,6%	98,7%
Euro-efficiency <sup>3</sup>	98,1%	98,3%	98,4%	98,5%
CEC efficiency <sup>3</sup>	98,2%	98,4%	98,5%	98,6%
<b>Protective devices</b>				
DC disconnect device	Motor-drive switch disconnecter			
AC disconnect device	Circuit breaker			
DC overvoltage protection	Type II surge arrester			
AC overvoltage protection	Type I surge arrester			
Auxiliaries overvoltage protection	Type II surge arrester			
Ground fault monitoring	•			
Overvoltage	•			
Undervoltage	•			
Overfrequency	•			
Underfrequency	•			
Anti-islanding	•			
Reverse polarization	•			
Short circuit on the output	•			
Overtemperature	•			
Asymmetrical current	•			
<b>General data</b>				
Ambient temperature	-10 °C ... +50 °C / +14 °F ... +122 °F			
Max. permissible value for relative humidity (noncondensing)	15% ... 95%			
Cooling concept	Air forced cooling			
Auxiliaries power supply	230 V			
Max. self-consumption (operation) / self-consumption (night)	1300 W / ~85 W			
Color	RAL 7035			
Altitude for rated conditions / Maximum operating altitude above sea level <sup>6</sup>	1000 m / 3000 m			
Dimensions (WxDxH)	2200 x 610 x 2000 mm / 86,6 x 24 x 78,7"			
Weight	1800 kg / 3968 lb			
Protection degree	IP20 / NEMA 2			
Protective class	I			
<b>Standards</b>				
CE marking	Yes			
Safety/EMC	EN 62109-1, EN 62109-2 / EN 61000-6-2, EN 61000-6-4			
Grid interface	IEC 62116, BDEW, P.O.12.3, Arrêté 23-04-2008, ABNT NBR 16149, ABNT NBR 16150, South African Grid code, Chilean Grid Code			
<b>Interfaces</b>				
Local Human Machine Interface	4.3" Color, touch screen			
Remote interface	Web Virtual HMI			
Communication protocols	Modbus TCP/RTU			
Data storage	Datalogger			
<b>Optionals</b>				
	Remote monitoring software			
	Reactive energy compensation module			
	Maintenance service			
	Warranty extension			

• Base feature

(1) - Other configurations can be used.

(2) - Other AC voltage, DC voltage and power classes can be configured.

(3) - Power factor > 0,98 at rated output voltage and power load > 15%.

(4) - The adjustable range can be extended and other values can be configured.

(5) - Efficiency measured without auxiliary power supply consumption and at input and output rated voltage.

(6) - Please consult Efacec with the specific operating conditions in order to characterize an eventual derate with altitude.



Efacec Energia, Máquinas e Equipamentos Eléctricos, S.A.

Rua Eng. Frederico Ulrich - Ap. 3078 | 4471-907 Moreira Maia | Portugal | Tel: +351 229 402 000 | Fax: +351 229 403 209 | inverters@efacec.com | solarinverters@efacec.com

